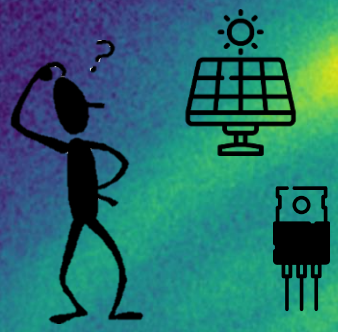

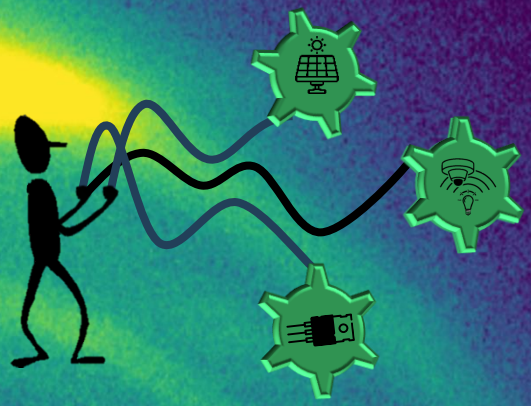

Structure-Property Interrelations in Non-Crystalline Semiconducting Polymers for Organic Electronics

Written by

Nicolás Ramos Gómez

eman ta zabal zazu

Universidad del País Vasco

Euskal Herriko Unibertsitatea

May 2024

Structure-Property Interrelations in Non-Crystalline Semiconducting Polymers for Organic Electronics

A dissertation submitted to the

University of the Basque Country (UPV/EHU)

presented by

Nicolás Ramos Gómez

In partial fulfillments of the requirements for the degree of

DOCTOR IN APPLIED CHEMISTRY AND POLYMERIC MATERIALS

Research conducted under the supervision of

Dr. Jaime Martín Pérez (UPV/EHU)

Donostia, May 2024

Universidad del País Vasco Euskal Herriko Unibertsitatea

POLYMAT

Iturri zaharretik

edaten dut,

ur berria edaten,

beti berri den ura,

betiko iturri zaharretik.

De la vieja fuente

bebo,

bebo el agua nueva,

el agua que siempre es nueva,

de la fuente que siempre es vieja.

Joxean Artze

Acknowledgements

I want to thank all the people that stay with me during this years and support me in this new knowledge field for me. The made me improve myself and expand my research career. This thesis it is not only the fruit of my work, it is made thanks also to all the people that was around me help me in and outside the job.

En primera instancia querría dar las gracias a mi director **Jaime Martín**, ya que entre los dos hemos sacado este trabajo adelante a pesar de todas las inclemencias debido a los cambios producidos durante estos años por la pandemia, traslados, etc. Ha sabido darme espacio pero también meterme caña cuando era necesario. También quiero dar las gracias al resto del grupo. Muchas gracias a **Sara** por acogerme y ayudarme cuando llegué a una ciudad completamente nueva y empecé en un campo totalmente diferente a todo lo que yo había estudiado. Gracias a ella le cogí el gustillo a las noches de sincrotrón y a tratamiento de datos con el maldito Fit2D. Por otro lado quería darle las gracias a mi postdoc **Edgar**. Entró casi igual de perdido que yo en la técnica de flash DSC pero conseguimos entenderla y buscarle truquitos juntos. Nos mejoró mucho la calidad de vida automatizando procesos tanto del flash como del sincrotrón poniendo en peligro su pelo al hacer una rasta inmensa! También quiero darle las gracias a **Valentina** por estar ahí y apoyarnos mutuamente en los peores momentos y ayudarme a centrarme y no dispersarme.

Gracias también a **Daniele Cangialosi** y **Valerio**, que desde el CFM me han enseñado lo complicado y bonito que puede llegar a ser el estudio de la fase vítrea de los polímeros.

Gracias también a todos mis compañeros de la universidad y de polymat por acogerme cuando quedé huérfano de jefe aquí en Donosti. Gracias a **Elena, Miryam, Marta, Xabi, Ainhoa, Paula, Aritz, Giulia, Lucas, los Iones, Emelin, Fermín, Álvaro…** Gracias a todos los que han estado y están ahora por todos los buenos momentos que hemos pasado y nos quedan por pasar!! También a **David** por acogerme en su grupo y enseñarme a trabajar happy pero también hard. A todo el personal de la de la

universidad como **Maite** o el personal de la cafetería y de limpieza que hacen que todo funcione como un reloj suizo.

Muchísimas gracias a mi novia **Raquel** que ha estado estos últimos dos años aguantándome y soportando todas las horas que he echado en casa haciendo la tesis. Ha conseguido que me sienta en San Sebastián como en casa y ha sido mi fuente constante de apoyo y aliento a lo largo de esta ardua travesía académica. Este logro no solo es mío, sino nuestro, y quiero expresar mi gratitud por su amor incondicional, su apoyo inquebrantable y su contribución invaluable a mi vida, tanto personal como académicamente.

Gracias por todo (menos por ayudarme en la tesis jejeje) a todos mis amigos y familia tanto de Salamanca, como mis abuelos **Abue** y **Cani**, mis tías **Sonia** y **Belén** y las primas. De Torrecaballeros a todos (que sois muchos) y los amigos de mi peña. También a los de toda la vida con los que he compartido todos los años de mi vida y mi educación Desde la infancia como **Mateo, Diego, Javi, Ana…** hasta la universidad y el master como **Carlitos, Ana, Eva, Samu, Maya, Silvia, Andres, Rulo, Pretus, Ferni**… Y también a los nuevos de San Sebastián como **Gabriel, Luna, David y Álvaro** y mis colegas del Atlético de San Sebastián.

Y por último, muchas gracias a toda mi familia en especial a mis padres **Jose Manuel** y **Susana** y a mis hermanos **María** y **Miguel**. En vacaciones me han echado la bronca y me han hecho avanzar en la tesis cuando menos me apetecía. Nos hemos ido de viajes y me han criado y han conseguido un (mini)doctor en la familia.

Summary

Nowadays, all the semiconductor industry is governed by the silicon technology. The increasing of the energy consumption and the use of electronic devices force to develop and found new materials with less energy consumption, less harmful and new properties. In the last decades the organic semiconductors (OSC), including semiconducting polymers, appear as a new, promising alternative. Flexible and transparent devices can be developed with these new materials. The scalability and the easy process from solutions compared to molecular beam epitaxy (MBE) or atomic layer deposition (ALD) used for the common semiconductor devices make the most important difference and make the OSC as a new promising technology. However, organic electronic technologies are still at their initial steps and the community is still focused on understanding these important materials.

This thesis presents 3 timely studies on materials science aspects of polymeric semiconductors. **The idea is to understand and control the morphology of the polymers to improve and tune their optoelectronic properties.**

The first chapter (chapter 3) deals with the study of the active layer of an organic solar cell. The glass transition of the bulk heterojunction is studied to determine the composition of the intermix phase on the active layer.

The second chapter (chapter 4) is focused on the study of the solid-state microstructure of the high-mobility polymer IDTBT, which has been claimed to be “nearly amorphous” polymer and thus confronts the general idea that good electrical properties stem from high crystallinity.

In the third experimental chapter (chapter 5) I stablish that, like crystalline regions, glassy regions can be also manipulated to optoelectronic properties in semiconducting polymers.

Resumen

Hoy en día, la industria de los semiconductores se rige por la tecnología del silicio. El aumento del consumo energético y del uso de dispositivos electrónicos obliga a desarrollar y encontrar nuevos materiales con menor consumo energético, menos nocivos y con nuevas propiedades. En las últimas décadas, los semiconductores orgánicos (OSC), incluidos los polímeros semiconductores, aparecen como una nueva y prometedora alternativa. Con estos nuevos materiales se pueden desarrollar dispositivos flexibles y transparentes. La escalabilidad y la facilidad del proceso a partir de soluciones en comparación con la epitaxia de haces moleculares (MBE) o la deposición de capas atómicas (ALD) utilizadas para los dispositivos semiconductores comunes marcan la diferencia más importante y convierten a los OSC en una nueva tecnología prometedora. Sin embargo, las tecnologías electrónicas orgánicas se encuentran todavía en sus pasos iniciales y la comunidad sigue centrada en la comprensión de estos prometedores materiales.

Esta tesis presenta 3 estudios puntuales sobre aspectos de ciencia de materiales de semiconductores poliméricos. **La idea es comprender y controlar la morfología de los polímeros para mejorar y sintonizar sus propiedades optoelectrónicas.**

El primer capítulo (capítulo 3) aborda el estudio de la capa activa de una célula solar orgánica. Se estudia la transición vítrea de la heterounión para determinar la composición de la fase de entremezclada en la capa activa.

El segundo capítulo (capítulo 4) se centra en el estudio de la microestructura en estado sólido del polímero de alta movilidad IDTBT, del que se ha afirmado que es un polímero "casi amorfo" y que, por tanto, se enfrenta a la idea general de que las buenas propiedades eléctricas se derivan de una alta cristalinidad.

En el tercer capítulo experimental (capítulo 5) establezco que, al igual que las regiones cristalinas, las regiones vítreas también pueden manipularse para obtener propiedades optoelectrónicas en polímeros semiconductores.

Table of contents

1) Introduction 3

2) Materials and Methods 15

2.1) Materials 15

2.1.1) IDTBTs 15

2.1.2) PFO 15

2.1.3) PBDBT-Cl and ITIC-Th1 15

2.2) Characterization Methods 16

2.2.1) Fast Scanning Calorimetry (FSC) 16

2.2.1.1) Protocols 18

2.3) X-ray techniques with synchrotron radiation 22

2.3.1) Grazing incidence wide-angle and small-angle X-ray scattering (GIWAXS and GISAXS) 24

2.3.2) NEXAFS 28

2.4) AFM 29

2.5) UV-vis spectroscopy 30

2.6) Electrical characterization 30

2.7) Sample preparation 31

2.7.1) FSC chip preparation techniques 33

3) Using the vitreous phase to unravel the morphology in bulk heterojunctions 37

3.1) Summary 37

3.2) Introduction 39

3.2.1) Evolution of donors 41

3.2.2) Evolution of acceptors 43

3.2.3) BHJ 45

3.3) Results and discussion 49

3.4) Conclusions 57

4) Solid-state microstructure of high charge mobility IDTBT polymer 61

4.1) Summary 61

4.2) Introduction 63

4.2.1) Transistor operation 63

4.2.2) FET structure 65

4.2.2.1) OFET 66

4.3) Results and discussion 67

4.4) Conclusions 79

5) Glassy Phase Engineering for Tunning Photoluminescence in PFO 83

5.1) Summary 83

5.2) Introduction 85

5.2.1) Organic light sensors 85

5.2.2) Fictive temperature 87

5.2.3) PFO 89

5.3) Results and discussion 91

5.4) Conclusions 100

6) Conclusions 103

7) Bibliography 107

1

“La ingeniería es la transformación del conocimiento en valor”

Anónimo

1) Introduction

A semiconductor is a material that is capable of acting as a conductor or insulator depending on the external stimuli. Normally the temperature, pressure, radiation, magnetic or electric field are the most common factors that change the semiconductor properties[1]. This type of materials is very interesting to use as detectors, sensors or amplifiers because their electrical conductivity can be tune changing, controlling or knowing the environment where is the device and *vice versa*.

Semiconducting materials revolutionized the electronic technology obtaining smaller devices (switchers and amplifiers) than with thermionic valves. The latter relies on the flow of electrons from a heated cathode to a positively charged anode in a vacuum-sealed glass tube. In contrast, semiconductors rely on the properties of materials like silicon and germanium to control the flow of electrons and can be much smaller[2].

The most common and well-studied semiconductor is the silicon (Si). The abundance of this material, together with its intrinsically good semiconductor properties are the reasons why silicon dominates the industry. Further widely used semiconducting materials are among others: germanium (Ge), sulfur (S), selenium (Se), gallium arsenide (GaAs), etc[3]. Semiconductors are divided in two types: intrinsic materials which possess inherent semiconductor properties and extrinsic ones which need to be doped with other atoms to obtain semiconductor properties. Doped semiconductors can be either N-type or P-type depending on whether the free charges are electrons (e.g. with boron (B), indium (I) and gallium (Ga) as dopants) or holes (e.g. with phosphorous (P), arsenic (As) and antimony (Sb) as dopants)[1].Combining N- and P-type semiconductors (e.g the invention of the p-n junction) the humanity has been able to create a wide range of electronic devices including diodes, transistors, sensors, solar cells, etc.

Nevertheless, the above inorganic semiconductors have shown some disadvantages. The most significant one is the complexity of fabrication because they need very expensive techniques such as molecular beam epitaxy (MBE), atomic layer

deposition (ALD), etc. These techniques require a high technology level like high vacuum or high intensity. Moreover, the classic semiconductors have not too much flexibility and ductility so they are not able to use for example in flexible devices.

Currently, the growth of the semiconductor industry is exponentially growing. The size of the transistors evolved from centimeters to nanometers in few decades. Moore developed a theory stating that the size of the transistors in an integrated circuit will be doubled every two years[4]. Nowadays, experts predicted that in this decade the physical limit to decrease the size of devices is almost reached due to the physical challenges associated with miniaturization.

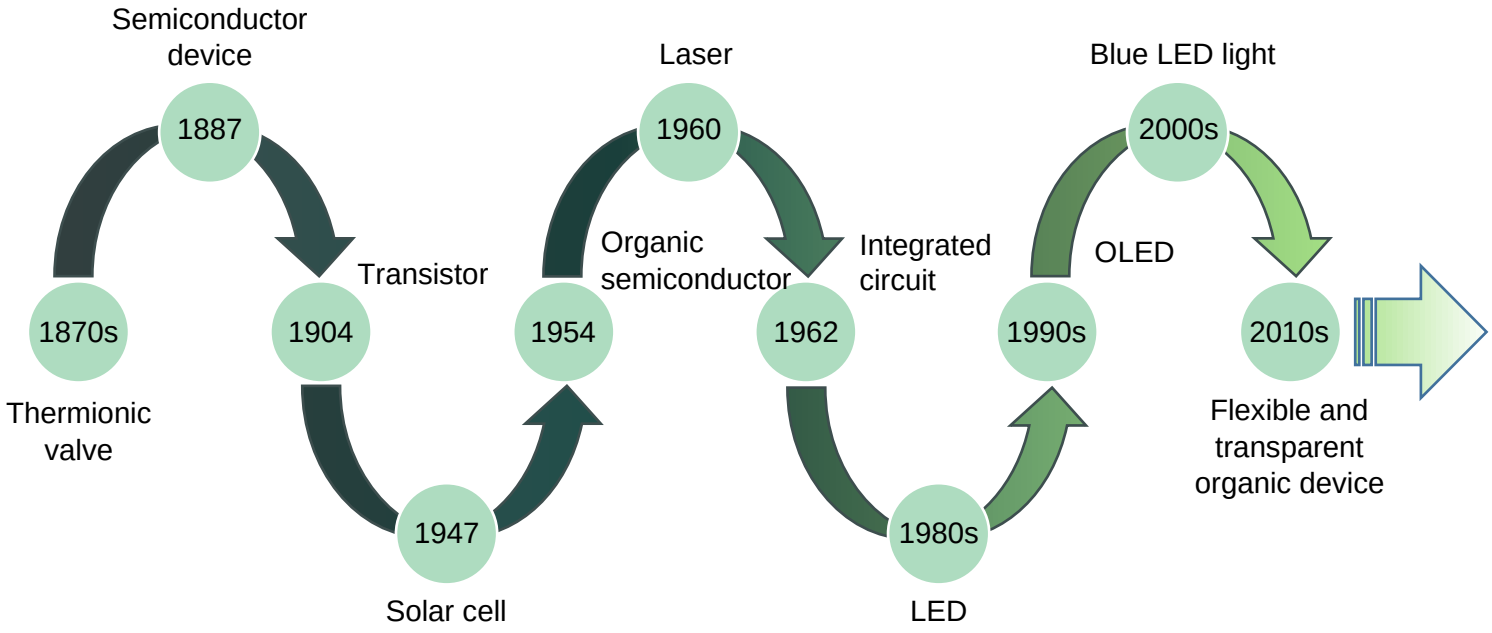

Figure 1 Milestones of the optoelectronic industry.

The first scientific publication on organic semiconductor materials dates from 1954, in which the electrical conductivity of organic polysulfones was described[5]. In the 70s, the first semiconducting polymer, i.e. doped polyacetylene (PA), was reported by Chiang et al. These development rises the possibility to break the barrier of the classical semiconductors and obtain better mechanical properties, non hazardous and biocompatible devices that allow to link the electronic world and biology , i.e.

bioelectronics[67]. During the 80s and 90s, different types of organic semiconductors were developed as small molecules or polymers.

The common and most used commodity polymers are insulators. These include. e.g. polyethylene (PE), polyethylene terephthalate (PET), acrylonitrile butadiene styrene (ABS), etc. These families are composed of repeating units connected by single covalent bonds. These sp^3 hybridization are strong, non-polar, and have low electron mobility. As a result, commodity polymers have limited electrical conductivity and are mainly used as insulators, films or for mechanical purposes[8].

If the polymers have aromatic rings or double bonds, a sp^2 hybridization occurs. With this configuration, the electron that is not linked with the adjacent atom is forming a π-bond instead of a σ-bond. The electrons that are in the π-bond are weaker and delocalized so the electrons can move more freely. If this explanation is moved to the electronic band structure, in the insulator polymers, the space between the valence band or highest occupied molecular orbital (HOMO) and the conduction band or lowest unoccupied molecular orbital (LUMO) is large so the electrons cannot climb to the conduction band to move freely[9]. In the case of conductor polymers, that space does not exist so the electron can move at will. Finally, in the case of the semiconducting polymers that space, named bandgap, is less so, applying some energy to the system the material can conduct the electricity[10].

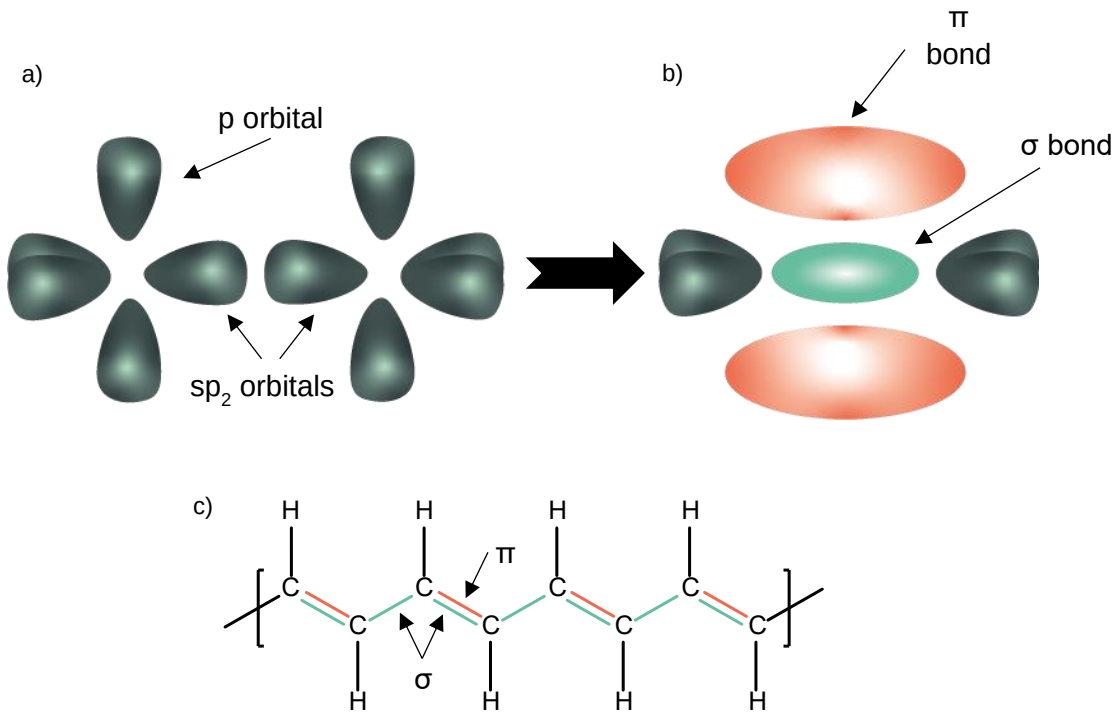

Figure 2 a) Hybridization sp2 of the orbitals, b) Link between two sp^2 orbitals and c) Chemical structure of the polyacetylene.

As described above, semiconducting organic molecules or conjugated polymers owe their optoelectronic and magnetic properties to the sp^2 bonds but also to the conjugation. Conjugation is the delocalization of multiple π-bonds that form larger and more stabilized molecular orbitals. It is achieved by alternating single and double bonds along the backbone. The orbital p that is not linked can either be in-phase or out-of-phase with neighboring orbitals, forming bonding (π) and antibonding (π*) interactions respectively. The planarity of the conjugated molecule is important to maximize the orbital interactions[1112]. The bandgap of these materials is usually in the range of visible light. This means the material can be excited optically offering new solutions in the field of optical sensors or photovoltaic applications[13].

Doping in these polymeric materials refers to chemical oxidation in the case of the p-type polymers and reduction in the case of the n-type. When the p-type polymers are excited the Fermi level is displaced to the valence band so electrons move to lower level of the bandgap and the transport of the charge occurs in the valence band (the positive hole that the electron left can move). If the material is n-type occurs otherwise and the

electron (negative charge) can move through the conduction band[14]. This process is the same as the exciton pair electron-hole in the classic semiconductors[15].

One molecule is not enough for the charge transport so some π-orbitals have to be overlapped with their contiguous to have a continuous path for the conductivity. Intrinsically, the materials with π-bonds try to heap them with the π-bonds of other chains to stabilize all the system so all these conjugated polymers have π-π stacking that also contributes to enhance the carrier mobility[16].

The traditional conjugated polymers have poor stability, which limits their efficiency and performance so, to overcome this issue, push-pull polymers were developed. This new family of conjugated polymers has two parts integrated in the same molecule. It has a donor and an acceptor part balancing the electron distribution and enhancing its stability. Also, this results in efficient charge separation and improved electrical conductivity.

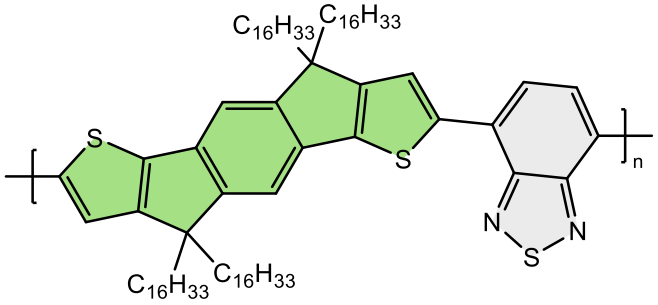

Figure 3 Indacenodithiophene-co-benzothiadiazole (IDT-BT) push-pull polymer. In green the donor part and in gray the acceptor part.

Keeping this in mind, the mobility of the electrons on the conjugated polymers not only depends on the formulation of the polymer. It depends also on the orientation of the backbone and the side chains, the planarity, the packing, the distribution… In other words, the microstructure.

There are several advantages of conjugated polymers with respect to inorganic materials. The fabrication of the devices is cheaper because they do not need complex

techniques like MBE. This is related to the easy and low-cost techniques to deposit the polymers like spin coating or blade coating and the facility to scale these techniques. Polymeric ones have, also, less fragility and more flexibility. This gives the option to develop curved displays or flexible microprocessors[17]. They are transparent or translucent so there is a possibility to develop transparent solar cells for windows for example. And one of the most promising advantages is the biocompatibility of the conjugated polymers to expand the devices to medicine and biological research due to the interaction with the environment which was previously unavailable[7]. With organic polymers actually, there are devices like transistors, diodes, integrated circuits, memory devices, solar cells, sensors and screens and displays based on them.

To understand properly how the optoelectronic properties vary in a semiconductor polymer is essential to study their microstructure. On the solid state, matter could have some microstructures depending on the order of their atoms. In the case of polymers, it depends on the order and conformation of the chains. If a material has a disordered molecular structure where the polymer chains are randomly arranged, it is referred to as amorphous. This microstructure has singular qualities as transparency or flexibility between others.

If the polymer was completely ordered, with the same periodicity between their atoms it would be a crystalline material. It is impossible in polymers to obtain a 100% of crystallinity so the polymers that crystallize are denominated semicrystalline. If the material has some degree of order but not enough to call it crystals (it could be crystals with a lot of defects) they are named paracrystalline polymers. They are characterized by the presence of a lot of structural defects that give them localized random domains with different structural properties but a certain periodicity in the system[18]. Between both models of organization of the polymer chains there are other one. The semi-paracrystalline model shows some degree of long-range order and regularity like the paracrystals but with a more limited degree of structural order. It has the dense arrangement of very small paracrystallites coexisting with more disordered sites in an amorphous matrix[19]. This opens the field to more flexible and adaptable devices than semicrystalline materials. Also, the last year, our group developed a new theory of the possible structuration of the polymers. The semi-para-cristallinity[19].

The last microstructure is the liquid crystal. This is a distinct phase in the liquid state that exhibits properties of liquids and crystalline solids. It has an intermediate state between solid and liquid, where their molecular structure aligns to some degree while still retaining fluid-like behavior. Liquid crystal polymers possess chains that can order themselves into a partially crystalline arrangement under certain conditions. This state is characterized by their anisotropic nature, meaning that their properties can vary depending on the direction. These polymers can exhibit different degrees of molecular alignment or orientation, which can be influenced by external factors.

Focusing on the transition between the states of solid matter, polymers have certain temperature named glass transition temperature or T_g. If the polymer is above this temperature, it can move and if the polymer is below T_g is freeze the system. This parameter is very important because the material experiences huge changes in the free volume, density, specific heat, mechanical properties, etc.

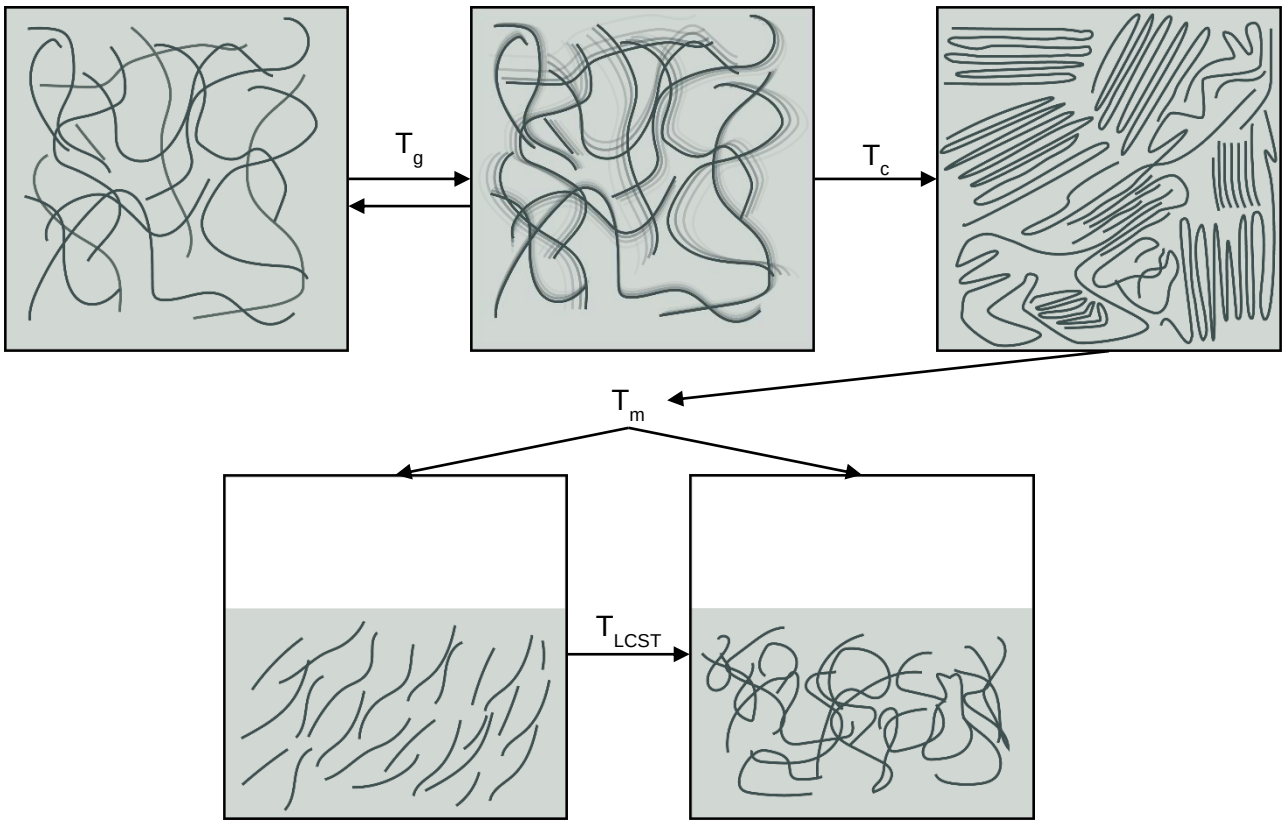

Figure 4 Scheme of the polymer thermal transitions.

There are four transition temperatures. The T_g that was explained before, the crystallization temperature (T_c), liquid crystal-liquid transition and the melting temperature (T_m). The crystallization temperature is the point when the polymer chains move from a disordered state to an ordered state. When the system equalizes and goes above T_c, the free energy of the polymer system is minimized and the polymer chains begin to arrange themselves into an ordered structure. This crystals are composed by a repeating, long-range structure and are a function of the polymer's chemical composition, molecular weight, and processing conditions[2021]. The melting temperature is the point when the polymer goes from solid to liquid state. At this temperature, the system takes enough energy (heat) to surpass the intermolecular forces that maintain the crystals linked. The last temperature, less knowledgeable and it has only a few polymers have it is the liquid crystal-liquid transition (LCST). The LCST is the temperature at which the polymer changes from liquid crystal to isotropic liquid. This is an important transition talking about processing due to its special mechanical properties being a viscoelastic liquid in a range of temperatures. The state of matter named liquid crystal has properties between liquids and solids. Is a partially ordered liquid with long-range arrangement who got it anisotropic properties like birefringence, polarizability or dichroism[22].

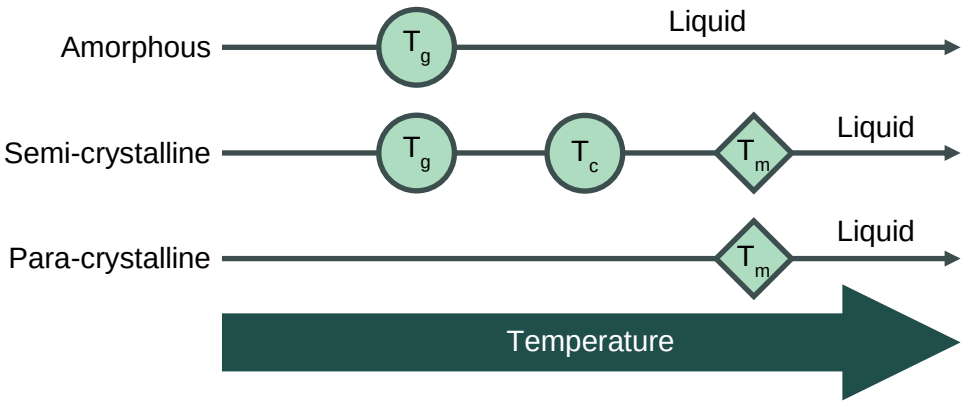

Figure 5 Classic solid-state structural models for polymers.

The classical theory of conjugated polymers said as many crystals, as much conductivity. This is because, normally, the defects and lattice disorder affect as traps reducing the conductivity[23]. For this reason, the theory of the conductivity in semicrystalline or paracrystalline polymers is through ordered domains interconnected. The most common “links” between ordered regions are the aggregates and the tie chains. Aggregates are clumpings of polymer chains with some order and tie chains are

flexible chains that connect crystals or ordered regions in a polymer network acting as wires through which electricity is conducted.

Therefore, the high mobilities in polymers are not dependent only on the crystallinity. They have many complex structures (some of them even considered amorphous) well connected that conduct electricity.

The charge transport always increases the temperature of the system like the Joule effect in the conductor materials. Due to this, optoelectronic devices based on polymers have to have high thermal stability. To be sure that the material will not change its structure and properties high T_g and T_m values are preferred. On the other hand, low T_g and T_m confers to the system more flexibility so there has to be a balance.

This work is focused on how control the optoelectronic properties in sundry promising devices for applications in transistors solar cells and sensors.

In summary, conjugated polymers are promising materials for advanced applications, such as flexible electronics and bioelectronics. To get the most out of conjugated polymers is necessary to understand, control and know how to tune their structure. Normally, classical studies are focusing on understanding the crystallinity but, nowadays, the vitreous phase is taking more importance. Knowing and switching the vitreous phase the optoelectronic properties also could change significantly.

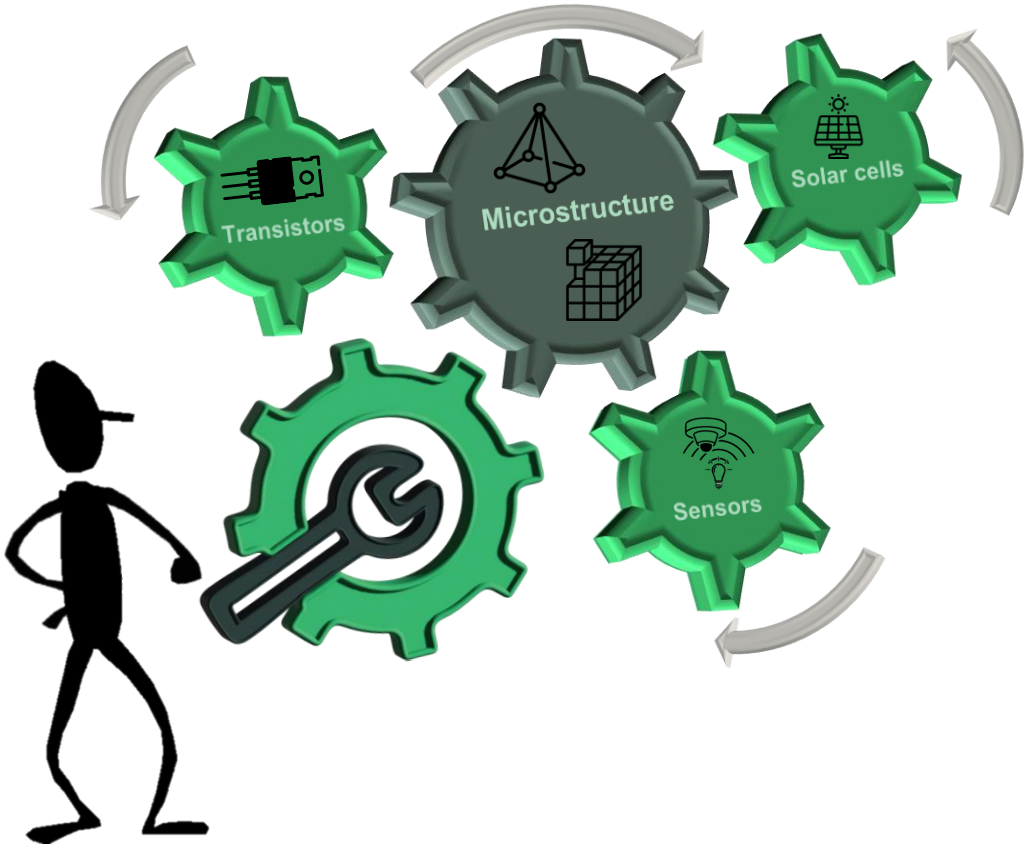
Transistors
Microstructure
Solar cells
Sensors

2

"El trabajo de la ciencia es la eliminación de lo imposible."

Isaac Asimov

2) Materials and Methods

2.1) Materials

The materials and solvents used are divided in three sections according to the chapters of the thesis.

2.1.1) IDTBTs

Developed at the Imperial College by Martin Heeney's group. Two different molecular weights of (indacenodithiophene-co-benzothiadiazole (IDTBT) were studied with Mn 121.4 kDa, Mw 321.6 kDa, PDI 2.57 and Mn 65 kDa, PDI 2.42.

2.1.2) PFO

Poly(9,9-di-n-octylfluorenyl-2,7-diyl) also named F8 or PFO.

Only one PFO synthesized at the Imperial College by Wenmin Xu with 20.68 kDa of molecular number, 33.56 kDa of molecular weight an polydispersity index of 1.62.

2.1.3) PBDBT-Cl and ITIC-Th1

The small molecule 3,9-bis(2-methylene-((3-(1,1-dicyanomethylene)-6-difluoro)-indanone))-5,5,11,11-tetrakis(5-hexylthienyl)-dithieno[2,3-d:2',3'-d']-s-indaceno[1,2-b:5,6-b']dithiophene or ITIC-Th1 purchased from Derthon Optoelectronic Materials Science Technology Co. Ltd.

The donor poly[(4,4'-bis(2-butyloctoxycarbonyl-[2,2'-bit-hiophene]-5,5-diyl)-alt-(3-chloro-2,2'-bi-thio-phene-5,5'-diyl)] or PDCBT-Cl were synthesized on Geng's group according to their previous report[24].

2.2) Characterization Methods

To study the physical and structural properties are required two principal techniques. They are used to uncover the relations between the structure, the morphology and their electronic and optoelectronic properties. The most important technique to study the amorphous part of the polymers is the Flash DSC or Fast Scanning Calorimetry (FSC) and the technique to study the order of the polymer chains is, in-situ and ex-situ, the Grazing Incidence Wide Angle X-ray Scattering (GIWAXS). Moreover, Grazing Incidence Small Angle X-ray Scattering (GISAXS), temperature-resolved Polarized Light Optical Microscopy and Spectroscopy (PLOM-S), Atomic Force Microscopy (AFM) and were used to support and understand better the morphology of the semiconductor polymers.

To see if the physical properties change the electronic and optoelectronic properties spectroscopic techniques (absorption, photoluminescence, Raman) and charge mobility measurements in organic field effect transistors were utilized.

2.2.1) Fast Scanning Calorimetry (FSC)

The idea of the FSC appeared when the users of the conventional DSC tried to increase the scan rates. The first approximation was reducing the sample obtaining rates of 200-750 °C/min. Thanks to the Micro-Electro-Mechanical Systems (MEMS) technology (developed in the 90s) could be possible to create the Flash DSC sensor chips obtaining heating and cooling rates of more than 10000 K/s[25].

The FSC used in this work is a *Mettler Toledo Flash DSC 1* fast scanning calorimeter based on a power compensation twin-type chip. It has attached a *Huber TC100MT* intracooler to reach temperatures of -100 Celsius. It has also a magnifying

glass to locate properly the sample and a continuous nitrogen purge flow of ≈ 20 mg/ml. The part where a substantial change has been achieved thanks to the technology is the sensor. *MultiSTAR UFS1* (24 × 24 × 0.6 mm3) MEMS chip sensors. It is composed by two identical quadratic silicon-nitride/oxide membranes (1.7 x 1.7 mm), 2 µm of thickness mounted on a 300 µm thick silicon frame. All of this technology is supported in a ceramic plate. Each membrane acts as a small furnace being the chip as a miniature DSC. The membranes are connected with the FSC by small paths in the ceramic plate and small wires between the ceramic plate and the silicon frame.

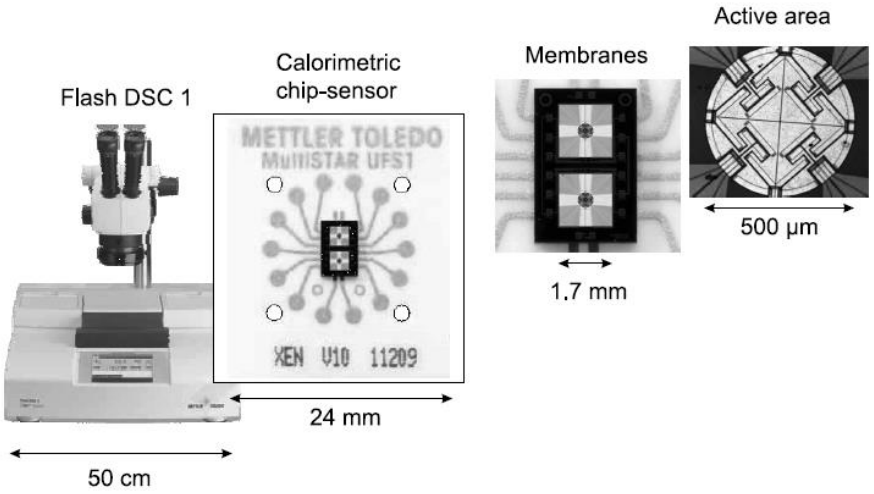

Figure 6 Size of the Flash DSC chip parts.[26]

The chip can be extracted from the FSC so the sample can be prepared with many different techniques. The sensor is very stable so it can be placed in liquids, autoclaves, furnaces, and so on. One important difference with other techniques is that it is possible to grow thin films in the chip. With this advance, it is possible to study exactly the thermal changes that occur in organic solar cells, transistors, sensor devices, etc. A second important difference is that cooling at very high velocity rates, overcoming the crystallization rates, vitrified materials can be obtained to study metastable phases and study isothermal crystallization with annealings from very short times (0.01 s) to simulate processes as injection molding. Another important difference is that, heating very fast the material, it is possible to go to very high temperatures avoiding the degradation of the material so, the melting of the material can be studied if it is overlapped with the degradation of itself, for example. The range of temperatures for this technique is -90 to 450 Celsius, enough to study polymers.

This technique is complementary with the conventional DSC due to there are a range of cooling and heating rates where they are overlapped.

2.2.1.1) Protocols

The most common experiments of FSC are the isothermal “annealings”. These experiments are used to study kinetics. In this case, three thermal protocols are used to elucidate the thermal properties of the materials. The so-called isothermal “annealings” to evaluate the nature of the peak[27]. The isochronous thermal protocol to identify the different thermal transitions in a wide range of temperatures. And the modulated DSC to avoid irreversible processes such as crystallization or study the behavior of the vitreous phase.

The word annealing is not well used always in a good way, the term annealing is correct only when the temperature constant step is up to the T_g of the polymer. If the isothermal step is at lower temperatures, is an ageing.

Before, the chip is heated and cooled it very times to remove the thermal stresses of the membranes and corrected with a baseline. Then, the sample is deposited on the chip, the range of temperatures to work is located and the heating and cooling rates optimized. With higher rates it is able to see smaller samples and more clear results but the sample could have thermal lag so the measurement is not correct. With less velocity rates, the thermal lag is deleted but the sensitivity of the FSC decrease (lower signal). When the optimization is finished, the thermal protocols can be made. Depending on what you are looking for, one protocol or another is selected.

2.2.1.1.1) Isothermal “annealing”

It consists on bring the sample to a high temperature to delete the thermal history and obtain the most isotropic material. This temperature has to be above the melting point to certify the isotropicity of the material. Then, the material is cooled at a given cooling rate (β)[25] to a certain temperature T_a (annealing/ageing step), below the T_g to freeze the material in a specific thermodynamic state[2829]. Then, the material is cooled

down to -80 or -90 Celsius (the minimum temperature is reached by the FSC) and immediately heated up to the higher temperature. Finally, the material is cooled with the same cooling rate and it is made another heating ramp to use it as a reference (heating without the isothermal step).

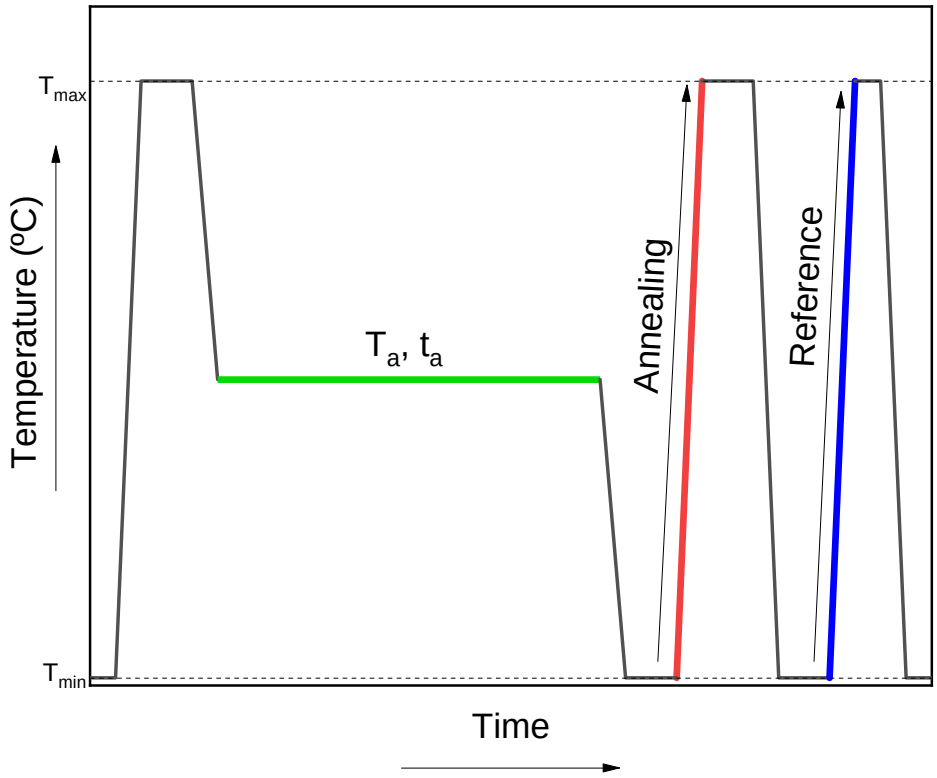

Figure 7 FSC protocol with T_a (annealing temperature) and t_a (annealing time).

The aforementioned overshoot can be explained with the own definition of the T_g. The glass transition temperature (T_g) is defined as the temperature (or range of temperatures) where the glassy phase undergoes a change between an immobilized state (out-of-equilibrium glass) to a molecular mobility state.[30] In the case of calorimetry, if the material in the immobilized state evolves through a less energy level (reducing its enthalpy) an endothermic overshoot can be seen at temperatures close to the T_g. This process is called physical ageing. In conclusion, the glass transition temperature and the metastable equilibrium of an order glassy phase below that temperature can be studied by researching the endothermic overshoots formed by ageings below T_g.

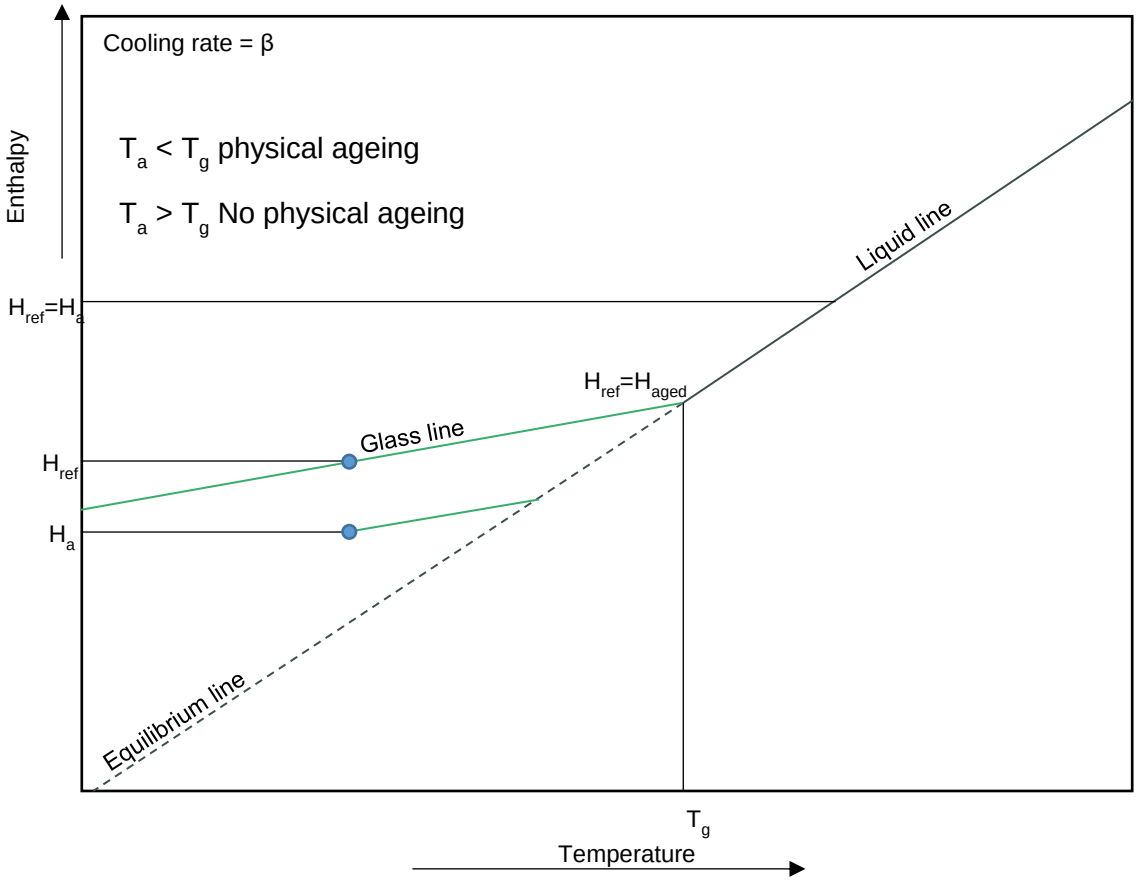

Figure 8 Temperature dependence of the enthalpy for a typical glass former cooled down at a given cooling rate β.

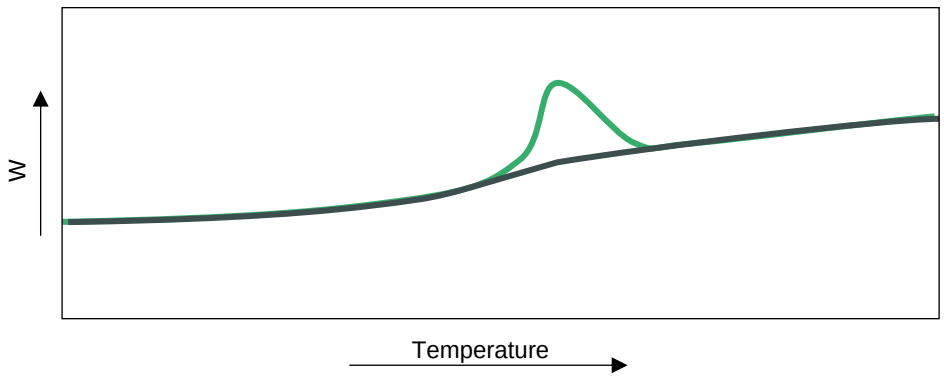

Figure 9 Effect of an ageing in a DSC experiment. In green the sample aged and in grey the sample unaged.

When the annealing time is changed (at the same temperature all de annealings), studying the evolution of the endothermic overshoot, the kinetics of crystallization and ordering can be studied to know if the peak is due to the glassy phase, nucleation or

growth of crystals. The total area of the endothermic overshoots are fitted with a sigmoidal-like law (e.g. Kohlrausch-Williams-Watts, Avrami, etc.). The parameter in which we are interested is β, the Avrami exponent.

$$\Delta H = e^{(kt)^{\beta}}$$

Equation 1 Kohlrausch-Williams-Watts or Avrami-like law.

Where ΔH the maximum enthalpy value measured in the experiments, k is a constant associated with the rate of the advance of the the calorimetric process, *t* is time and β, is a parameter related with how the advance of the process depends on temperature and it is typically referred to as the Avrami constant.

2.2.1.1.2) Isochronous “annealing”

Developed by Cangialosi et all, it is used to identify the T_g of the samples by FSC.[31] The same protocol as in the isothermal Figure 7 is used but, instead of varying the time of annealing, is varying the temperature of the annealings. In this way, when the temperature is below the T_g, in the isotherm the vitreous phase is ordered (every time the materials try to reach the low energy state) that is translating into an endothermic overshoot in the heating curves of the DSC. The point when the overshoot becomes 0 can be extrapolated when some measurements are made increasing the annealing temperature. At this point, the vitreous phase cannot evolve. Therefore, this means that we have reached the early part of the T_g region called T_g onset[32].

The evolution of the crystalline phase above T_g can also be studied with this method.

2.2.1.1.3) Modulated DSC

The idea of this protocol is, instead of using a linear heating ramp, to use a periodic temperature modulation (step response or sinusoidal usually) of a certain amplitude and frequency.

Thanks to this protocol, we can separate processes due to reversible C_p and irreversible C_p. In this way, for example, cold crystallization processes and reversible processes such as the glass transition can be separated.

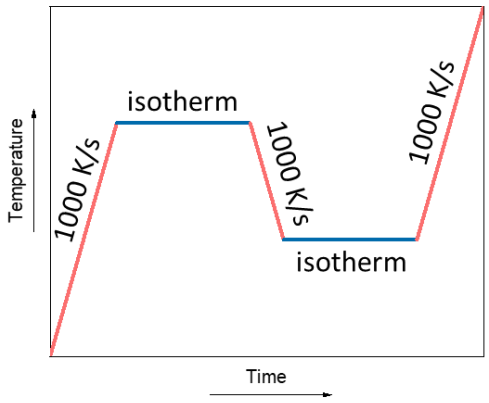

Figure 10 Schematic scheme of one pseudo-wave of the modulated DSC.

This protocol in FSC consists in a pseudo wave that simulates an harmonic heating protocol. One heating ramp of two degrees, a small isotherm, one cooling ramp of 1 degree and another isotherm with the same time of the previous one. Repeating this four steps x cycles a modulated DSC is obtained with a step of 1 degree[33]. The maximum velocity of the equipment for the data acquisition with this small heating and cooling ramps is 1000 K/s. Changing the time of the isothermal steps we are able to change the modulated frequencies (typically between 1 and 20 Hz). It is necessary to use the Fourier transform to treat the data and separate the C_p reversible from the non reversible[34].

2.3) X-ray techniques with synchrotron radiation

A synchrotron is a light source emitted by electrons moving very fast (almost light speed) inside a ring. The spectrum of synchrotron light reaches from the far infrared to near γ-rays. The radiation is emitted tangentially and forward from the particle orbit due to the nature of the relativistic particles. The angle of the collimated light corresponds to 1/γ where γ is the Lorentz correction factor for the particle relativistic motion: $\gamma = (1 - \beta^2)^{-0.5}$, where $\beta = v/c$ and v is the electron velocity and c the speed of light in vacuum. The wavelengths obtained from the synchrotron radiations include from the far

infrared to near γ-rays.[3536] We leverage the hard X-rays of this light thanks to the monochromators.

Due to the wave-particle duality, the electrons can be considered “wave packages” and, therefore, particles named photons in the case of the light. Also, they can have all the wave properties such as diffraction, reflection, etc. [37] This is because they can be considered “matter waves” with their own wave function so knowing the mass and the velocity, the wavelength can be known thanks to the de Broglie equation λ=h/mv where lambda is the wavelength, h is the Plank’s constant, m is the mass of the particle and v the velocity.[38]

The synchrotron has 5 differentiate parts. The electron generator or “Electron gun” where the electrons are generated by heating a metal up to 1000 Celsius (tungsten with barium oxide normally), a linear accelerator (Linac) where the electrons were accelerated up to 100 MeV using radio frequency cavities. Then, the electrons accelerated up to 3 GeV in a booster ring with electromagnetic fields. Finally, the electrons are delivered into the storage ring. Maintaining under vacuum to minimize the scattering of air, it keeps the electrons spinning until the extraction of them tangent to the ring in the beamlines with the help of magnets. Then, in the beamline, they are used some slits, mirrors and monochromators to obtain the desired wavelength.[3940]

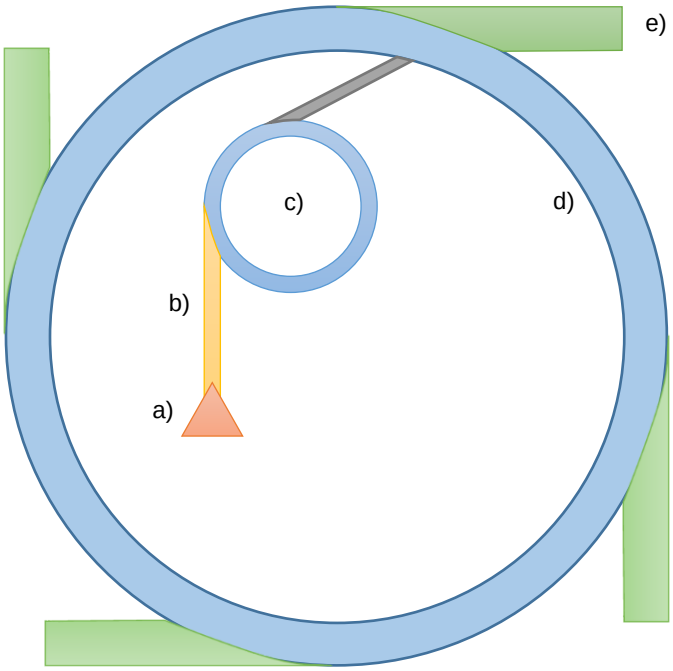

Figure 11 Synchrotron graph. a) Electron gun b) Linac c) Booster ring d) Storage ring e) Beamline.

The synchrotron radiation light source is used because the intensity is higher than in the conventional X-Ray tubes and the light is very polarized and collimated.

2.3.1) Grazing incidence wide-angle and small-angle X-ray scattering (GIWAXS and GISAXS)

X-Ray techniques are good to study the structural and morphological aspects of the semiconductor polymers in a broad range. In our case, the maximum range we use is between 0.006 and 25 nm^{-1} approximately. All the distance data are expressed in scattering vector, momentum transfer or wavevector transfer scattering vector, momentum transfer or wavevector transfer (q) which is inversely proportional to the real distance (d).

Moreover, the Bragg law[41] relates the distance between adjacent periodic planes (d), the wavelength (λ) and the angle between the scattered wave and the incident wave (θ). If this law is fulfilled, the periodic distances of the material can be studied.

a) $$q = \frac{2\pi}{d}$$ b) $$n\lambda = 2d\sin\theta$$

Equation 2 a) q-d relationship and b) Bragg's law.

In the specific case of GISAXS and GIWAXS, instead of knowing the interplanar distances, the shape, texture and orientation can also be shown.

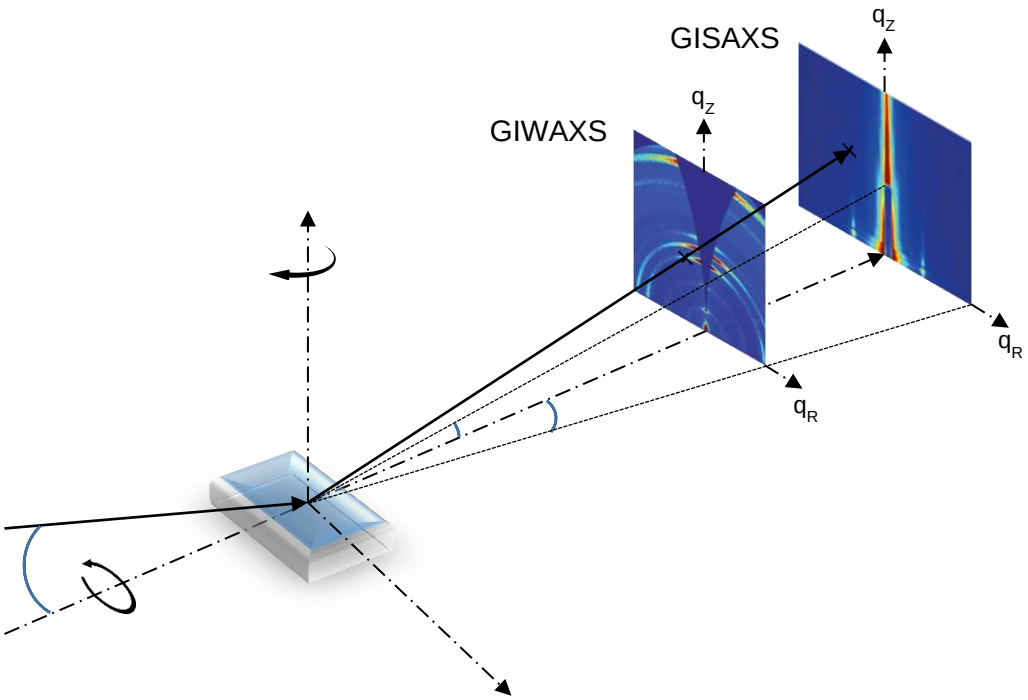

Figure 12 GIWAXS and GISAXS geometries.

The detector where the intensity values of the scattering are collected is planar so it is necessary to make some corrections in GIWAXS. In the case of GISAXS, the detector is very far from the source so it is considered that the image in the detector is veracious. The scattering of the sample is isotropic (vectorially speaking) so, having a planar detector, the distances in the planar detector are not the real value of q. A spherical detector is needed to obtain the real distances in the reciprocal space to have all the detectors equidistant to the detector. With the planar detector, the Ewald sphere correction is used[4243] as you can observe in *Figure 13*.

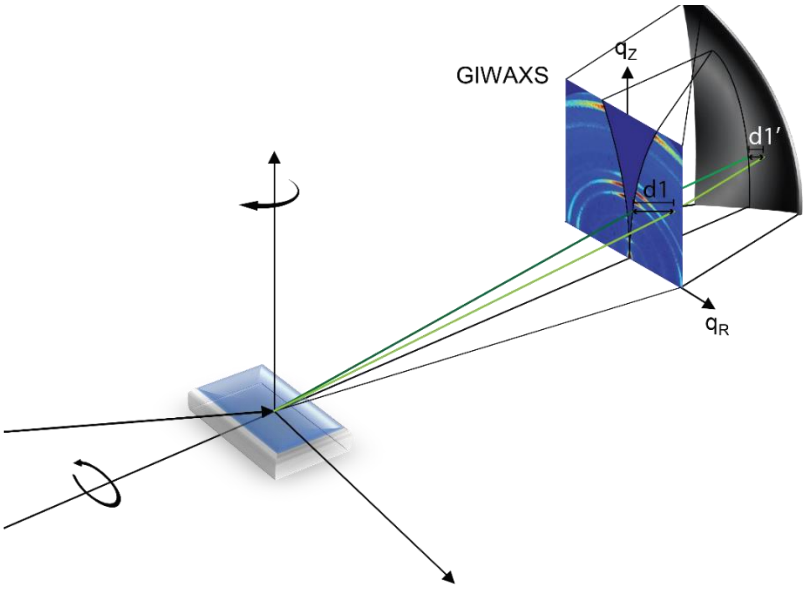

Figure 13 Ewald sphere correction scheme.

Moreover, as much ordered the material (more perfect is the periodicity), the peak observed in the detector is sharper. Knowing the width at the halfway up the peak (FWHM or full width half maximum) and the position in the q range, can be determined the coherent length (L_c) thanks to the Scherrer equation (*Equation 3*)[44] where k is the shape factor (between 0.9 and 1)[45] and Δq is the FWHM.

$$L_c = \frac{2\pi K}{\Delta q}$$

Equation 3 Scherrer equation.

This parameter is directly related with the paracrystalline parameter (g). With this parameter is measure de statistical fluctuation of individual lattice spacings[45]. For highly disordered systems, the g parameter can be extracted from the width of the first order diffraction peak[19] only if the peak is entirely described by cumulative disorder and if paracrystallinity is more significant than lattice parameter fluctuation[46]. If these two conditions are fulfilled

$$g = \sqrt{\frac{\Delta q}{2\pi q}}$$

Equation 4 g parameter equation.

where Δq is the FWHM and q is the maximum peak position. The g parameter can oscillate a lot between 0.01 (1%) and more than 0.20 (2%) using as scale-based material the a-SiO2. Ig g > 1% the material is highly crystalline, if 1% < g < 10% the material has imperfect crystals and/or mesophases and, if g < 10% the material is amorphous[30].

For GIWAXS the incidence angle used was 0.12º (little below the Si angle) but the measurements were carried with 4 different angles between 0.08 and 0.2 to obtain the best data. 3 different types of integrations were carried out. Complete (in the whole directions), in-plane taking the 45 degrees below to see the order in the chains that are parallel to the substrate and out of plane to study the perpendicular substrate direction planes. The temperature experiments were conducted in a Linkam® in a N_2 atmosphere. All the experiments were performed at the BL11 NCDSWEET beamline at ALBA Synchrotron Radiation Facility (Spain). The incident X-ray beam energy was set to 12.4 eV using a channel cut Si (1 1 1) monochromator. A Rayonix® LX255- HS area detector was used. The setup was calibrated using Cr_2O_3 as reference.

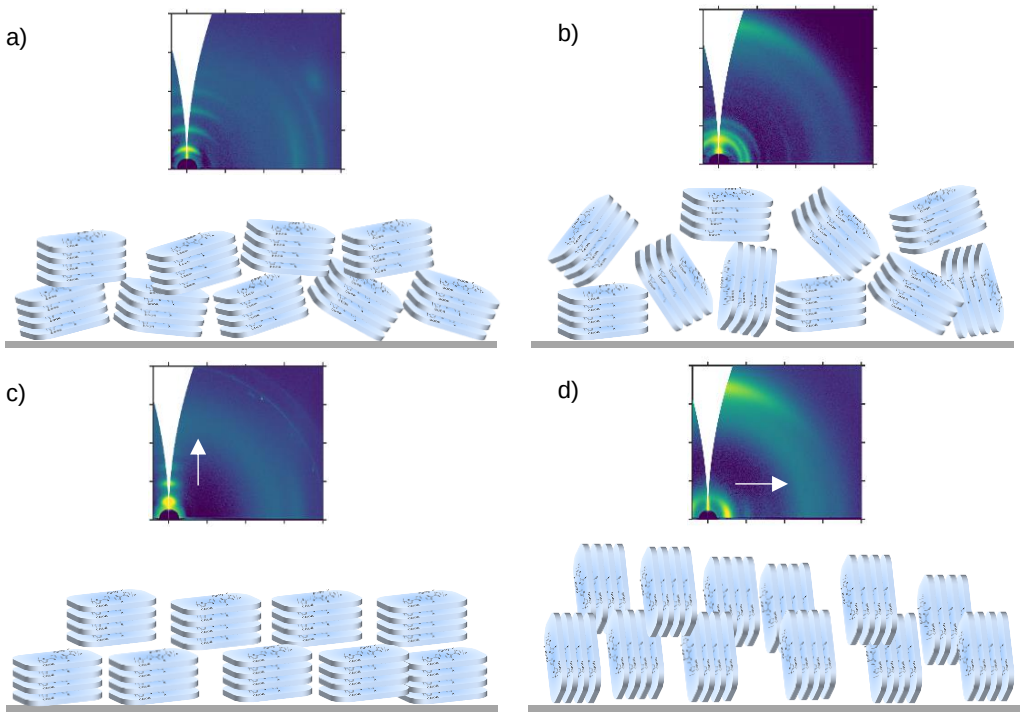

Figure 14 GIWAXS pattern and scheme of a) Low disorder out of plane, b) Totally disorder, c) Out of plane and d) In plane.

For GISAXS the horizontal integration was used at the Yoneda peak to obtain the maximum range of intensity. The experiments were developed at Alba and Elettra

synchrotrons. In both cases the calibration sample was AgBH (Silver Behenate) and the detectors were the Pilatus 1M detector from Dectris®[4748]. For the temperature experiments a Linkam® in a N2 atmosphere was used at Alba and an Anton Paar model DHS1100 was used at Elettra[48].

2.3.2) NEXAFS

Understanding the molecular arrangement and orientation of polymer chains is pivotal in tailoring the properties of advanced materials. In this pursuit, Near Edge X-ray Absorption Fine Structure (NEXAFS) spectroscopy was employed as a powerful tool to elucidate the intricate details of polymer electronic structures. The unique advantage of utilizing synchrotron radiation as the X-ray source further enhances the precision and sensitivity of NEXAFS, offering unprecedented insights into the orientation of polymer chains.

NEXAFS is based on the principle that X-rays incident on a sample can be absorbed by core-level electrons, causing them to transition to unoccupied states. Near the absorption edges of specific elements, such as carbon or nitrogen, the absorption spectrum exhibits fine structures that are sensitive to the local electronic and molecular environment. The orientation of polymer chains can be inferred by exploiting the polarization dependence of NEXAFS. The absorption cross-section is sensitive to the orientation of the absorbing molecule with respect to the polarization vector of the incident X-rays.

Analysis of the NEXAFS spectra involves comparing the intensities and shapes of spectral features for different polarization directions. This information can be used to deduce the average orientation of the polymer chains in the sample.

2.4) AFM

Atomic Force Microscopy is a very versatile technique. It is composed mainly by a cantilever that has at the end a very small tip that is in contact with the sample. At the top of the cantilever a laser is focus. Controlling the movement and the optical characteristics of the reflection of the laser (with a photodiode) the topography can be seen transforming the light changes in a voltage oscillation and this in height contrast[49].

The equipment can be operated under a lot of modes: contact mode, non-contact mode, tapping mode, etc.

The best mode for soft materials, more concrete polymers, is the tapping mode because the cantilever could have higher mechanical properties than the sample so the material to be measured can be dragged by the tip (lateral forces are practically eliminated)[50]. Also, the material is less damaged than in contact mode due to the less contact with the tip. In tapping mode, an oscillation (close to its resonant frequency) in the cantilever is induced. The information is collected through the amplitude of the cantilever. If the surface of the sample is not flat, the oscillation (amplitude and frequency) of the cantilever will change concerning the original oscillation resulting in lighter areas and darker areas. For that reason, the topographic picture (3D) of the sample is mapped line by line[51].

3 different picture sizes were carried out. 1x1 microns, 3x3 microns and 10x10 microns with 512 scan lines for each picture with a Bruker Multimode 8 AFM with a Nanoscope V controller.

The samples were prepared by spin-coating and the thermal treatments were performed in a Linkam® hot stage under N2 atmosphere.

2.5) UV-vis spectroscopy

UV-Vis Shimadzu UV-2550 was used to measure the absorbance of the samples. The thin films were made with the same conditions of the rest of the experiments and measured in a glass.

Photoluminescence spectra were measured using Witec equipment. We excited it through a UV high transmission 40× objective using a solid-state laser with a peak wavelength at 355 nm. Power of 60 μW. We made 500 μm × 500 μm images of the samples directly on the FSC sensor chips to know the region where it works. Cluster analysis of the data revealed three different regions for each chip:

- The inner part, likely very thick as deduced from the apparent self-absorption features in the spectra.
- The region above the heating resistance.
- The border between the inner part and the heating resistance region.

The data explained in this work corresponds to the material fraction just over the resistances because is the region where there are more material and it is more homogeneous.

2.6) Electrical characterization

The device architecture was a standard top-gate bottom-contact configuration. Channel width was 0.1 cm, while channel length was ranging from 2.5 to 20 μm. Low alkali 1737F Corning glasses were used as substrates and cleaned in an ultrasonic bath of acetone and isopropyl alcohol, and further exposed to O_2 plasma at 100 W for 5 min. Bottom electrodes were defined by a shadow mask and deposited by thermal evaporation of Au (35 nm), with a Al adhesion layer (5 nm). Patterned substrates were cleaned by ultrasonic bath in isopropyl alcohol and by O_2 plasma at 100 W for 5 min. IDTBT was dissolved in oDCB (10 mg/ml), stirred overnight at ~ 100 ˚C and spin coated

at 1000 rpm for 60 seconds, followed by thermal annealing at 100 ˚C for 1 hour in a nitrogen filled glovebox. Further, devices were thermally annealed at the given temperature in a nitrogen filled glovebox and subsequently stored overnight in air. A cytop layer is then spin coated (4000 rpm 400 acc for 90 seconds), before the thermal evaporation of the Al electrode.

Devices were then transferred into a nitrogen-filled glovebox for the measurement of the electrical characteristics with a probe station (EVERBEING) and a Keysight B2912A Precision Source/Measure Unit.

2.7) Sample preparation

For the experiments, we can prepare the sample dissolving the polymer (solution-processed) or using the neat material. The only case where the bulk material can be used is in FSC, putting a small piece of the material in the sample support.

For the rest of the characterization methods, and also for some FSC measurements, solution-casting techniques were required:

- Spin-coating: is the most used technique in this work. It consists of putting a certain amount of solution on the substrate and then spinning the substrate at a certain speed (normally between 1000 and 5000 rpm) and a certain time[52][53]. Finally, the film is formed and it is allowed to dry or to receive a thermal or solvent treatment. The spincoater used in this work was supplied by *Ossila Ltd*.

- Wire-Bar-coating: one metallic bar with a thread wrapped around is used to form the film. With this technique the substrate can be heated so the temperature can be used as a variable. The solution is spilled between the bar and the substrate, then, the bar is moved through the substrate at a certain velocity obtaining different thicknesses varying the velocity of the bars and the thickness of the wires[54]. The wire-Bar-coating used in this work is a K101 control coater with a K101 heated bed of *RK Print Coat Instruments Ltd*.

- Drop-casting: some solution is pipetted (10 – 50 µl) on a substrate creating a bead. Then, the drop is dried in ambient conditions[55]. If it is necessary to study the behavior of the dropcast by FSC, the drop can be deposited on a glass slide and then scratched the drop to obtain a powder to measure the bulk material.

Before depositing the solution-processed samples, the solutions were stirred minimum 1 hour at a certain temperature (lower than the boiling point of the solvent). For chlorobenzene and it derivates 80 °C, for tetrahydrofuran 60 °C and for chloroform 55 °C.

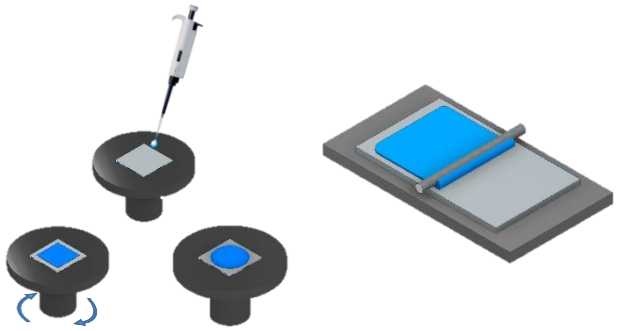

Figure 15 Schematic illustration of the different deposition techniques. On gray is the substrate and blue is the sample.

After the deposition, the films can be treated by different ways. The most common is heating the sample at a specific time giving it a thermal treatment. The other way is maintaining the sample in a saturated atmosphere of a solvent for some time (solvent vapor annealing). The idea is to give time to the polymer chains to be ordered better than in the deposition step.

The films were deposited in glass substrates (*deltalab*) and pieces of one side 100 silicon wafers polished undoped (*neyco*). All the substrates were cleaned with an ultrasonic bath (*Fisherbrand* FB 15047). First, 10 minutes in acetone and the other 10 minutes in isopropanol. Afterwards, the substrates were dried in air and exposed to ozone for 10 minutes in a chamber of *Ossila Ltd*.

2.7.1) FSC chip preparation techniques

In this work only two techniques are used to attach the sample to the chip: bulk and spincoating (*Figure 16*). The membrane where the sample is placed is very film so it must be handled very carefully. The weight of the sample is very low (10 ng – 10 µg) to avoid the thermal lag.

a) b)

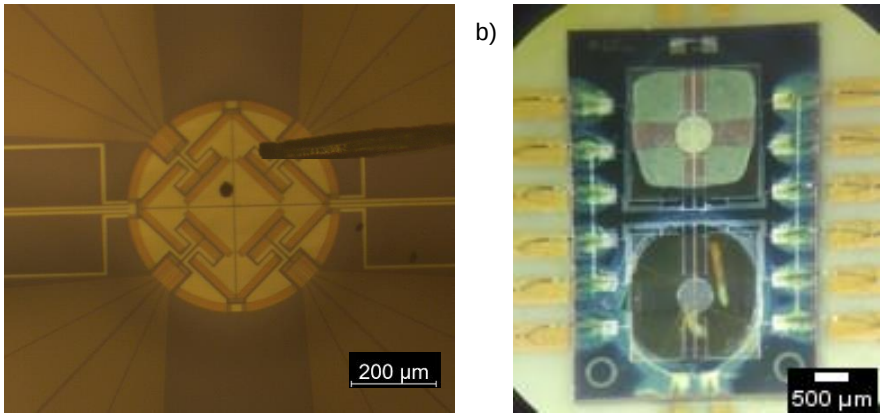

Figure 16 Optical microscope images of a) Bulk sample and b) Spincoating sample.

To place the bulk sample a small piece of the polymer is taken with a brush hair and posted in the chip.

Make a film is more complicated but all the polymer devices for electronic and optoelectronic applications are made with thin films to have the best volume:surface area relationship. The first step is to cover the reference with a small drop of glucose dissolved in water and wait until the droplet is partially solidifies/gelates. Then, the polymer solution is spincoated in the sample place. The glucose is insoluble in halogenated solvents so when the sample is deposited, the reference continues covered. To conclude, the glucose is removed with water. The thin film is deposited in the back part of the de chip because it is raised and it is easier to deposit the film.

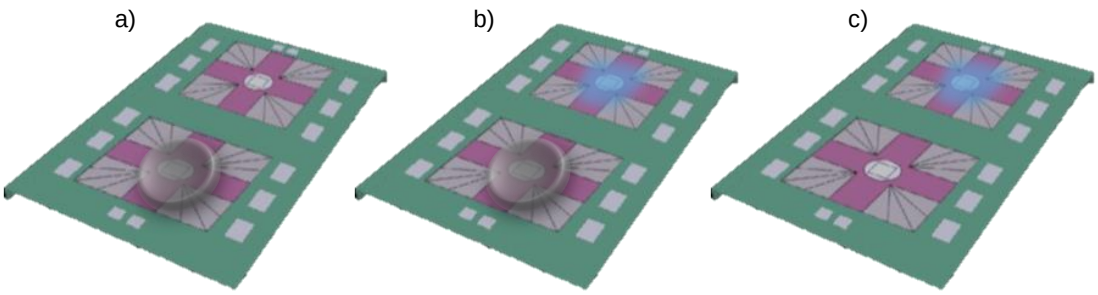

Figure 17 Thin film deposition steps of a sample in a FSC Chip. a) Glucose deposition, b) Spincoating of the sample and c) Removing the glucose.

The final result is a thin film covering only the sample part of the chip. If it is needed a post processing, it can be made directly on the film without damageing the chip.

3

"La ciencia y la tecnología revolucionan nuestras vidas, pero la memoria, la tradición y el mito nos agrupan como seres humanos."

Michael Crichton

3) Using the vitreous phase to unravel the morphology in bulk heterojunctions

3.1) Summary

Organic solar cells are the future for sustainable and environmental friendly energy. The study of how is the behavior of the active layer (Bulk Heterojunction) is key to improve this technology. Thanks to the Flash DSC, X-ray scattering and other techniques is possible to understand it.

The study of the mixture of PBDBT-Cl (donor) and ITIC-Th1 (acceptor) is used for this work. Thanks to the previous work of Liang et al the better concentration of the mixture is 50:50 %wt with a solvent annealing. With this knowledge and studying the vitreous phase of the mixture, the proportion between the mixed phase and the single component phase can be determined in the same development conditions of the real solar cell.

3.2) Introduction

The energy consumption in the world is increasing exponentially in the last decades. The petroleum reserves are not infinite and, nowadays, nuclear energy has the potential to be the best option but from the point of view of the population it is very dangerous. Due to these handicaps, renewable energies are taking the lead. The renewable energies are taken from the wind, the sunlight, the biomass, the movement of the water and the geothermal heat[56].

Focusing on the sun's energy, there exist three ways to extract energy. Heating a fluid to boil it and produce energy with a turbine, heating water or some spaces like a pool or a restaurant and directly convert the solar energy into electricity[57].

To extract electricity from the sun is necessary to have a material or materials that are able to absorb the energy of the sunlight and generate free charge carriers (electrons and holes). This mechanism is called the photovoltaic effect. When the photons of the sunlight arrive at the solar panel are absorbed by the atoms of the semiconductor material. If the energy of the photons is enough, an electron of the atom can "jump" from the balance band to the conduction band and become free from their atom. The released electrons move through the semiconductor material towards an electrode, creating an electric current[585960].

There are several types of solar cells depending on the materials and the deposition of the active material techniques. The most common are perovskite solar cells, silicon solar cells and organic solar cells[61].

As for organic solar cells, they could not be viable without the discovery of Alan Heeger in the 1980s who later received the Nobel Prize in Chemistry for his work[62]. The first viable organic solar cells or organic photovoltaics (OPVs) consist on a single layer of organic material between two electrodes. In the next decade more complex structures started to develop like multi-layer or tandem but without good results. Since 2000, the combination of improved materials (polymers and fullerene or non-fullerene acceptors),

device architectures and understanding the fundamental physics of them had improved significantly their efficiency.

The solar cells that are being studied are primarily composed of two main materials. A donor that “repels” electrons and an acceptor that attracts electrons. These two materials are typically blended, forming a so-called bulk heterojunction (BHJ) morphology., so that the blended material contains three well-defined regions: donor domains, acceptor domains and intermix face between both where the charge separation occurs.

Nowadays, organic solar cells continue having less efficiency than silicon ones but they have the potential to dethrone them thanks to the easier and cheaper manufacture. This makes them ideal for large-scale applications reducing a lot the energy consumption in the process of develop them. Also, they are lighter and, thanks to their flexibility, they can be integrated into a wide range of applications like clothing, building materials or portable electronics. They need to improve their lifespan because they lose properties when the time exposure is too long or in some environments.

One of the most auspicious advantages is the tuneability of the materials. They can be chemically or physically altered to have specific properties. The absorption spectra of the materials can be modified by selecting the light wavelengths depending on the country or region, the season or the things that are below it. For example, if you want to have a solar cell in the ceiling (transparent or semitransparent) of a greenhouse and you are planting lettuces, you can make a device that absorbs in a range of solar light but avoiding the wavelengths that the lettuce needs to grow[63].

Organic solar cells have the potential to be a key technology in the transition to a low-carbon economy. They use a clean and renewable energy source and can be cheap and easily processable. With their transparency and flexibility they can be used, not only on the top of buildings or solar farms, but also in areas where it was previously impossible such as windows, greenhouses, or irregular surfaces among others.

Of course, there are a lot of variables to have into account. The angle of incidence of the sunlight, the resistance of the materials, the joule effect, etc. This work is focused on how the microstructure of the bulk heterojunction affects the photovoltaic properties.

3.2.1) Evolution of donors

As was mentioned in the introduction of the thesis, the traditional conjugated polymers are homopolymers composed by only one repeating unit. In the 70s polyacetylene was discovered.

Afterward, in the 80s, thanks to the incorporation of ring structures in the backbone, 2D structures, more stable and better soluble polymers than the precursors polyacetylene-based could be made. This is the case of a few specific structural polymer families such as polyfluorenes, polyphenylenes or polythiophenes like well-studied P3HT (poly(3-hexylthiophene-2,5-diyl))[646566]. These new materials allowed for better control over the polymer's electronic properties, resulting in high efficiencies in organic solar cells.

In the next decade, the donor-acceptor or push-pull polymers were developed. As it was briefly explained in the introduction, this type of polymers is composed by two different structures alternated so it is possible to say that the monomer is made by two components blended. One compound is electron-rich trying to catch an electron. They usually have a high concentration of electron-donating groups such as nitrogen or sulfur to increase their mobility and electron density. The other compound is the opposite, electron-poor that decreases the electron mobility thanks to electron-withdrawing groups like carbonyl[67]. These new polymers emerged as the most promising materials in the field of OLEDs and OPVs since the 90s to nowadays.

The most used polymer for solar cells actually is the PBDB-T. The poly[(2,6-(4,8-bis(5-(2-ethylhexyl)thiophen-2-yl)benzo[1,2-b:4,5-b']dithiophene))-alt-(5,5-(1',3'-di-2-thienyl-5',7'-bis(2-ethylhexyl)benzo[1',2'-c:4',5'-c']dithiophene-4,8-dione))] was first reported in 2012 by Qian *et al* and an era in the polymer solar cells started thanks to it and it derivates[68]. PBDBT has a lot of names but the most known one is PCE12. This

material has a high power conversion efficiency (PCE) due to its broad absorption spectrum, high charge carrier mobility, and good morphological stability. The derivates consist on add atoms to the principal structure to improve its properties as the PBDBT-Cl, PBDBT-2F, etc.

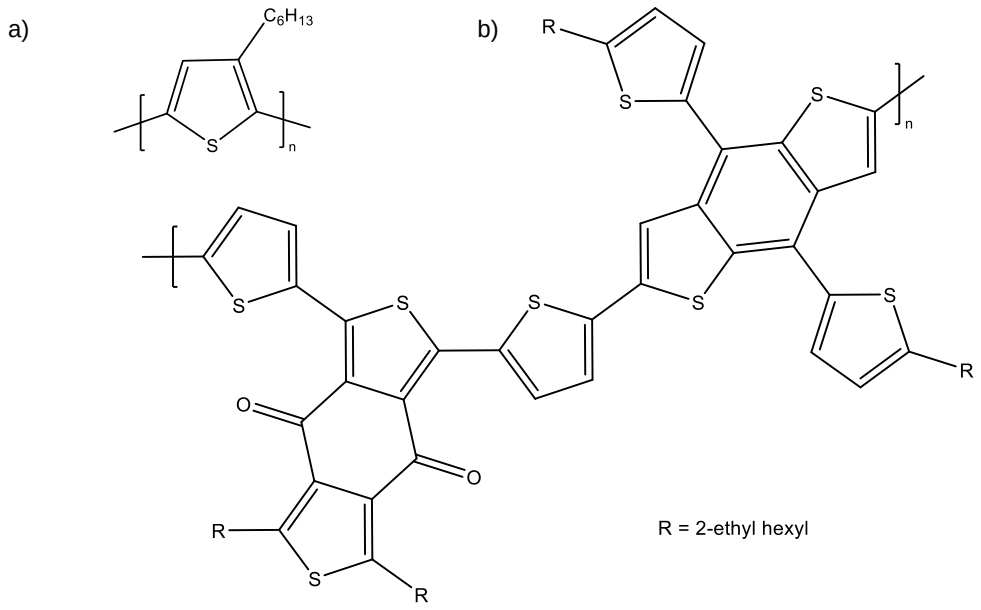

Figure 18 a) P3HT molecular structure and b) PBDBT.

Actually, the ongoing research has focused on developing new conjugated polymers with higher processability, stability and solubility to be a promising rival in the solar energy career.

In summary, while homopolymers are composed of identical repeating units, push-pull polymers have a more complex chemical structure with both electron-donating and electron-withdrawing groups. This structure leads to improved charge transfer and broader absorption spectra, resulting in higher efficiency and performance of organic solar cells.

3.2.2) Evolution of acceptors

The first acceptors developed for OPVs consist on phthalocyanines and perylenes. Created in the 70s, these organic dyes conferred low efficiencies due to their limited absorption and electron mobility. During the 90s the perylene diimide (PDI) was synthesized as a better acceptor[69] and, during the 2000s, PDI derivates obtained better and strong absorption in the sunlight range and upgraded the hole mobility.

It was not until 2002 that fullerene derivatives were developed. These structures composed by carbons offer excellent compatibility with conjugated polymers resulting in a good power conversion with a relatively good efficiency. The inconveniences are the relatively low hole mobility compared with the conjugated polymers, the aggregation, low solubility and the limited range of absorption[70]. The most important fullerene acceptors are [6,6]-phenyl-C61-butyric acid methyl ester (PCBM), [6,6]-phenyl-C71-butyric acid methyl ester (PCBM70) or [6,6]-phenyl-C61-butyric acid butyl ester (PCBB) between others.

In 2009 the non-fullerene acceptors (NFAs) began to be explored owing to the limited sunlight absorption range. These acceptors consist on small molecules synthesized and designed with precise control over their properties[71]. The pioneering were the quinolines and diimide derivates (more complex). In 2012 the development of fused-ring electron acceptors (FREAs) incorporating more electron-deficient aromatic rings in the core like fused thiophene or benzothiadiazole marked a breakthrough. The most important problem is the aggregation, but, changing their chemistry or structure, it is possible to tune the absorption range and the energy levels maintaining the high mobility and stability[72].

3 years later, in 2015, Zhang et al synthesized the milestone of the NFA. The indacenodithieno[3,2-b]thiophene or ITIC[73]. The core structure of ITIC is formed by fusing two thiophene rings to an indacene core conferring a planar and rigid structure. It is a push-pull acceptor with a donor part between two acceptor parts. Also, the electron mobility and the charge separation increase thanks to the sulfur atom of the thiophene and the fused ring. A wide range of derivatives is obtained by changing the side chains

or substituents that are attached to the core structure. Some derivates were developed by the introduction of an electron-rich group like methyl into the end-capping units (ITIC-M)[74], by the incorporation of electron-deficient atoms such as fluorine (ITIC-2F)[75] or chlorine (ITIC-2Cl)[76] or by the substitution of the phenyl units by thienyl groups (ITIC-Th)[77]. Another promising type of small molecules in this field were the acceptor-acceptor (A-A) type polymers like poly[N,N′-bis(2-octyldodecyl)-naphthalene-1,4,5,8-bis(dicarboximide)-2,6-diyl]-alt-5,5′-(2,2′-bithiophene) (P(NDI2OD-T2)[787980] and its derivates.

In the last years of the 2010s, Y6 or ITIC-4F (a derivate of the ITIC) increase the PCE up to 13% (combined with a donor polymer) consolidating the NFA as a viable alternative against the fullerene acceptors[8182]. O-IDTBR or IDIC were developed also.

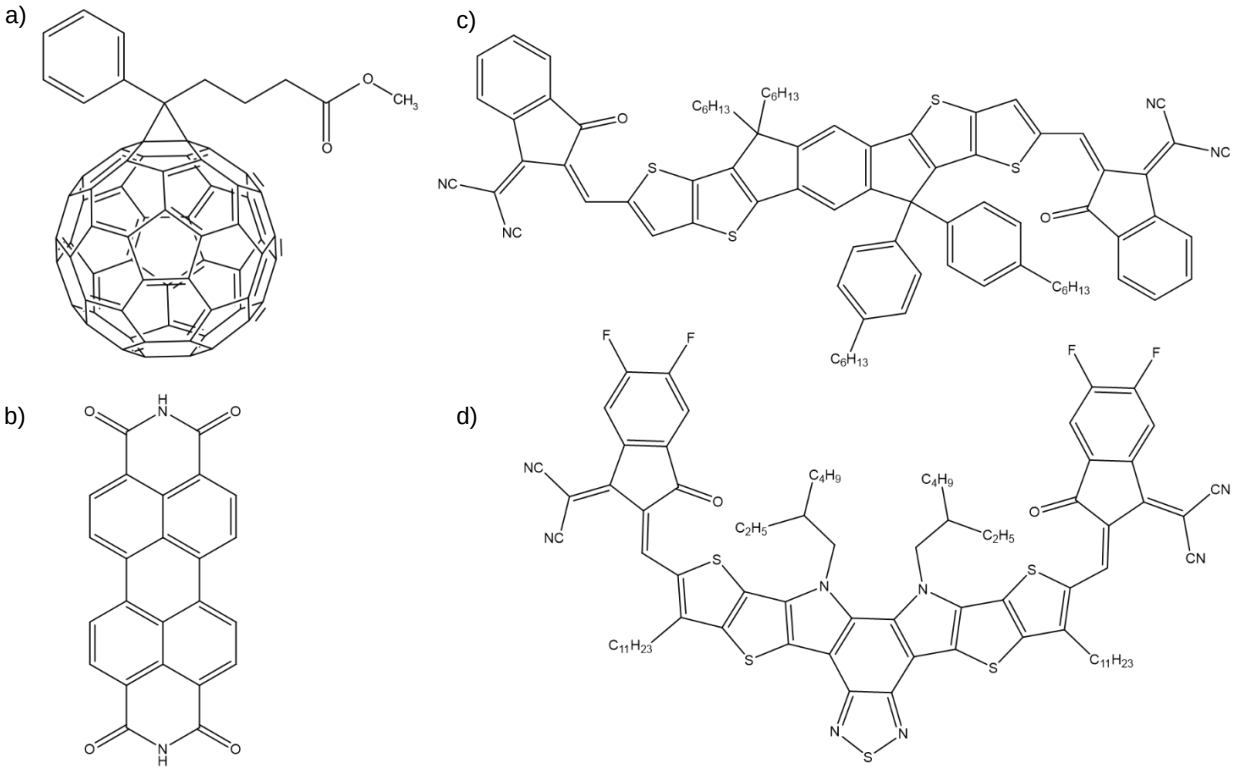

Figure 19 Chemical structures of the most important small molecules: a) PCBM, b) PDI, c) ITIC and d) Y6.

Nowadays, in this decade, the tendency is to continue with the ITIC derivates developing new small molecules more symmetric as N3 (derivate of the Y6) for example.

3.2.3) BHJ

The p-n junction opened the field to improve semiconductor materials to generate electricity from the sunlight. In 1986, Tang developed the first p-n organic junction based on two separated layers of copper phthalocyanine and a perylene tetracarboxylic derivative[83]. This first device consisted on a planar heterojunction (PHJ), one layer growth against the other creating an intermix between both. The problem was that the interface was very low so the charge separation was negligible.

The concept of bulk heterojunction (BHJ) was introduced in 1992 by Mark Thompson's team[84]. In this case, both materials were mixed and used as a single active layer. This architecture allows the charge separation and increases the PCE due to the higher intermix surface. On the one hand, the term "bulk" refers to the fact that some materials are mixed very well and distributed at the nanoscale instead of separated domains. On the other hand, heterojunction is used to allude the interface between the donor and the acceptor[81].

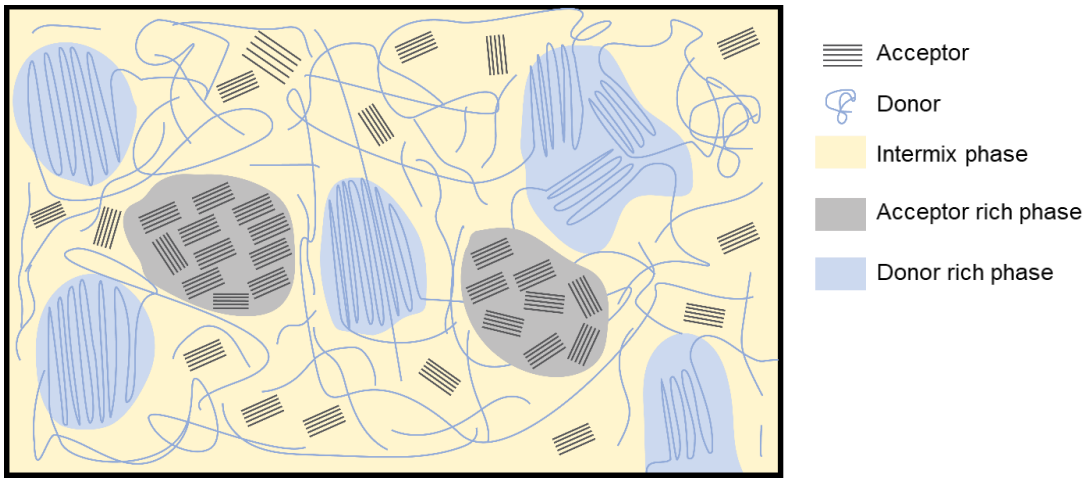

Figure 20 Scheme of a cross-section of a BHJ.

At the beginning of the millennium, polymer solar cells had only 1% of PCE. Overcome that 1% opens the door for BHJ structures to work in practical solar cells applications. In 2006 the PCE surpasses the 5%, bringing the technology closer to commercial viability. In 2009 it exceeds the 7% and finally, in 2012, the barrier of the

10% of power conversion efficiency was reached[85]. This level of efficiency made polymer solar cells more competitive with other thin-film solar cell technologies.

Since its inception, research and development in the field of BHJ solar cells have been dedicated to continuously improving their efficiency, stability, and scalability. While significant progress has been made, several challenges have emerged, including device stability, material optimization, and large-scale manufacturing.

One key focus area has been enhancing the stability of BHJ solar cells over extended periods. Researchers have explored innovative approaches such as encapsulation techniques and the incorporation of stable electrode materials to mitigate degradation and ensure long-term performance and durability. Material optimization has also been a major area of emphasis. Scientists have worked on developing organic semiconducting materials with enhanced light absorption characteristics, improved charge transport properties, and increased stability in BHJ devices[86].

Furthermore, the scalability of BHJ solar cells has been a crucial factor for their commercial viability. Researchers have aimed to develop cost-effective manufacturing processes that can be scaled up for large-scale production. Techniques such as roll-to-roll printing, blade coating, spin coating and spray coating have been explored to enable high-throughput and low-cost fabrication of BHJ solar cells.

Despite the challenges encountered, the bulk heterojunction architecture continues to hold immense promise for the development of efficient and cost-effective organic solar cells. Ongoing research collaborations between academia and industry are driving further advancements, positioning BHJ solar cells as a competitive solution for renewable energy generation.

Nowadays, NFA continues evolving and leading to higher PCEs. Also, ternary blend systems are emerging as the next step in solar cells. These advancements have led to the commercialization of polymer solar cells, with products now available on the market[8788].

The most studied systems of BHJ were the P3HT:PCBM[81] and the PBDBT:ITIC[89] blends, both studied in our group. The first blend is composed by a classic homopolymer very well studied (P3HT) and the most acquaintance fullerene acceptor (PCBM). This solar cell had an efficiency of 3.5 % approx. and was the first viable, well-studied system[90]. The problem of this BHJ (in addition to its low PCE) is the aggregation of the acceptor part.

The other system is composed by more new materials. One push-pull polymer commonly used in OSC (PBDBT) and the milestone of the non-fullerene acceptors (ITIC). Using this BHJ as model, a lot of OSCs were developed.

Quickly explained the mechanism, the electricity current is produced thanks to the dissociation of an exciton. When the light is more energetic than the bandgap of the material electrons can climb from the HOMO to an energy state close to the LUMO generating a pair electron-hole closely bound by Coulombic attraction. This pair of charges is named exciton. They can move through the material but their lifetime is very short, they can be displaced only a few nanometers until the recombination of the charges[91]. The goal of the solar cells is to separate the charges of the exciton and move them to the electrodes to extract electricity. This separation occurs in the frontier where there is a material that wants electrons (acceptor) and a material that wants to give electrons (donor). This interface acts as a p-n junction and is maximized in the intermix face[92]. Then, the electron or/and positive hole travel through the pure domains to the electrodes creating an electronic current[93].

Pure domains are necessary to create the excitons and move the charges to the electrodes. There has to be a balance between pure domains and the mixed phase. The degree of mixed phase within a material has a direct impact on the potential for charge separation. While a higher degree of mixed phase allows for increased charge separation, it is also essential to create pure domains within the material. These pure domains are responsible for generating excitons, and they need to be effectively connected to the electrodes (percolation pathways) in order to facilitate efficient charge collection[94]. They are strongly affected by the bandgap, absorption range spectra, energy level, morphology, size, order, miscibility with the other pure domain, etc. Having all of this in account, the most important parameter in a solar cell is the power conversion

efficiency which is the relationship between the output power and the incident light power.

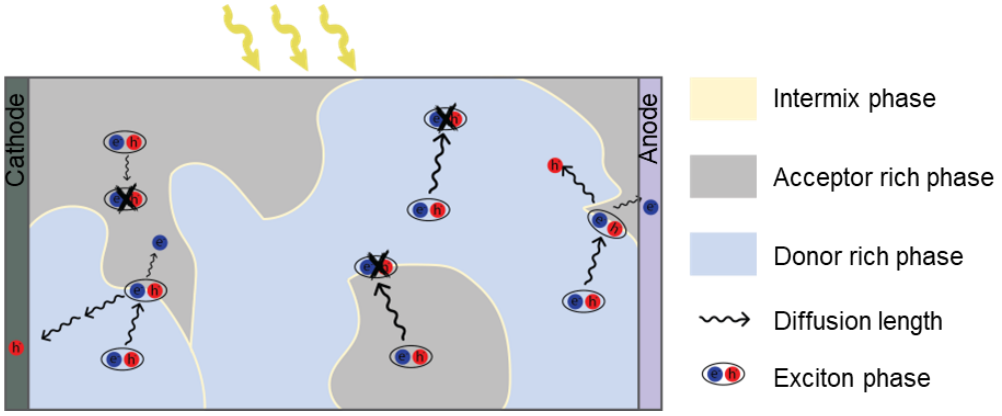

Figure 21 Schematic electron hole excitation in a BHJ.

The working principle of a polymer BHJ can be summarized in four steps (Figure 22):

- Absorption of Light: the absorbed photons transfer their energy to the material, creating excitons.
- Exciton Dissociation: in the intermix phase the exciton is separated in an electron and a hole.
- Charge Separation: the electron migrates to the acceptor material, which has a lower electron affinity, while the hole remains in the donor polymer. This charge separation creates an electric field across the active layer.
- Charge Collection: The separated charges are collected by the respective electrodes in the solar cell. These charge carriers can then be utilized to power external devices or stored in a battery.

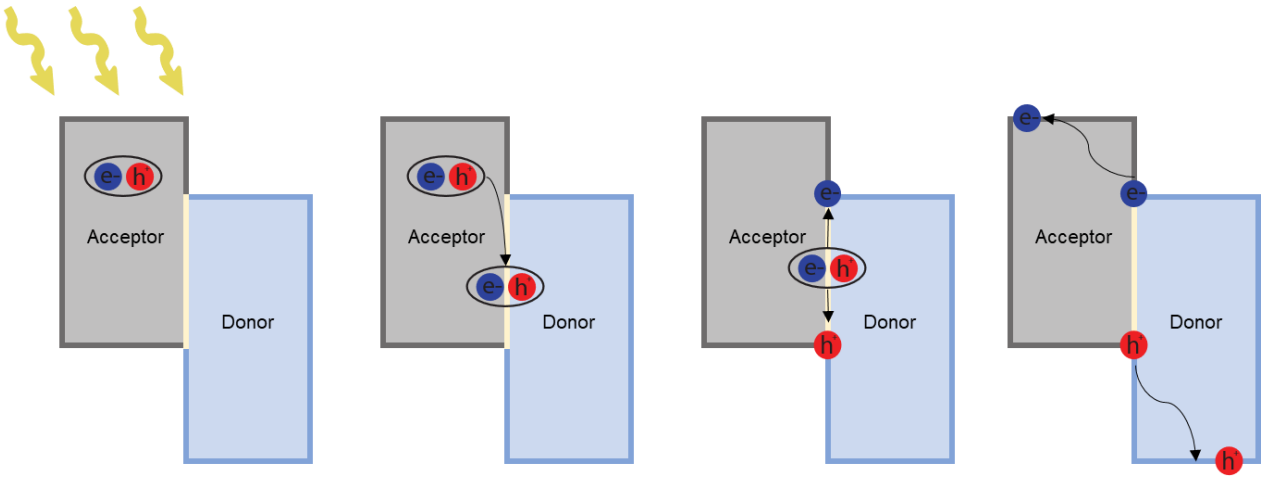

Figure 22 Charge generation croquis.

The key advantage of the polymer BHJ structure is the large interfacial area between the donor and acceptor materials, which promotes efficient exciton dissociation and charge separation. Additionally, the blend morphology at the nanoscale level allows for improved charge transport and reduced recombination losses, leading to enhanced power conversion efficiency in organic solar cells.

The objective of this part of the work is to study the concentration of a BHJ changing the concentration of the materials in the solution and see what happens in the intermix phase using an analysis of the vitreous phase. This system was selected due to the potential to be a commercial solar cell with efficiencies higher than 12 %.

3.3) Results and discussion

In this chapter the system used was: On one hand, the polymer used is a derivate chlorinated of the ITIC, the poly[2,2''''-bis[[(2-butyloctyl)oxy]carbonyl][2,2':5',2'':5'',2'''-quaterthiophene] -5,5'''-diyl] or PDCBT-Cl. It is composed by two thiophenes, one with a Cl and two thiophene derivates. On the other hand, the acceptor is a derivate of the ITIC, the difference is one flour at the beginning and the other one at the end of the molecule. The name is ITIC-Th1 or 3,9-Bis(2-methylene-(3-(1,1-dicyanomethylene)-6/7-fluoro)-indanone))-5,5,11,11-tetrakis(5-hexylthienyl)-dithieno[2,3-d:2',3'-d']-s-indaceno[1,2-b:5,6-b']dithiophene.

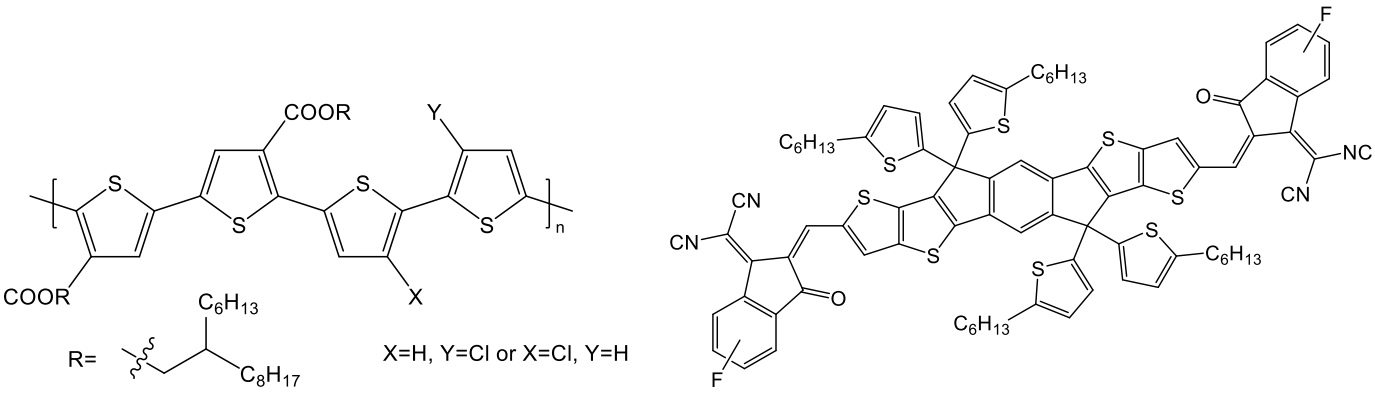

Figure 23 PDCTBT-Cl and ITIC-Th1 molecular structures respectively.

More than 12 % of power conversion efficiency had been obtained with a mechanical mixture of 50/50 % in weight of both materials in chloroform (18 mg/ml). A solvent annealing treatment in CS_2 were induce in the sample to obtain the best OPV values. *Liang et al.* selected these materials due to their good electronic properties, easy synthetization and the option to do large scale to commercialize it.

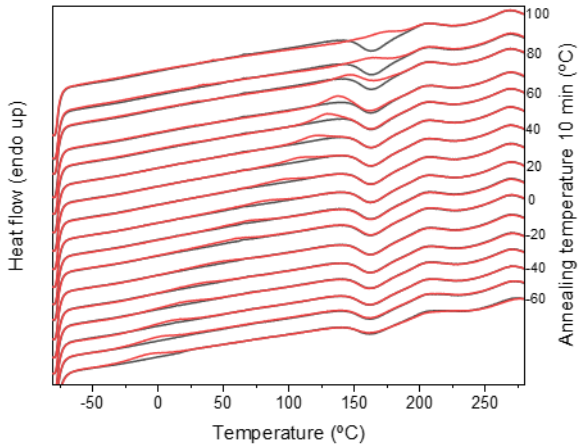

Figure 24 Isochronous annealings of 75:25 mechanical mix phase of PDCTBT-Cl and ITIC-Th1 respectively.

To understand properly this system it is necessary to study the neat materials and some different compositions of the mix phase neat materials and composition of 25-75 %, 50-50 % and 75-25 % were developed in addition to the most valuable solar cell of his system. Flash DSC has been used to determine the glass transition of all the compositions. With the T_g of the neat materials and some T_g of intermix compositions it

is possible to extrapolate a calibration curve to know the T_g of one unknown intermix composition but knowing its T_g.

By the isochronous annealing method, it was impossible to determine the T_g of the intermix phase due to the overlap of the cold crystallization on the heating ramp of the small molecule and the ageing overshoot of enthalpy recovery of the PDCBT-Cl. This issue can be clearly seen in the Figure 24. It can be observed also how in this 75:25 chip of polymer and small molecule respectively at the annealing of 70 or 80 Celsius for example, the crystallization and the peak due to the physical ageing are superposed.

For this reason, the modulated method has been used. With the temperature modulated DSC, the non-reversible processes, such as cold crystallization, are ridded. All the systems were studied by this method to maintain the same criteria with all the samples.

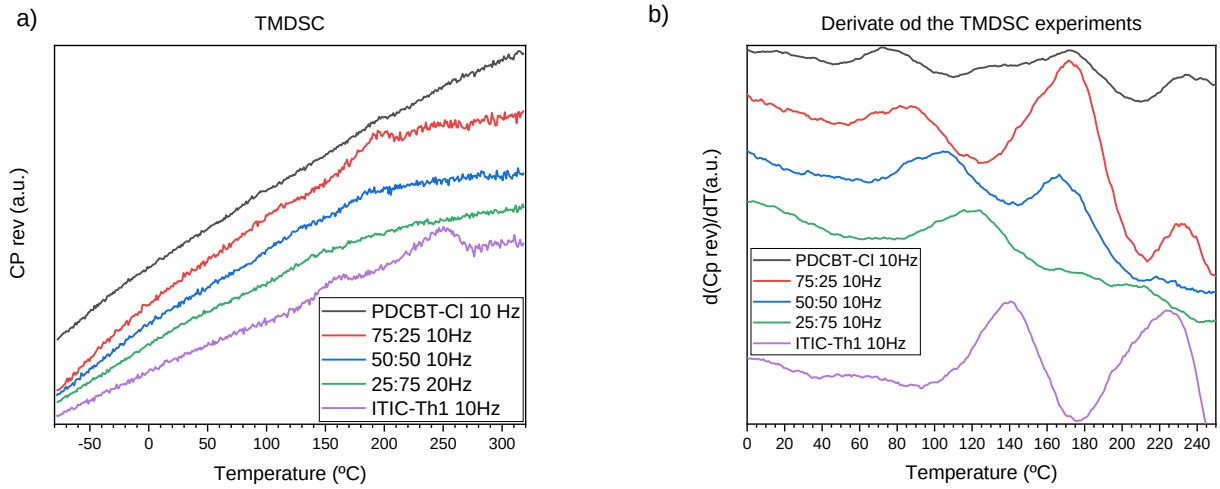

Figure 25 Temperature modulated DSC of all the systems (a) and their derivates (b).

To estimate the T_g of the intermix phase in all the measurements, 10 Hz were used in the experiments.

After the Fourier-transform of the data, it is more visible that the cold crystallization is deleted and can be clearly the glass transition and the melting of the neat materials. To have a common criterium with all the results, the 1st derivate was develop. The maximum of the peak of the derivate in the region corresponds with the T_g. To not make mistakes, the peak was fitted to a Gaussian function and extracted the maximum.

Intuitively, in the panel b of the Figure 25, a clear observation emerges: the T_g of the intermix phase is displaced from the T_g of the polymer to the T_g of the small molecule when the weight percentage of the last one is increased. It is appreciated also the melting of the two neat materials, making sure that the measurements are well done. In the next figure, it can be observed a table with the extracted T_gs from de modulated experiments and their fitting to a Gordon-Taylor equation to have a calibration curve of the system PDCBT-Cl:ITIC-Th1.

% wt PDCBT-Cl:ITIC-Th1	T_g (°C)
1:0 (PDCBT-Cl)	73
75:25	87
50:50	105
25:75	122
0:1 (ITIC-Th1)	140

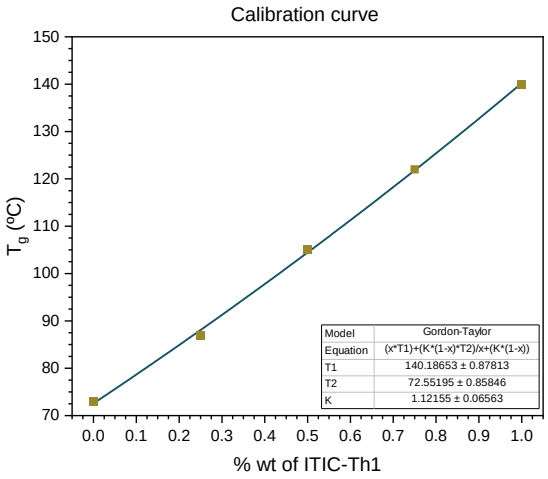

Figure 26 T_gs of the different intermix phases and Gordon-Taylor fit calibration.

Figure 9b shows that the experimental data can be adequately fitted to the Gordon-Taylor equation. Once the calibration curve is done, the solar cell with the best electronic properties can be studied. To study the solar cell a thin film of 50:50 % in weight was deposited in a silicon wafer with the conditions of *Liang et al.* Immediately, a solvent annealing in CS_2 at room temperature 2 minutes. The T_g of this system only can be measured in the first heating because the SA confers to the solar cell better properties.

If we use the second heating to extract the T_g the thermal history of the system was deleted so we are not seeing the real T_g. For that, the thin film was deposited in a silicon wafer. Having this, we are able to scratch this film and take a small part to measure. We can take many samples from the same film to measure many first heatings of the same sample.

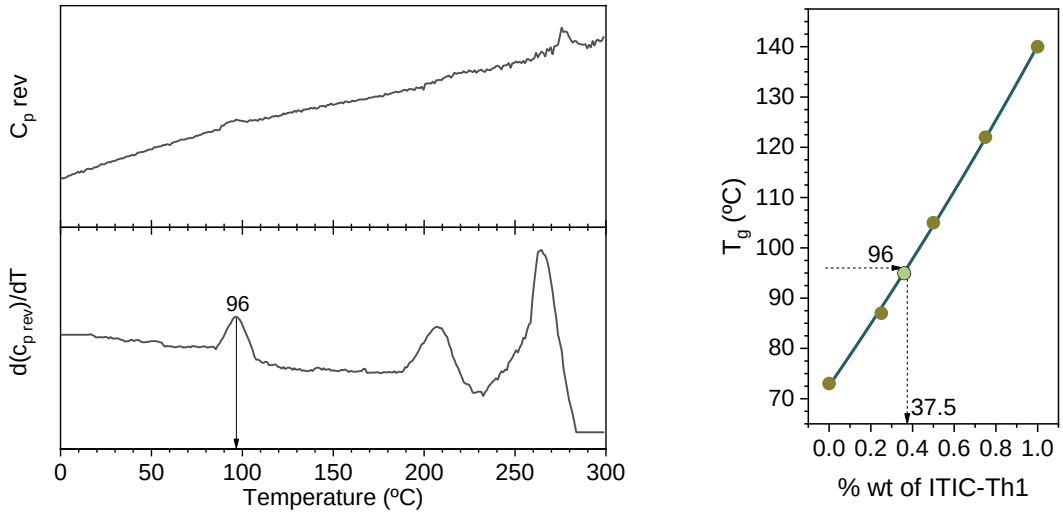

Figure 27 T_g of the solar cell improved by Liang et al. and the extracted composition of it.

This result show how, with the solvent annealing, the percentage in weight of the small molecule in the intermixed domains decreases considerably to 37.5 %. This can be rationalized in terms of migration of the ITIC-Th1 from the intermixed phase to a compositionally pure phases, for example into the crystalline domains.

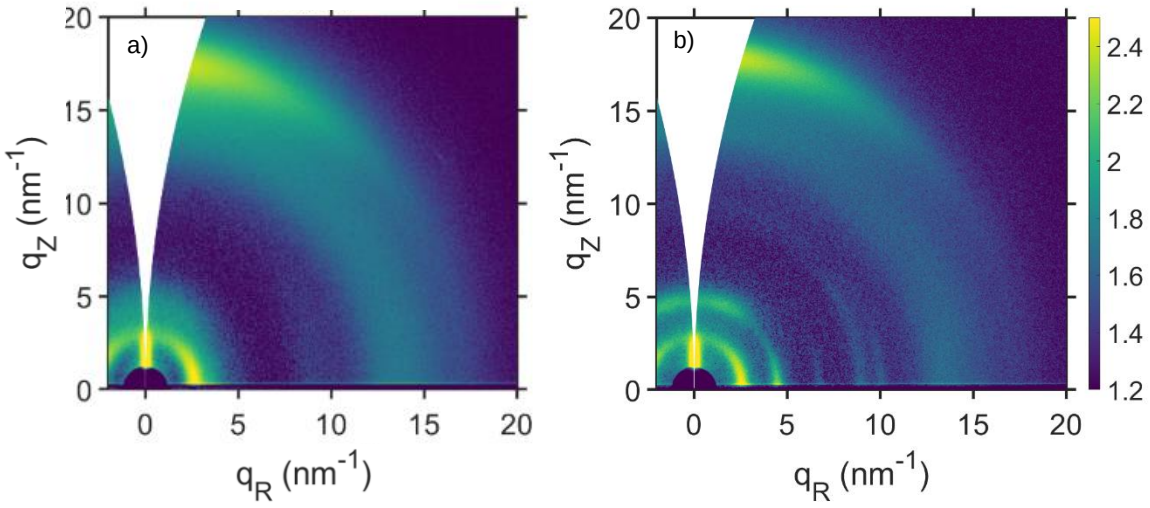

Figure 28 GIWAXS patterns of 50:50 %wt of PDCBT-Cl:ITIC-Th1 without (a) and with (b) solvent annealing of 2 minutes.

Indeed, in the Figure 28 it can be observed how the solvent annealing improve the crystallization of the small molecule conferring to the system more PDCBT-Cl in the intermix phase. This is congruent with the results of the flash DSC because the T_g is lower than in the case 50:50 without solvent annealing.

To see the morphology the AFM technique was used. An image of the best system was analyzed to see the domains. In the phase image of the AFM it is clear that there are separated domains and between them a visible boundary were the intermix phase is located. The domain size is approximately 85 nm of diameter and it was measure by image J software.

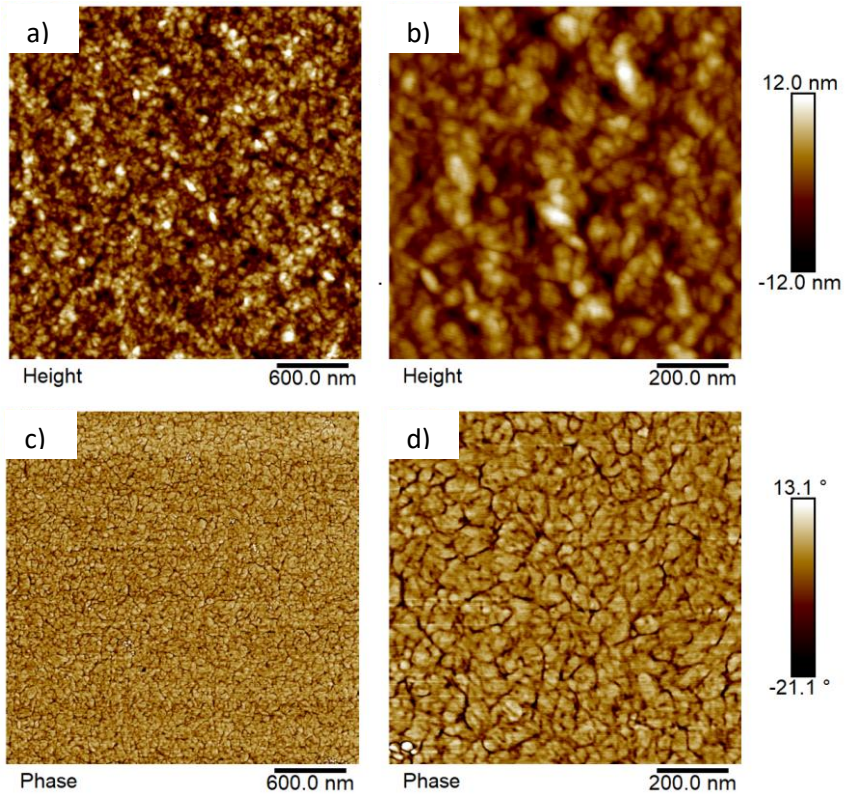

Figure 29 Height and phase AFM images of 50:50 with solvent annealing thin film.

To support the AFM images a small GISAXS study was carried on. The mixtures have more scattering than the neat materials due to the higher electronic contrast in the film. When the film does not have solvent annealing, the domains have a plane disc shape with 30 nm of radius approximately. Then, after the SA, the domains increase their size to 45 nm of radius and the discs swell until they acquire the shape of a fractal sphere.

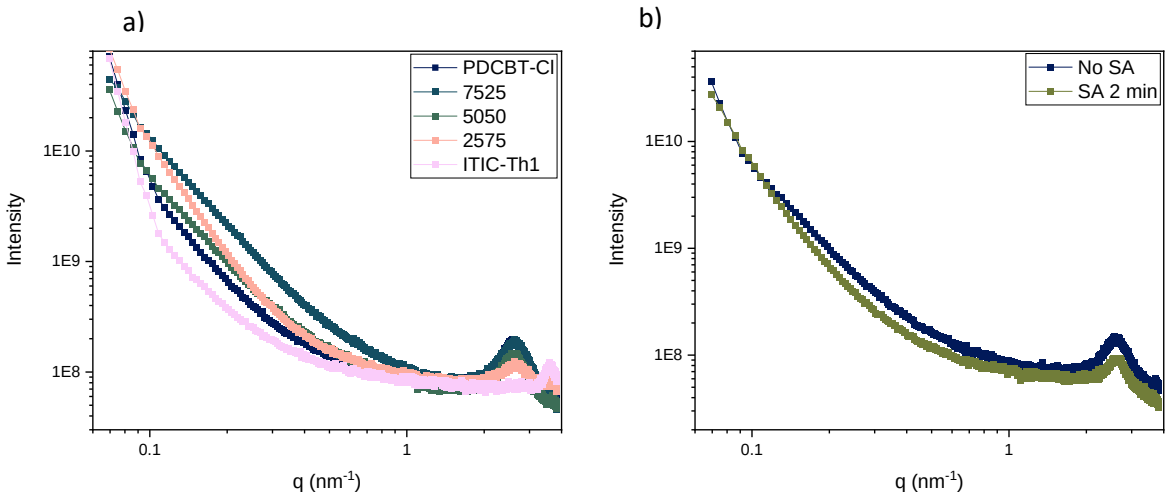

Figure 30 GISAXS integrations of the Yoneda peak of a) different systems and b) the thin film 50:50 with and without solvent annealing.

Knowing the structure, it is important to check the optical properties. For this, the UV-Vis absorption of the system was analyzed. In the next figure, it is shown how with the 50:50 mechanical mixture is obtained the highest range of absorption of the light in all the range between the neat materials. In addition, with the solvent annealing, it is demonstrated that the absorption range is increasing a little bit increasing also the total area of the light absorption but decreasing the maximum of absorption.

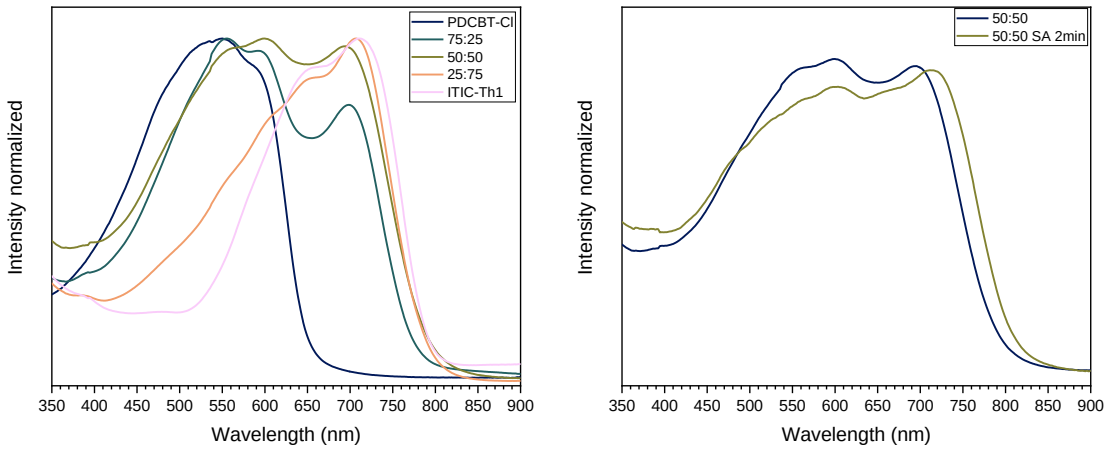

Figure 31 UV-Vis spectra of all the system.

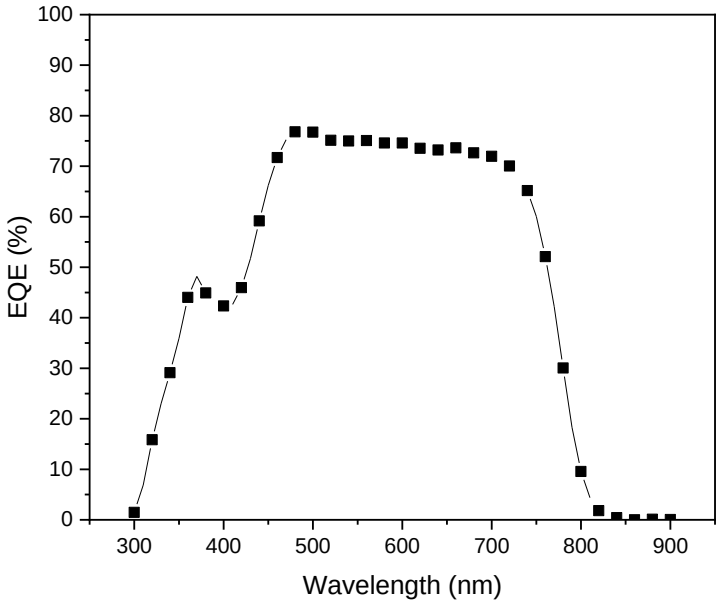

Figure 32 External quantum efficiency of the reference solar cell.

Finally, in the Figure 32 we can observe that it has the same shape of the absorption spectra. This indicates that the electronic current generated is along all the absorption of the photons corroborating the good solar cell properties.

3.4) Conclusions

In summary, the utilization of the TMDSC (Thermal Modulated Differential Scanning Calorimetry) has enabled precise reproduction and compositional analysis of solar cells. By faithfully replicating the solar cell using a flash DSC chip, we can investigate the morphology of the real active layer through calorimetry.

An intriguing finding is that the Intermix phase of the solar cell, when combined with the SA (Solvent Annealing) process, deviates from the 50:50 composition expected from the precursor solution. Instead, it comprises 37.5% of the weight of ITIC-Th1, attributed to its favorable crystallization behavior during solvent annealing.

Additionally, the examination of the vitreous phase allows for a detailed analysis of the solar cell's composition. This comprehensive approach sheds light on the intricate aspects of solar cell structure and behavior, providing valuable insights for further advancements in solar technology.

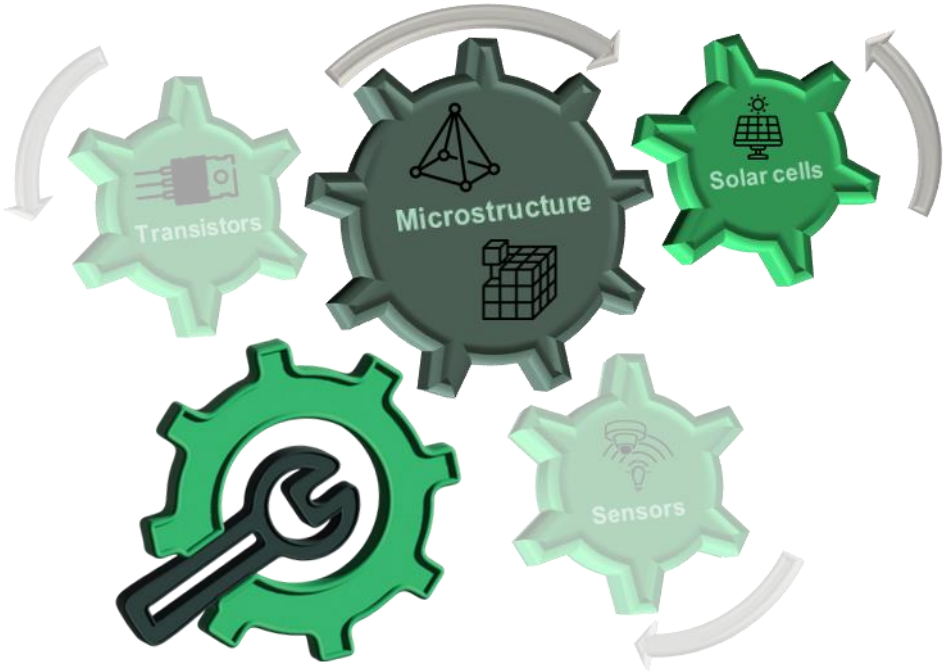

4

"El descubrimiento consiste en ver lo que todos han visto y en pensar lo que nadie más ha pensado."

Albert Szent-Györgyi

4) Solid-state microstructure of high charge mobility IDTBT polymer

4.1) Summary

OFET is the emerging technology to dethrone the silicon-based transistors. Historically, the organic electronics community has accepted that the higher the structural order (i.e. crystallinity) of the organic semiconductor, the higher the charge carrier mobility. In the second half of the last decade IDTBT polymer was developed questioning the statement above. IDTBT exhibited one of the highest charge-carrier mobility among polymers, yet lacking of crystallinity. As a matter of fact, it has been typically referred to as amorphous. This study unravels the actual solid-state microstructure of IDTBT.

.

4.2) Introduction

Computers or smartphones have a microprocessor whose main building blocks are transistors. Transistors are, basically, essential electronic devices that regulate the electricity movement.

With this idea in 1947 John Bardeen, Walter Brattain, and William Shockley at Bell Laboratories invented the point-contact transistor, which was the first working transistor. In 1951 the first commercial transistors become available. In 1959 appears a transistor made with the material on which this industry is based, the silicon[95].

A lot of types of transistors were developed during the years. Metal oxide transistors (MOS), junction field-effect transistor (JFET), bipolar junction transistor (BJT), field-effect transistor (FET), etc. Semiconductor polymers were introduced in this discipline via the FETs[96–98].

At the end of the 80s, the first organic FET (OFET) was developed using a cooper thiophene derivate. This breakthrough opens the possibility to use semiconductor polymers in transistors. More specifically, substituting the classic doped semiconductor materials as channel of the device. With this change, flexible, transparent and lighter transistors are able. A couple of important dates in the recent years for this OFET are 2008, when were developed the first organic complementary logic circuit which use both p-type and n-type organic transistors and 2018 when, at Stanford University, the first biodegradable organic transistor was created, paving the way for environmentally friendly electronic devices[99100].

4.2.1) Transistor operation

More in detail, a transistor is a fundamental electronic device that controls the flow of current or voltage in a circuit. It acts as a switch or an amplifier, and its operation is based on the properties of the semiconductors.

They are typically composed of three parts, known as the emitter, base, and collector, which form two p-n junctions. Changing the voltage applied on the base (or gate) the flow of current between the emitter and collector (source and drain)[101]. One of the most visual examples to understand a transistor is a water tap or an irrigation dam imagine that water is the flux of electrons. The base or gate is the dam or the water tap in the examples, the source is the input water and the drain is the output.

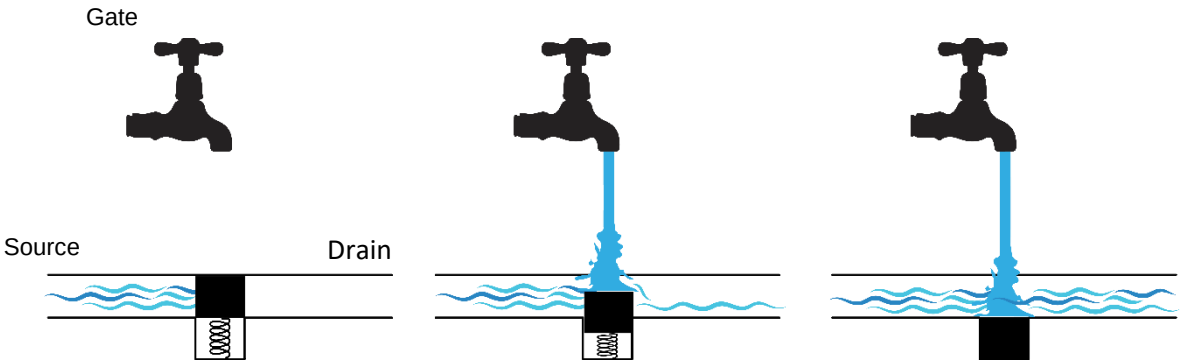

Figure 33 Simile of a transistor with a water tap.

If the dock in the Figure 1 is very lax, it works as a switcher because with a minimum of water from the gate all the source current can go. One example of this use is a phototransistor. This transistor allows the current to pass only if it receives a certain light. Another one is how electronic devices work, the binary code. Is based on 0 or 1 which translates to the transistor is if it allows or forbids the electricity flux.

If the dock is robust, the transistor acts as an amplifier. Depending on the current of the gate there is a different flux between the source and the drain. One very easy example is the use to amplify the sound. If you connect the phone to a speaker, the transistor takes a small voltage from the phone (the music codify) and multiplicate the voltage of the signal to obtain a loud volume.

There are two main types of transistors where conjugated polymers are used: bipolar junction transistors (BJTs) and field-effect transistors (FETs). BJTs are commonly used for analog amplification, while FETs are often used in digital circuits. The BJTs use the flow of minority carriers (electrons or holes depending on the material) to control the current, while FETs use electric fields to regulate the conductivity of a channel.

In summary, transistors have played a pivotal role in the advancement of technology, enabling the development of smaller, faster, and more efficient electronic devices controlling and amplifying electrical signals[102]. Transistors are crucial components in modern electronic devices and systems.

4.2.2) FET structure

FET or Field Effect Transistor is composed principally of three different parts. The electrodes that are the electrical contacts or electrodes where the current flows, the active layer and an insulating layer made of a dielectric material.

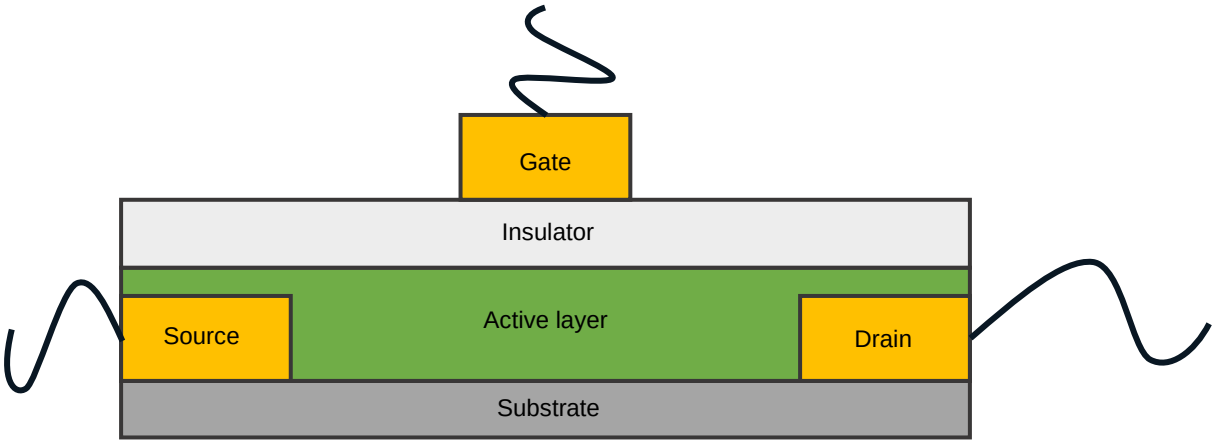

Figure 34 Cross section scheme of a FET.

In this type of transistors, the gate is separated from the active layer by an insulator. The electricity that passes through the gate generates an electric field in the insulator layer. This electric field tunes the behavior of the organic semiconductor in the active layer. By varying the gate voltage, the conductivity of the organic material can be modulated, allowing control over the flow of current between the source and drain[103100].

This type of transistors has several advantages over other types. They have high input impedances so they require very little current in the gate to tune the active layer making them perfect for sensors or amplifiers. This is translated also in a low power consumption with low noise and high switching speeds. Other advantage in the temperature stability due to the encapsulation of the active layer with an insulator[104].

Depending on the semiconductor material of the active layer, the FET transistor has a lot of names. MOSFET if it is a metal oxide semiconductor, JFET if it is an n-p junction, CNTFET if carbon nanotubes are the active layer, etc. In this case, a polymer acts as the semiconductor so the name is OFET (Organic Field Effect Transistor).

4.2.2.1) OFET

OFETs offer several advantages over traditional transistors. The active layer of these transistors (organic materials) can be processed at low temperatures and with low-cost manufacturing (like solution-based techniques) and large area production. Due to their elastic properties, they can be deposited on flexible and light materials[105].

The insulator layer presents some problems. When a current travels along the active layer, it is heated due to joule effect. The insulator layer has to be an electrical insulator but, normally, it is also a thermal insulator so the transistor tends to overheat. If the material has a thermal transition near the working temperature of the transistor it could affect to it efficiency. In the other hand, as it is encapsulated, the degradation due to the environment is retarded. Also, organic materials typically have lower charge carrier mobility compared to inorganic semiconductors, limiting their speed and performance but not preventing it. For this, is important to improve the materials to enhance the electronic transport values of the non-polymeric materials[106].

4.2.2.1.1) Active Layer

As it was explained before, the active layer has the key role on the transistor operation. The properties and performance of the active layer determine the OFET's overall characteristics, such as its switching speed, current-carrying capability, and stability so it is important to study the material behavior[107][108].

One of the most promising materials to set aside the classic semiconductor materials is de IDTBT[109]. Recently, some semiconducting polymers have challenged the

paradigm (much order, better properties) exhibiting high mobility while lacking of crystalline-like long range order[109–116]. IDTBT is a push pull polymer composed by indacenodithiophene and benzothiadiazole. Its backbone has a very low torsion angle conferring it a rigid and planar structure[115117]. These characteristics give to the polymer a low disorder structure but not crystalline. Also, in the free carbon of the thiophene groups, aliphatic chains are located to give solubility to the system.

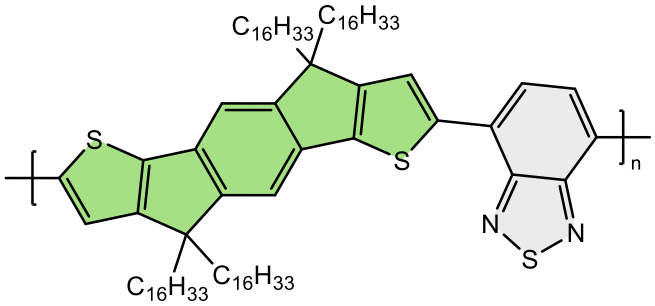

Figure 35 IDTBT chemical structure.

In summary, the FETs have revolutionized modern electronic. Their low power consumption, ease to integration and precise control of the current make them an invaluable tool for new complex integrated circuits. The ability to manufacture the organic active layer on flexible and transparent substrates using low-temperature deposition techniques open the door for new emerging applications.

The objective of this part of the work is to understand the thermal behavior of the IDTBT family to determine why is one of the best organic materials for transistors and is called amorphous.

4.3) Results and discussion

In this chapter the IDTBT and derivates were studied. An exhaustive analysis of the IDTBT (two different molecular weights) was made and a superficial one for the

derivates. After several experiments, the dichlorobenzene was decided as the best solvent to made films.

One of the most important results is that the mobility does not change with the thermal treatments given to the transistors. For the thermal treatment of the transistor, it is important to say that it was made when the active layer (IDTBT in this case) is on the top. Then, after the treatment, the insulator layer and the top gate was grown so the annealing was made with the same conditions of the samples of the other techniques.

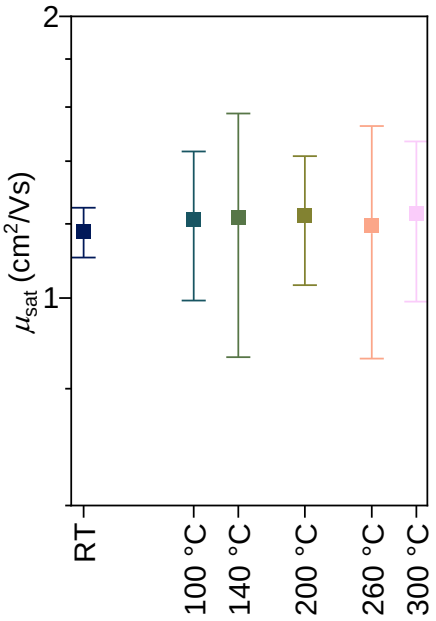

Annealing temperature (ºC)	Mobility saturation (cm2/Vs)	Standard deviation
RT	1.17674528	0.07222518
100	1.21399166	0.21989346
140	1.21949628	0.35537115
200	1.22493352	0.19324101
260	1.19403097	0.33225271
300	1.23069779	0.23940238

Figure 36 Mobility data of the IDTBT transistors.

The charge carrier mobility values are more or less the same in each sample. The small differences might be associated with changes in the ideality of the I-V curves, which do not seem to be microstructure-related. If there are changes in the mobility due to the annealings, the results are shielded by the intrinsic error related to the extraction of parameters from the I-V curves of transistors.

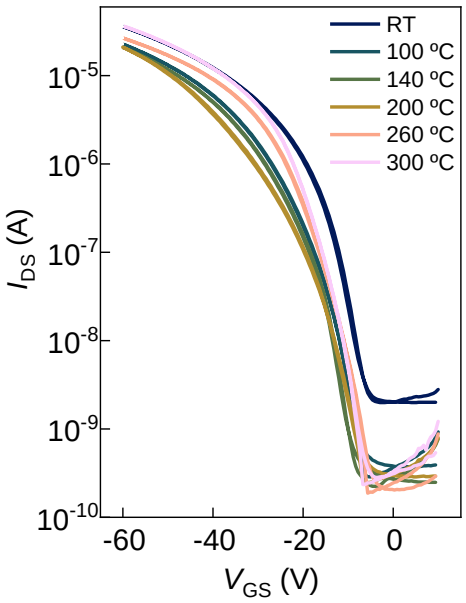

Figure 37 I-V data IDTBT transistors.

In order to understand the electrical behavior, it is important to know if there are changes on the solid-state microstructure.

On the as cast GIWAXS pattern of the IDTBT they are observed essentially three diffraction peaks. One thick in the out of plane (010) at q = 14 nm^{-1} related with the stacking of the π-π bonds or π-π stacking and the refection in the in plane (001) due to the periodicity of the backbone of the polymer. It is curious that the IDTBT does not have the typical out of plane refection (100). This means that it does not have periodic alternation of aliphatic and aromatic regions contrary to what usually happens with conjugated polymers.

The molecular orientation was also measured by NEXAFS showing less energy peaks on the π-π* bonds. This means that the chains are preferably horizontal, although there is a small proportion of chains in a vertical orientation, sustaining the GIWAXS results.

a) b)

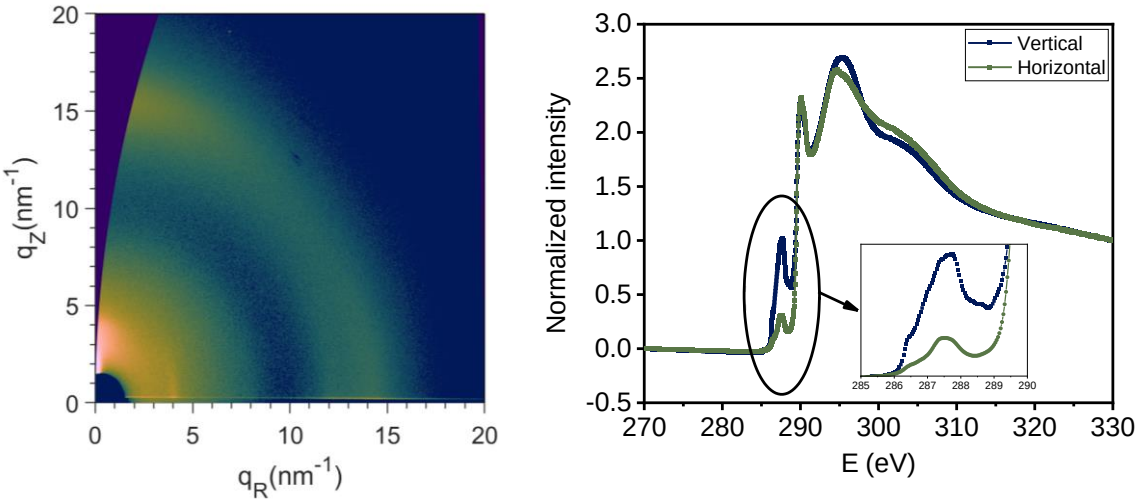

Figure 38 a) GIWAXS pattern and b) NEXAFS of the IDTBT.

To determine the thermotropic behavior, two different temperature-resolved experiments were taking. *In situ* taking GIWAXS patterns every 5 degrees and *ex situ* images (annealings of 10 minutes) every 20 degrees. The data recorded was integrated along the in plane and out of plane directions as a function of the scattering vector (q).

The structural behavior of this polymer at temperatures between room temperature and 300 ºC where it is totally melted. Increasing the temperature, the polymer acquires more energy so it is able to move easily. Thus altering the short-range molecular order and promoting the supramolecular one. In other words, switching to les *q* the π-π stacking reflection and appearing the (100). This changeover can be explained like the transition from crystal to liquid crystal in other conjugated polymers like PBTTT.

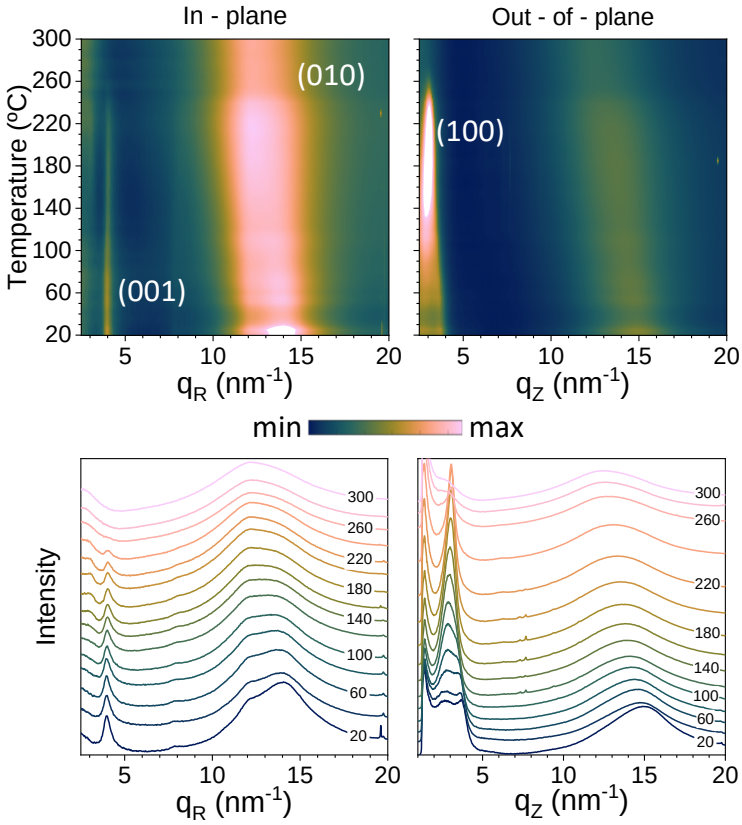

Figure 39 Integrations of IDTBT *in situ* experiment.

Thermotopic materials, in the field of semiconductor materials, are semicrystalline or semiparacrystalline (partially ordered) in the low-temperature region but in this case it happens the opposite. At low temperatures it is disordered but, increasing the temperature, it becomes more ordered until 260 ºC approximately. The most rational thing of why it becomes more order is the formation of crystals but by GIWAXS it is demonstrated that no. There most accurate alternative is the undercooled liquid. In this case, the molecules tends to self-assemble spontaneously into a more-or-less ordered structures. In addition, the order increase during the heating reorganizing and compacting the lattice. Consequently, when semiconducting polymers are heated up (below the order-disorder transition temperature, $T_{O\text{-}D}$) both (100) and (010) diffraction peaks tend to increase and/or become narrower. When this temperature is surpassed, the structural order disappears.

To study this we used the parameter g[118119]. In the Figure 40 is represented the evolution of this parameter in the three representative reflection on the GIWAXS experiments. In the (001) and the π-π stacking reflections, the order increase modestly

from 150 ºC approximately that correspond exactly with the formation of a clear (100). This process means that the chains are more near between them and the periodicity of the backbone becomes more regular. Also, in the same way, the decreasing of the (100) g parameter with the temperature indicates the appearance and arrangement of the lamellar stacking.

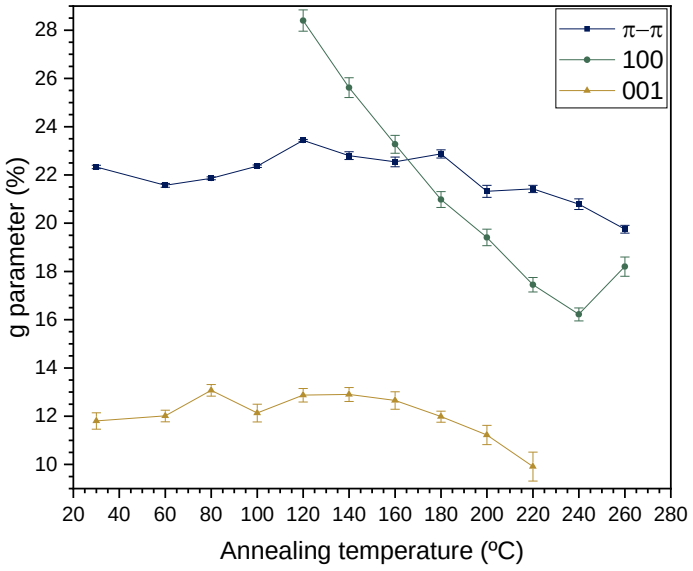

Figure 40 Evolution of the *g* parameter in the *in situ* GIWAXS experiment.

Based on these findings, a more comprehensive investigation into the thermal characteristics of this material is warranted, prompting the application of Flash DSC.

The first experiment was carried out using the isochronous annealing explained in the materials and method chapter. The time isotherm time was 1h each annealing, the maximum temperature 400 Celsius and the minimum -80. All the coolings were at 4000 K/s forcing the material to be freeze in the state of the ageing. In the next chart are represented the heat flow against the temperature for each ageing (the heating ramp just after the ageing and a reference).

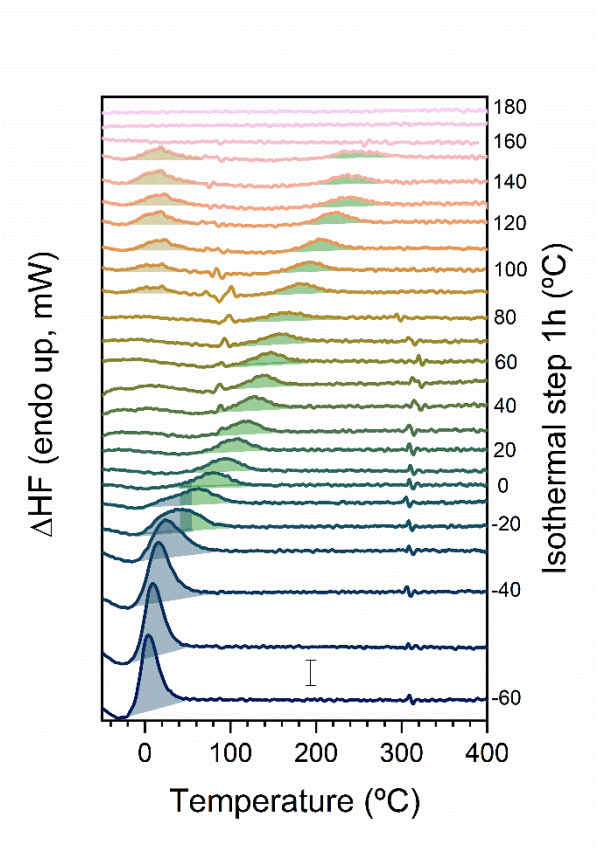

Figure 41 Isochronal annealings of 1h from -60 ºC to 180 ºC.

To clarify the information of the Figure 41, the excess of the heat flow (ΔHF) was represented versus the temperature. ΔHF was calculated subtracting the reference line to the measurement. With this simple operation, any peaks (not near zero values) evidence calorimetric features. In this case, IDTBT reveal 3 different endothermic peaks which means three different thermal transitions[27].

The third process is easy to determine. It is strange because the endothermic peak is located at 10 ºC, very low temperature having in account that the minimum ageing temperature where it appears is 80 ºC. Therefore, this process cannot be associated with something physical that occurs in the ageing like physical ageing or crystallization during the annealing. During the cooling it cannot be also a crystallization because the material does not have enough time to order so the peak (for rejection) is the melting of crystals. In this thermal region, the IDTBT tries to self-assemble into an ordered structure composed by layers of aromatic and aliphatic nanodomains. Then, the aliphatic regions are able to crystallize. The peak of the process 3 is due to the melting of this crystals.

The first process (blue) is due to the physical ageing of a region of the IDTBT. It occurs at -10 Celsius and we think that is associated to the T_g of the lateral chains. We are not able to link this transition with the lateral chains but observing the shape, the position and the behavior we can say that it is a vitreous transition. We can discard the degradation and the melting of crystals due to the low temperatures and the shape of the endothermic peak.

The second process is the most intricated one. It encompasses a very wide range of temperature so is important to explain properly this. It is important also to mark that appears above what we associate as the T_g of the lateral chains. When this T_g is exceeded, the system starts to gain mobility. It could lead in three different reasons: a melting of the ordered domains in the system, structural relaxation of the glassy phase or a transition from liquid crystal to isotropic liquid. The liquid-liquid transitions the endothermic peak is not shifted so much so this theory can be discarded. Also, the appearance of the peak at an annealing at 20 Celsius starts at 60 degrees and, visually, at room temperature the material seems solid. As if this were not enough, at this annealing temperature, the π-π stacking begins to deteriorate in the GIWAXS analysis. It is inferred that this disruption is associated with the disorder of intermolecular aggregates characterized by a limited short-range order. This transition is very broad suggesting a very big heterogeneity due to the large range in which this process appear. It is also agreed with the (100) GIWAXS peak. It is visible until room temperature (when the process 2 in Flash DSC starts to contribute) but starts to acquire importance at 140 Celsius approximately and disappear at the same temperature in both techniques (temperature order-disorder or $T_{O\text{-}D}$ = 260 ºC) when the domains become disordered.

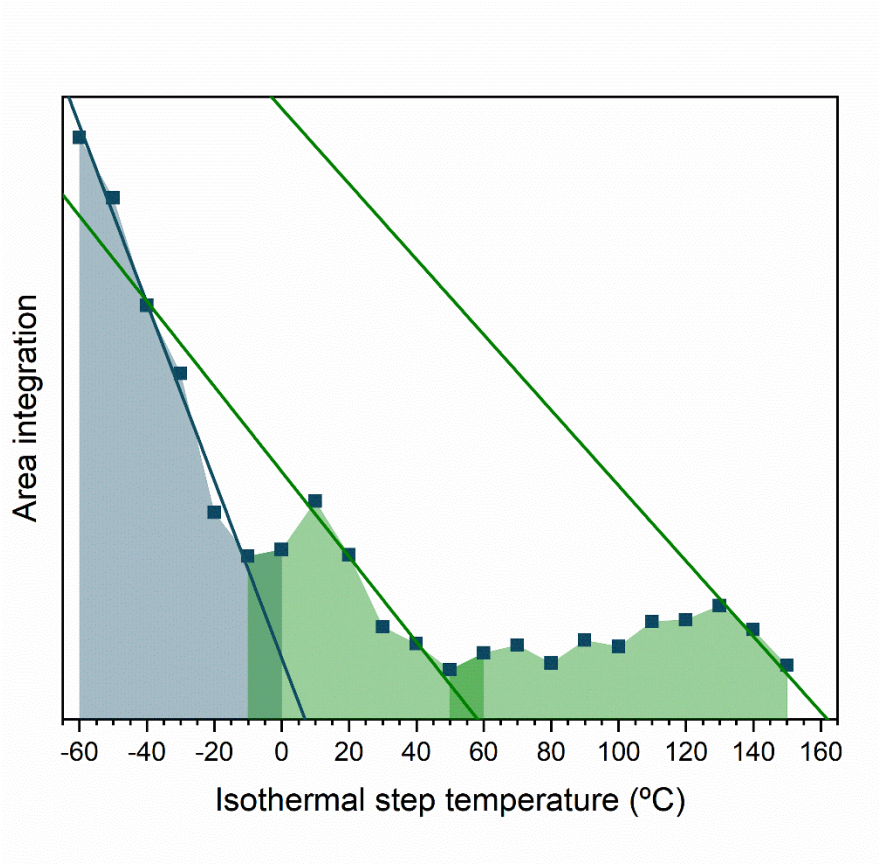

Figure 42 Integration of the ΔHs values and extrapolation of the thermal transitions.

Last of this, the third process seems to be related with the side chains only. It is interesting because the overshoot appears when the ageing temperature is above 80 degrees but the peak is located at 10 degrees approximately. At this temperature, the (100) peak in the GIWAXS starts to take importance. That means that in this thermal region the backbone and the alkyl chains of the IDTBT increases its order into a layered structure. When the nanodomains are formed, maybe the linear chains can crystallize or physically aged during the cooling step. It is possible because this endothermic peak disappears when the material does not exhibit more peaks (in the rest of the ageings) and not before.

The process 2 explained before is only a theory. This experiment does not bring light to clarify totally this. It is not clear if this process is due to the melting-like transition of the ordered regions or if it is related with the glass transition. To disclose this paradigm, a sequence of 2 or 3 consecutive isothermal steps in an ascending or a descending way were developed.

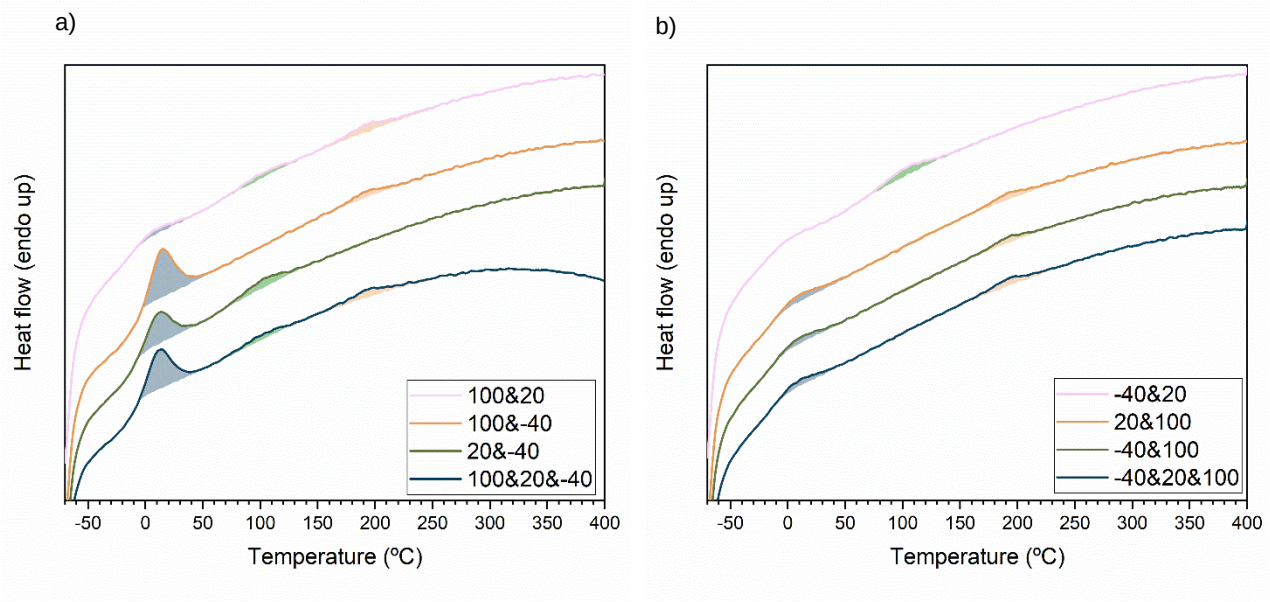

Figure 43 Descending (a) and ascending (b) isochronal annealings.

The physical ageing was finally discarded because in the ascending sequence with the annealings at 20 and 100 Celsius and the annealing at 100 does not have the same result. If this process were due to physical ageing, the annealing at 100 after the annealing at 20 should delete the thermal history generate by the less temperature ageing. Furthermore, when 100 and 20 degrees of annealing are done, three peaks appear due to the three processes but if the same sequence is done in ascending order only the peaks at 20 and 200 ºC approximately pop up. This implies that, when there was an annealing at 100 Celsius, it effectively erases the thermal changes that occurred during the prior isothermal treatment at 20 ºC. However, when the order is reversed, the annealing process at 20 ºC induces further modifications in the material, resulting in the appearance of an additional peak.

This discrepancy between the results from ascending and descending sequences explain the compatibility with the ordered regions theory. When there is an annealing of 100 preceded by another of 20, the melting temperature increase due to the improve of the growth and arranged of the ordered regions. Conversely, when the 100 ºC is followed by the 20 ºC annealing, with the first step ordered regions are created that melt at 200 ºC approx. During the subsequent annealing at 20 ºC, these crystallites formed at 100 ºC remain unaltered, maintaining their melting point at around 200 ºC due to their origination under more thermodynamically favorable conditions. However, it's important

to note that the annealing at 20 ºC has the potential to stimulate the formation of additional ordered regions through nucleation processes.

According to our data, the side chains glass transition occurs at a maximum temperature of ≈-10 ºC, maybe the melting of side-chain crystals between 0 and 50 ºC, the melting of backbone ordered regions at a maximum temperature of ≈150 ºC and an order-disorder liquid-liquid transition at ≈ 250 ºC. Thus, with respect to structural organization, the primary phase transitions of significance are the breakdown of short-range order occurring at temperatures below 150 °C, marked by the system's transformation into a liquid state, and the subsequent loss of conformational and translational order at 250 °C.

In the panel a and b of the Figure 44, it can be appreciated a notably reduction in the roughness below 200 ºC which is consistent with the transition temperatures identified previously. GISAXS results indicate starting from 120 ºC there are some small but appreciate structural changes in the range between 500 and 1.5 nm. There are structures of 20 nm until 160 ºC that start to disappear and 100 nm size structures start to growth. This study corroborates the idea if the 20 nm structures correspond to aggregates and the 100 nm structures are domains layered liquid crystalline structures characterized by the (100) GIWAXS peak. Annealing near 300 ºC disrupts also these larger structures, as suggested by the reduction of the scattering in the region of low q.

a)

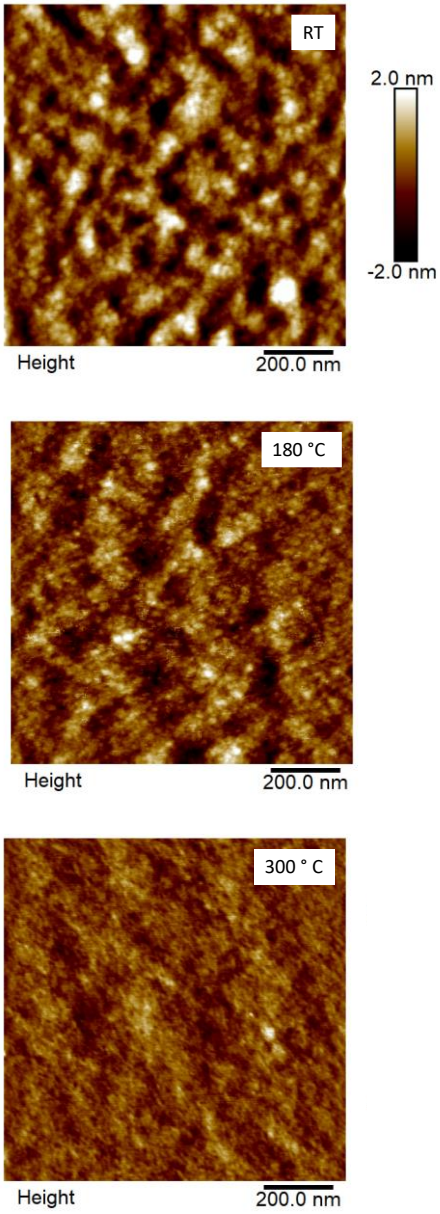

b)

Temperature (ºC)	RT	180	300
Rq (nm)	0.747	0.559	0.359

c)

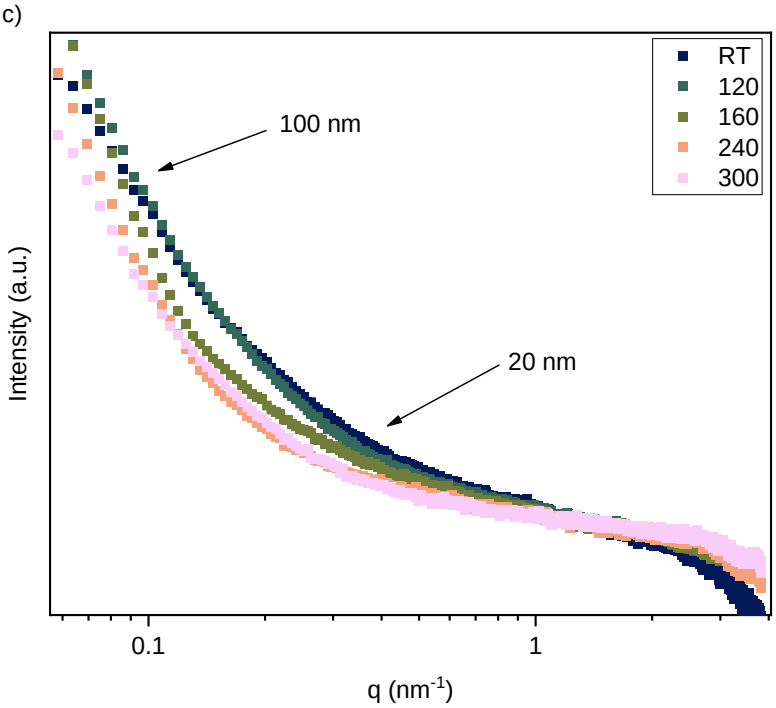

Figure 44 a) AFM images with the roughness values b) and GISAX ex situ integrations c).

4.4) Conclusions

In this chapter, the IDTBT is studied. It is demonstrated that this known “near amorphous” polymer, in reality, has a high order at nanoscale. This type of polymer named high performing were considered amorphous-like but, in recent works and our study is demonstrated that are highly ordered at the nanoscale.

On other side, the charge mobility (around 1 cm^2/Vs) is independent from the annealing temperature and thereby from the microstructure. The movements of the electrons are along the backbone. The planarity of the chains is maintaining during the range of temperatures studied so the change in the microstructure does not affect their electronic properties.

To summarize, our conclusions are visually captured in the *Figure 45*. This investigation delves into four key transitions while examining the material through the application of Flash Differential Scanning Calorimetry and Grazing Incidence Wide-Angle X-ray Scattering principally. A primary emphasis on two transitions occurring below 50 degrees. These transitions are associated with the formation of backbone aggregates and alterations in the side-chain regions. A pivotal shift is observed at around 150 °C, marking the beginning of backbone mobility. Lastly, a transition at 250 °C is indicative of the loss of backbone order.

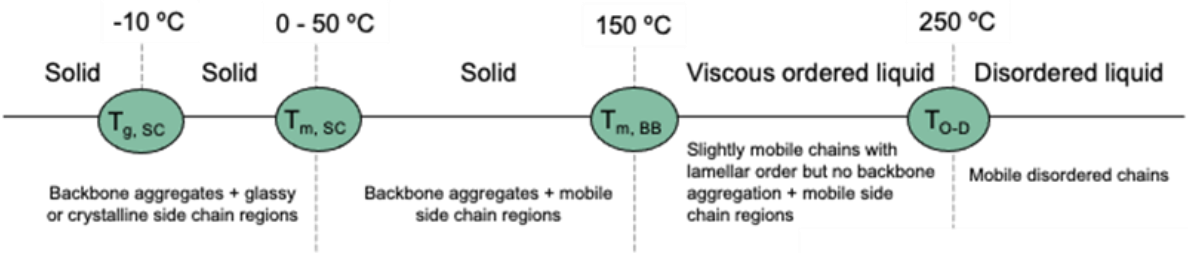

Figure 45 Summary of the transitions of the IDTBT.

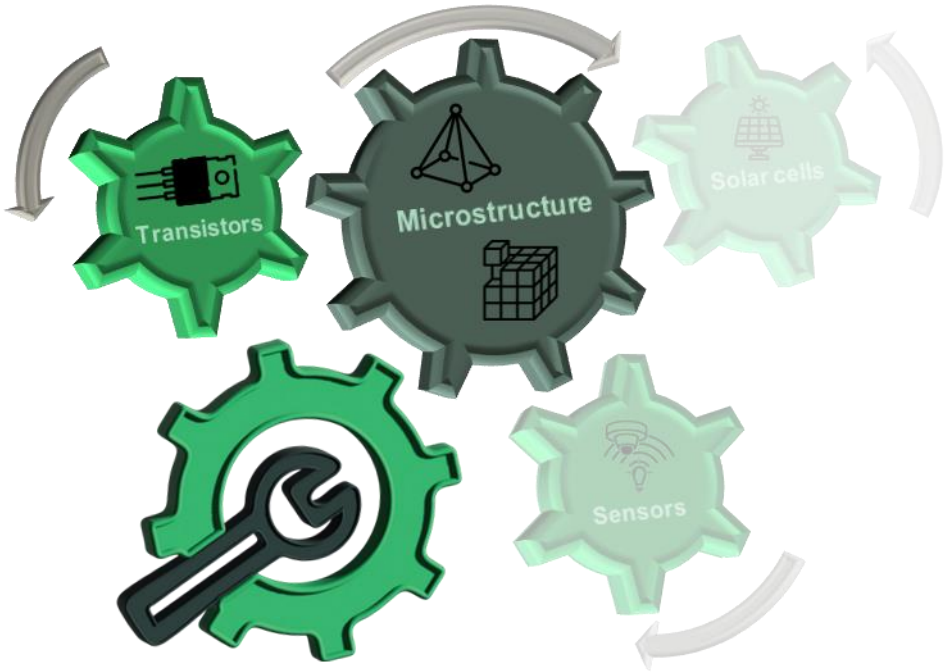
Transistors
Microstructure
Solar cells
Sensors

5

"La ciencia no tiene patria, porque el conocimiento pertenece a la humanidad, y es la antorcha que ilumina el mundo."

Louis Pasteur

5) Glassy Phase Engineering for Tunning Photoluminescence in PFO

5.1) Summary

The chapter analyzes vitreous polymers' thermodynamic state, focusing on the concept of fictive temperature (T_f). Poly(9,9-di-n-octylfluorenyl-2,7-diyl) (PFO) is scrutinized, revealing crucial insights into its glassy behavior connected to optoelectronic properties. It is established that the control of T_f is key (like crystallinity) in shaping the optoelectronic properties of semiconducting polymers.

5.2) Introduction

Light emission and detection are important milestones for scientists, aiming to understand how to make efficient emitters and photodetectors. They catch environmental light and transform it, thanks to the cones and rods, into electricity and an image is interpreted by the brain. Nowadays, a wide quantity of different sensors is developed to cover an extensive wavelength range.

This type of sensors is used in diverse applications, from measuring the light radiation in the desert to adjust the time exposure in a camera. Also, they are important in microscopy and astronomic observations but the most important one is the data transmission. To use light pulses (faster) than electric pulses to send information.

In recent decades, technological advances have led to significant innovation in the field of light sensors, particularly in the development of organic light sensors (OLD). These new materials based on organic materials have provided significant advantages in terms of flexibility, production costs, and energy efficiency.

5.2.1) Organic light sensors

The organic light sensors (OSD) are one of the most innovative materials in the field of light detection and optic properties. Modifications on the conjugated polymers or small molecules properties are used to detect light changes in the environment. They have also high sensitivity and a very wide range in the light spectrum acting from UV to near infrared wavelengths. This makes them an attractive option for applications such as digital cameras, lighting control systems, medical devices or motion sensors.

The light detection process of these sensors is almost the same as the work of each component in an organic solar cell. Firstly, the light that is going to be detected hits the OSD. Then, the energy of the photons is absorbed and, if this is enough, an electron of the material is excited and jumps to a high energy state level. When electrons have energy in excess, they can return to the basal energy and emit light with another

wavelength or separate from the atom and move freely. In the latter case, they can be collected (applying a potential to help them to move) and used to extract electrical current or be recombined with a hole and also emit the energy.

With respect to inorganic sensors, OSD present the advantage of being flexible and light, therefore exhibiting the possibility of being integrated in clothes or bandages. Changing the chemical structure, they are able to sweep a broad spectrum of wavelengths, thus providing specific sensors for particular purposes. Furthermore, their efficiency is very high, it means that almost all the photons that fall into the sensor are absorbed by the OSD. Last but not least, one of the most important advantages is their scalability. Normally, the way to produce them is by solution casting on a substrate. By this method, large quantities of OSD can be made with low costs and in a sustainable way.

In contrast, there are some obstacles that need to be overcome. The first one is the competitiveness with traditional semiconductors based on the silicon technology. They are very well established in the market and the whole niche currently is covered by them. Related to it, they must fulfill some standards and regulations that nowadays are set up for conventional inorganic semiconductors.

To be competitive with the actual sensors, OLDs have to improve their quantum efficiency and, more importantly, their stability and durability. These materials should be very sensitive to the humidity because the water acts as tramps for the hole and electrons. Also, they have to overcome their resistance to the oxidation, sharp temperature changes… All of these factors can affect their stability, durability and, therefore, their usability.

These materials find their most crucial applications in the realm of organic light-emitting diodes (OLEDs) for image-related devices. In the market, we can witness a proliferation of televisions and smartphones equipped with OLED screens, primarily due to their exceptional ability to deliver deep blacks and high-resolution displays. Moreover, the adaptability of these materials has given rise to flexible screens and sensors for digital cameras, contributing to their widespread adoption.

Another significant application area is the domain of data transmission via optical fiber, where these materials shine due to their high efficiency and cost-effectiveness, making them ideal for addressing a wide range of bandwidth requirements. Beyond this, they play a pivotal role in proximity and gesture/movement recognition technologies, enhancing user interfaces and interaction with various devices.

In the context of image-related devices, these materials extend their importance to the field of biomedical detection, serving as near-infrared (NIR) detectors for the analysis of tissues and the diagnosis of diseases. This diverse range of applications underscores the versatility and significance of these materials in our modern technological landscape.

Normally, the tuning of the principal characteristic of OLDs are achieved by two main strategies, that are the development of new materials by changing the chemical structure and by changing the crystalline structure. However, the glassy phase is also emerging crucial to tune material performance. This work will be focused specifically on the characterization of the glass thermodynamic state via the fictive temperature, whose definition will be introduced in the next subsection.

5.2.2) Fictive temperature

The fictive temperature (T_f), originally formulated by Tool[120] and associated with the 'frozen-in' liquid structure in the glassy state, serves as a conceptual tool for characterizing the non-equilibrium state of a glass previously cooled from its high-temperature, molten state[121]. T_f is defined as the temperature at which a glass with given thermodynamic state would be at equilibrium. Hence, T_f quantifies the extent of deviation from equilibrium that persists in the glassy state[122]. If the glass has reached equilibrium, its T_f is identical to the actual temperature.

Given its definition, T_f is identified as the point where the glass line intersects the extrapolated equilibrium line at a specific enthalpy. In calorimetric measurements, where the first derivative of the enthalpy is characterized, T_f is typically derived from heat flow curves during a heating scan after cooling. When employing identical heating and cooling rates, with the heating scan immediately following the cooling scan, the resulting T_f is

referred to as the limiting fictive temperature, denoted as T_f'[123]. The fictive temperature (T_f) is generally determined by using Moynihan's method[124]. This defines T_f as the temperature at which the area of the aged sample and that of the unaged sample are the same. The equation is the next:

$$\int_{T_f'}^{T>T_g} (C_{pl} - C_{pg})dT = \int_{T<T_g}^{T>T_g} (C_p - C_{pg})dT$$

Equation 5 Moynihan's method to calculate T_f.

Where, C_{pl} and C_{pg} are the heat capacity of the liquid and glass, respectively, and C_p is the apparent heat capacity of the sample at each temperature. It is noted that the differences in T_f between the same material having two different thermal histories are related to the differences in their enthalpy overshoots[124].

T_f exhibits a decreasing trend with prolonged ageing time or diminished cooling rate. As the glassy structure approaches equilibrium, Tf converges toward the value of the ageing temperature itself.

In essence, the glass transition temperature (T_g) marks the shift of an amorphous material from a supercooled liquid to glassy state. Determined by observing changes in heat capacity or thermal expansivity during cooling, often using dilatometry, T_g is highly sensitive to the cooling rate, yielding distinct values for the same material under different rates. Conversely, the fictive temperature (T_f) defines the structural state of a glass during heating. It is the temperature at which specific properties, like specific volume or enthalpy, intersect with the equilibrium liquid line when extrapolated along the glass line. Both, T_g and T_f, depend on the cooling rate, with a common assumption of their approximate equality under similar conditions. T_g signifies a fundamental transition impacting mechanical properties, while T_f reflects the structural aspects of the glass, capturing the degree of relaxation during cooling and heating.

Together, these temperatures provide insights into the dynamic behavior and structural transformations of glass-forming materials, enhancing our understanding of their thermal properties and practical applications[125].

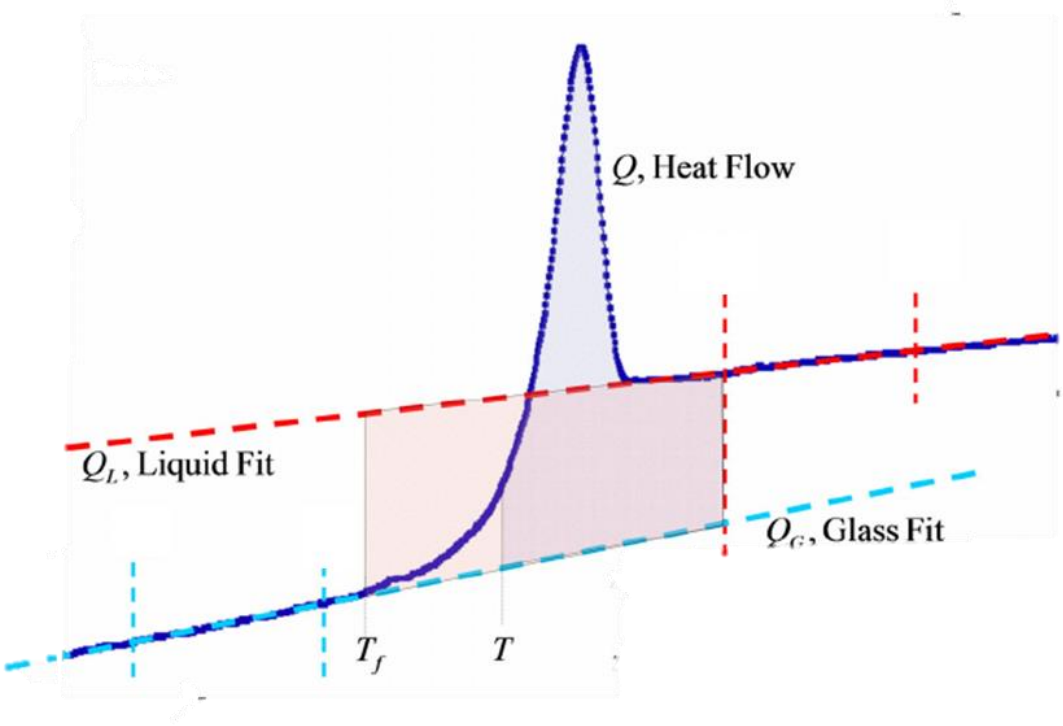

Figure 46 Fictive temperature scheme.

In this chapter, the T_f of poly(9,9-di-*n*-octylfluorenyl-2,7-diyl), a renowned polymer with a very intense photoluminescence, is characterized following a wide variety of thermal histories.

5.2.3) PFO

Poly(9,9-di-*n*-octylfluorenyl-2,7-diyl) or PFO was synthetized in the 80s as parrot of the emerging field of organic electronics, particularly in OLEDs and organic photovoltaic cells. It was developed to exhibit strong electroluminescence properties. This made it a promising material for new technologies for flat-panel displays and lighting. PFO and its derivatives played a crucial role in the development of OLED

technology. OLED displays offered advantages over traditional liquid crystal displays (LCDs) in terms of better color reproduction, faster response times, and flexibility[126–130].

It is flexible, almost transparent, low weight and all the properties related to the polymers and, also, it can be dissolved in the common organic solvents giving it the advantage in the industry field.

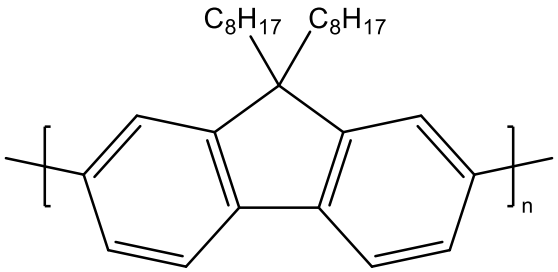

Figure 47 PFO chemical structure.

PFO solid state shows all the morphological behaviors mentioned in the Chapter 2) . In particular, PFO has reported α phase, β phase and liquid crystalline, all influenced by alterations in the surrounding solution environment[131132].

The α-phase of PFO is characterized by a well-ordered hexagonal lattice structure. The repeating units align in a way that maximizes π-π stacking interactions, leading to good charge transport properties with high crystallinity and stiffness which contributes to PFO's favorable optoelectronic properties[133]. This crystalline structure tends to be the most stable and dominant crystalline phase in PFO at room temperature[129].

The β-phase is another crystalline phase of PFO, typically observed at lower temperatures than the α. The exact structure and properties of the β-phase can be influenced by factors such as cooling rates during solidification and the presence of additives or impurities[126]. The β-phase structure may involve a different lattice arrangement compared to the hexagonal lattice found in the α-phase[130134]. Compared to the α-phase of PFO, the β-phase often exhibits lower charge carrier mobility[135128].

In the nematic phase, the long flexible polymer chains of PFO tend to align along a common axis, but they lack positional order. This means that, while the chains have orientational order, they are not arranged in a regular pattern as they are in a crystalline solid[136137].

The objective of this part of the work is to tune the photoluminescence changing the physical behavior of the vitreous phase of the PFO.

In summary, the flexibility, lightness, and easy processability make organic light sensors a pertinent successor to inorganic sensors, creating a new frontier in flexible sensor technology. The current focus is on enhancing efficiency, stability, and versatility, while maintaining their affordability, sustainability, and potential for large-scale production.

5.3) Results and discussion

This polymer can explore all thermodynamic states mentioned in the chapter 2) . It may be either in the amorphous, crystalline or liquid crystal phase. It has relatively low thermal transition temperatures well defined. Therefore, suitable thermal protocols can be designed to minimize the risk of significant degradation issues. In addition to (at least) two crystalline forms, PFO exhibits a nematic liquid-crystalline mesophase (here after referred to as the NEM state) in the temperature range immediately above the crystalline phase(s) along with an isotropic liquid phase (here after referred to as ISO state) at higher temperatures.

To understand the thermal behaviour of the polymer, samples were aged for 30 min over a wide temperature range between -80 and 280 Celsius, followed by heating scans at 4000 K s^{-1} that are showed in Figure *48*. Following the development of calorimetric features resulting from ageing, this procedure allows unveiling the thermal events triggered by a given thermal protocol. In this way, three regions can be distinguished: isothermal annealing at or below 70 ºC results in the arise of an endotherm at low temperatures (gray areas of Figure *48*), between -20 and 100 °C depending on

the annealing temperature, testifying the physical ageing of the glassy polymer and the subsequent recovery in proximity of the glass transition. Then, between 70 and 110 ºC crystallization to the α form takes place during the annealing step, highlighted by a sharper and more intense melting endotherm taking place at 130-140 °C (purple areas, Figure *48*). Annealings between 110 °C and 220 °C allow the formation of the liquid crystal phase, that eventually disrupts during the weak endothermic transition at 260 °C (red area, Figure *48*).

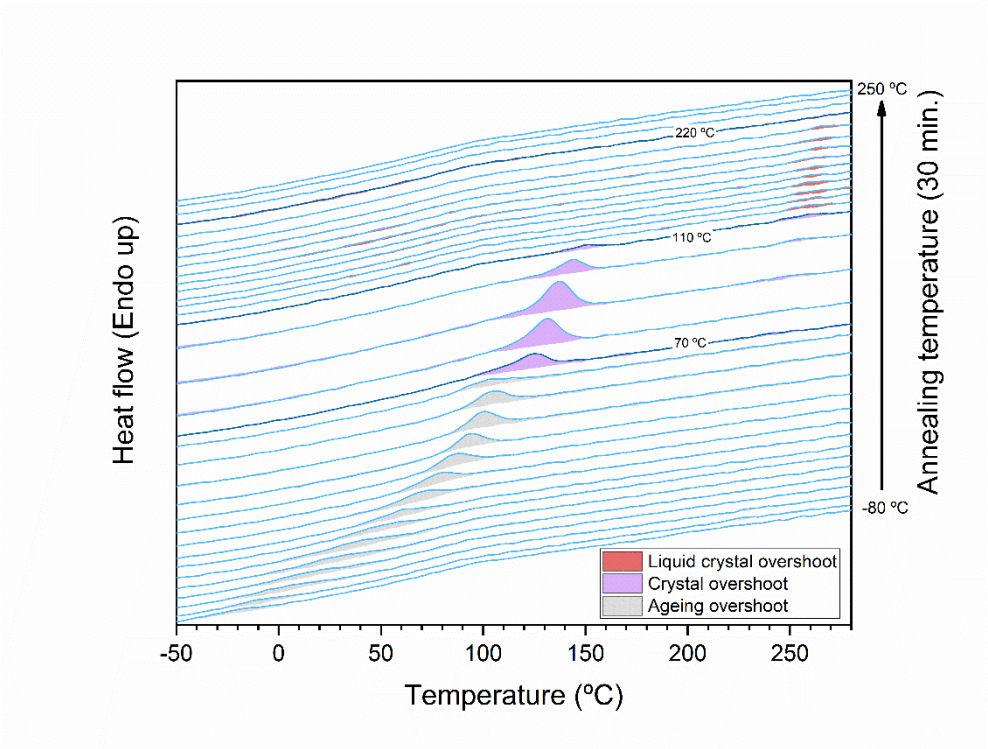

Figure 48 Isochronous method applied to the PFO polymer.

To provide a quantitative picture, the endothermic peaks were integrated to assess the enthalpy variation resulting from each thermal event. The outcome of this analysis is plotted in Figure *49*. As in the Figure 48, the grey data are associated to the physical ageing of the glassy polymer, the purple one to the crystals and the soft red one to the liquid crystal.

Extrapolating the high temperature part of the enthalpy variation by a straight line, the upper temperature limit of each thermal event can be determined. This procedure delivers the upper limit of T_g about 70 ºC, that of the crystallization process of 110 ºC and that of the liquid crystal formation at 220 Celsius.

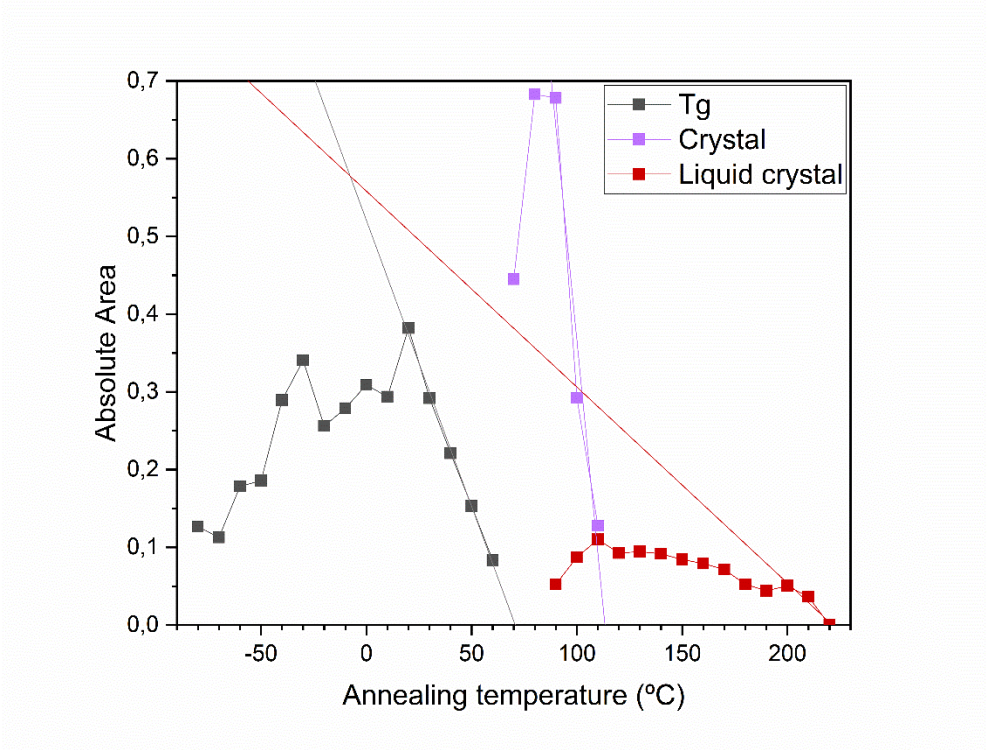

Figure 49 Integration of the excess heat flow in the isochronous method.

The present work is focused on the tuning the T_f by modifying the glass thermal history and inspecting the dependence of the photoluminescence on T_f and physical states. Following previous work by *Valentina et al.*[122], a thermal protocol to reliably obtain the desired physical state of PFO was developed. The temperature programs to obtain the isotropic and the liquid crystal phase at the beginning of FSC experiments, as well as the protocol to assess the vitrification kinetics of PFO, were showed in Figure *50*. The isotropic liquid (LQ) is obtained simply by cooling the polymer at 4000 K s^{-1} from 300 °C up to 80 °C (Figure 50 a). On the other hand, the maximum amount of liquid crystal (LC phase) is achieved by performing an isothermal annealing at 90 degrees for 30 minutes (green step, Figure 50 b) to attain maximum crystallinity, then heating at 4000 K/s to 170 °C to melt crystals, and cooling down to 80 °C, thereby obtaining the liquid crystal (purple steps, Figure *50* b). After these pre-treatment steps, the kinetics of vitrification of PFO could be assessed by cooling the system from 80 °C up to -80 °C at a specific rate β_c (orange step, Figure *50* a and b), and by acquiring a heating scan from -80 °C up to 300 °C at a fixed rate of 4000 K s^{-1}. The temperature programs in Figure *50* a and b have been looped by varying the cooling rate β_c in a range between 4000 and 0.01 Ks^{-1}. In this way, the thermodynamic state of the glass can be tuned by varying the cooling rate from

the melt. The slower the cooling rate, the lower the enthalpy state attained by the glass, and therefore the lower its T_f, resulting in a more pronounced endothermic peak associated with physical ageing.

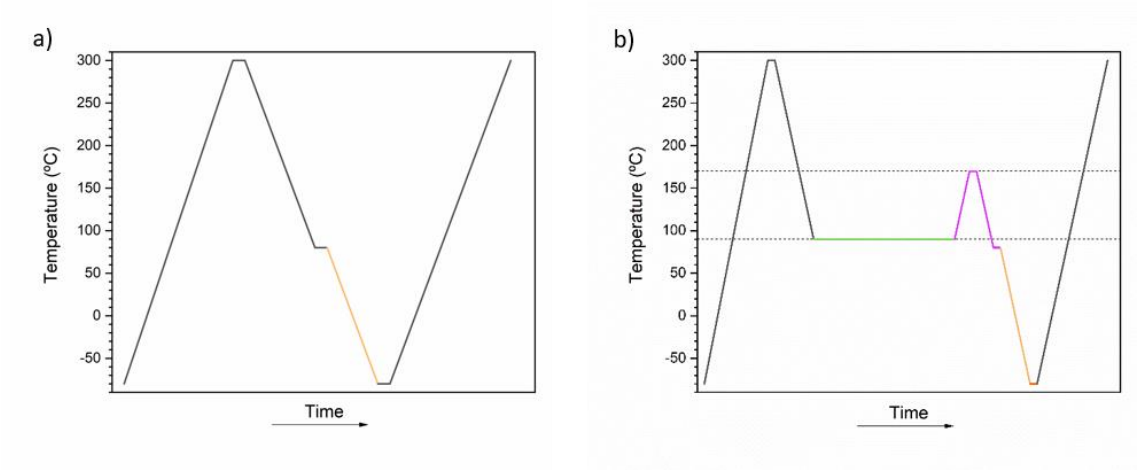

Figure 50 Methods to tune the Tf from a) the isotropic liquid and b) the liquid crystal states.

In the Figure 50 b in green and purple is plasmed the following protocol to obtain the liquid crystal structure avoiding the crystals. Then, in orange, varying the cooling rate from the melt with this method, the thermodynamic state of the glass can be altered. The slower the cooling rate, the lower the enthalpy state attained by the glass, and therefore the lower its T_f, resulting in a more pronounced endothermic peak associated with physical ageing.

Similarly, the typical signature of glass equilibration resulting from physical ageing is the development of an endothermic overshoot with magnitude increasing with ageing time (Figure *51*). The magnitude of the overshoot and temperature interval where this is located depends on the ageing time and temperature. Shortly after the beginning of ageing, it grows on top of the specific heat step underlying the glass transition. At longer ageing times, the endothermic overshoot shifts to higher temperatures, indicating that accessing low energy states delays devitrification when heating the aged samples[138].

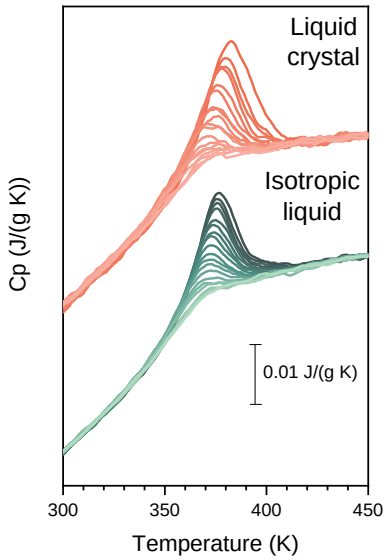

Figure 51 Endothermic peak associated to the physical ageing at different cooling rates from the liquid crystal and isotropic liquid.

Using the Moynihan's method (Equation *5* and Figure *46*), the T_f could be calculated for each scan characterized by a different cooling rate β_c and for both LC and LQ physical states of PFO. Figure *52* represents the vitrification kinetics of PFO, in which the cooling rate β_c, that is the inverse of a characteristic time of perturbation, is graphed as a function of the inverse fictive temperature. In this way, the super-Arrhenius temperature dependence of vitrification could be assessed for both physical states of PFO. Noteworthy, the liquid crystal (LC) shows higher T_f than LQ, considering that the isotropic liquid exhibits a more disordered system than the liquid crystal.

Another performed approach to characterize the two phases of PFO was to study the spontaneous fluctuations of the system related to the main α-relaxation, in terms of thermal susceptibility. To do that, step-response FSC analyses were employed to assess the frequency dependent dynamic glass transition temperature (T_g^{dyn}), that is the glass transition obtained for linearly perturbated systems.

As was explained in the Chapter 2) the inflection point of the reversing specific heat ($C_p$rev, corresponding to the modulus of C_p^*, is identified to determine the temperature-

dependent relaxation time (τ). This relaxation time represents the characteristic time scale of the alpha relaxation process at different temperatures. By conducting multiple step-response experiments at varying temperatures, the alpha relaxation dynamics can be characterized across a wide frequency range, spanning approximately six orders of magnitude. This rigorous characterization approach offers valuable insights into the molecular dynamics and thermal behavior of glassy materials, enabling a comprehensive understanding of the alpha relaxation phenomenon[139140].

In Figure 52, the temperature dependence of spontaneous fluctuations of PFO, has been plotted together with the vitrification kinetics in an activation graph. It was conducted for the samples measure from the Isotropic liquid and the liquid crystal.

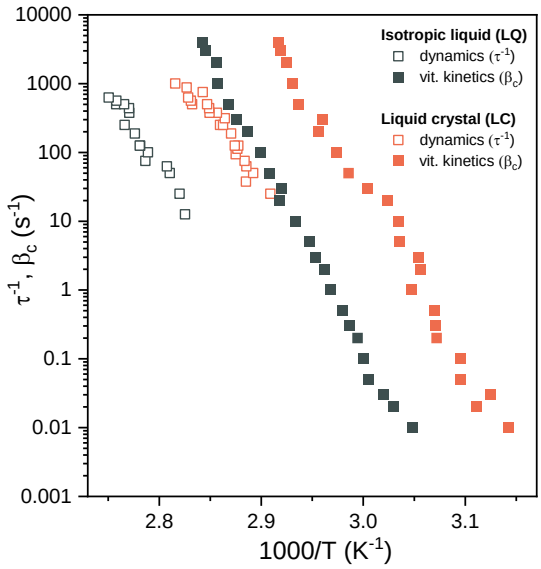

Figure 52 Liquid dynamics of PFO (open symbols), showed as the inverse relaxation time (τ^{-1}) as a function of the inverse dynamic glass transition temperature ($1000/T_g^{dyn}$), compared to the vitrification kinetics (full symbols) of LQ and LC phases of PFO.

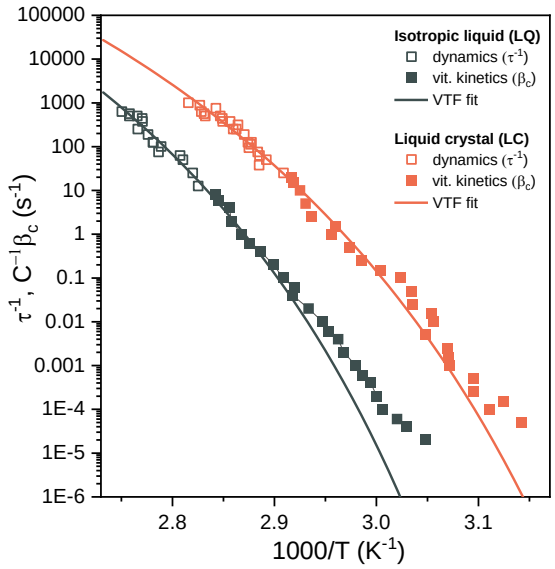

Figure 53 Comparison between α-relaxation dynamics (τ^{-1}) and vitrification kinetics (β_c), the latter divided by the Frenkel-Kobeko-Reiner constant C (equal to 500 and 200 for LQ and LC, respectively), of PFO in isotropic liquid (LQ) and nematic form (LC).

The α-relaxation dynamics, characterized by τ^{-1}, reflect the rate at which molecular rearrangements occur within the material, offering insights into its relaxation behavior and molecular mobility. A higher of τ^{-1} value indicates slower relaxation dynamics, suggesting decreased molecular mobility and longer relaxation timescales. On the other hand, vitrification kinetics, D, provide information about the rate of cooling required for the material to transition from a mobile to a rigid glassy state. A higher value of D implies a faster vitrification process, indicating the material's propensity to undergo glass transition under specific cooling conditions[141142].

All of this is given by the approximation of the data to the Vogel-Fulcher-Tammann (VFT) equation. It is commonly used to describe the temperature dependence of relaxation times (τ) in glass-forming materials. The parameters include the logarithm of the characteristic relaxation time at a reference temperature ($\log \tau_0$), the temperature coefficient (D), and the characteristic temperature (T_0) [31143].

$$\tau = \log(\tau_0) + \frac{D * T_0}{T + T_0}$$

Equation 6 Vogel-Fulcher-Tammann (VFT) equation.

This equation parameters provide insights into the temperature dependence of the relaxation timescale (τ) and into vitrification kinetics, particularly in relation to the temperature at which the relaxation timescale becomes extremely long, signifying the onset of glass transition. However, differences in the temperature coefficient (D) and the characteristic temperature (T_0) suggest variations in the temperature sensitivity and fragility of the relaxation process. From the other side, A lower T_0 value suggests that the material approaches the glass transition temperature at a lower temperature, indicating a higher propensity for vitrification.

Table 1 VFT parameters.

VTF parameters	Log τ_0	D	T_0
LQ	-14	6.71	288.1
LC	-14	6.90	278.0

Focusing on the LC and LQ (*Table 1*), both forms exhibit the same log(τ_0) value. This similarity implies that, at a specific temperature, the materials in both forms have similar molecular mobility and relaxation behaviors. While the log(τ_0) values are identical, there are differences in D and T_0. The LC form has a slightly higher D value but not enough indicating that both have a similar fragility. The LC form has a lower T_0 value compared to the LQ form, indicating that it approaches the glass transition temperature at a lower temperature. This suggests that the LC form may have faster vitrification kinetics compared to the LQ form, as it reaches the critical relaxation timescale at a lower temperature.

To see if the T_f variation has a significant effect on their optoelectronic properties, photoluminescence of the samples deposited on the chip with the thermal protocol (T_f determined) is performed. Four temperatures were selected, two from LQ and two from LC to discard the effect of the pre-structure of the polymer. Also, an as-cast sample was measured and plasmed on the Figure 54.

There is a clear tendency for both peaks of the spectrum to shift towards higher wavelengths regardless of the initial state of the polymer (isotropic liquid or liquid crystal). With the decreasing of the T_f, the first peak is shifted to higher wavelengths allowing us to tune the light emission.

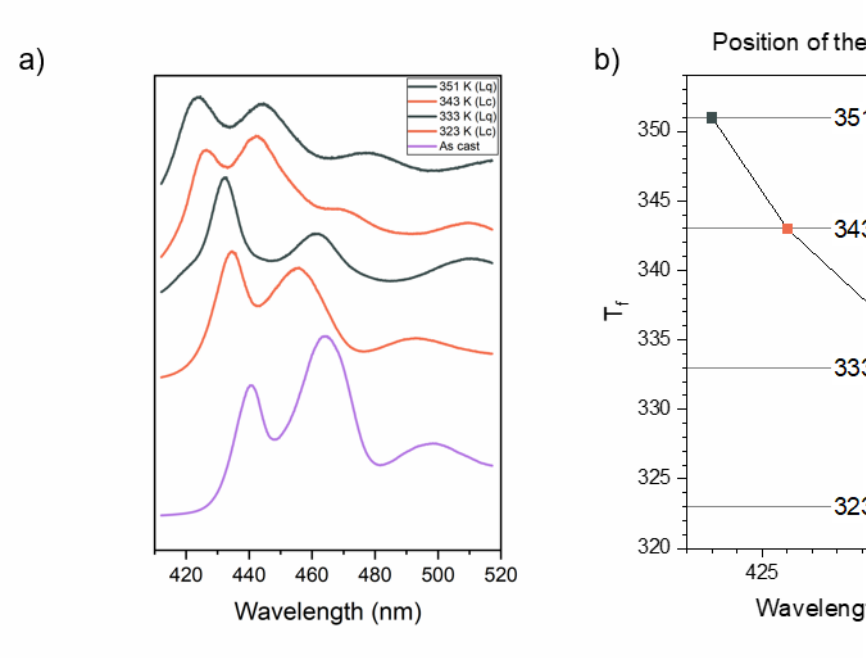

Figure 54 a) Photoluminescence spectras of the selected samples and b) position of the most relevant peak vs the fictive temperature of the samples.

With this first overview of the possibility of controlling the thermodynamic state of the vitreous phase to tune the photoluminescence new possibilities for optoelectronic devices are opened. Not only improving the crystallization better devices are obtained. With this approximation, also amorphous or near amorphous polymers can be used for new electronic technologies.

5.4) Conclusions

The thermodynamic state of the vitreous polymers is a difficult field of knowledge. Thanks to the flash DSC, we are able to distinguish and understand how the T_f behaves. In this case, the LC form appears to have a greater temperature sensitivity and a tendency for faster relaxation and vitrification compared to the LQ form.

The behavior of PFO in a 2D structure is the same as in bulk so active layers on thin film devices are possible. Also, a wide range of T_f were obtained controlling only the cooling rate. To enlarge the range the cooling rate control were developed from the isotropic liquid state and liquid crystal state.

But the most important and relevant conclusion is that the control of the T_f is also determinant to control the optoelectronic properties of organic semiconductor polymers.

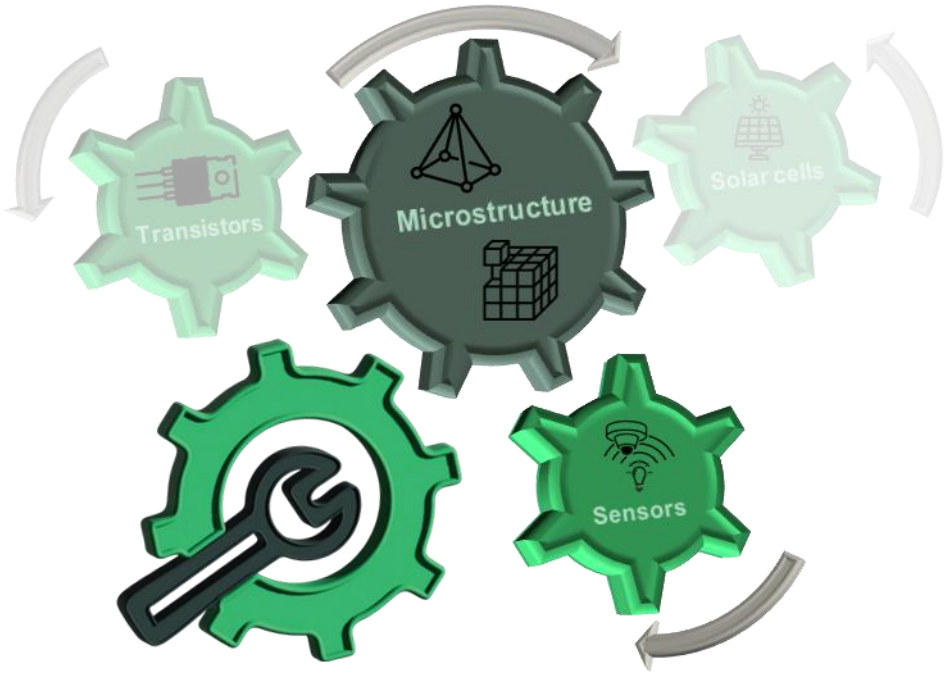

6

"La ciencia no consiste en acumular datos, sino en unirlos."

Sir William Lawrence Bragg

6) Conclusions

As main conclusions, the utilization of the TMDSC (Thermal Modulated Differential Scanning Calorimetry) has enabled precise reproduction and compositional analysis of solar cells and the active layer morphology on sensors and transistors. By faithfully replicating the solar cell and the transistor/sensor active layer using a flash DSC chip, we can investigate the morphology of the real active layer through calorimetry. Also, the GIWAXS and GISAXS provide a lot of information understanding the direction and the range of order. These techniques, along with other complementary approaches, allow us to understand and modify nano and microstructures at our discretion.

To know the real composition on the bulk heterojunction in a solar cell as in the Chapter 3) discovering that a 50:50 weight mechanical mixture has, in real, 37.5% of the small molecules and the rest polymer in the intermix phase.

To study a “near amorphous” polymer as active layer on a thin film transistor like in the Chapter 4) In this case is demonstrated that IDTBT is, at a glance, amorphous because there are no order at microscale but has a high order at nanoscale with 4 key temperatures. -10 and around 50 Celsius associated to the aggregation of the backbone and the sidechains, one at 150 when the backbone mobility starts and the order increases a 250 ºC associated to the melting of the material.

To understand and tune the amorphous phase of the polymers modifying the cooling rates and the start state (isotropic liquid or liquid crystal) to control the changes on the optoelectronic properties. In Chapter 5, the fictive temperature (T_f) of PFO was adjusted to manipulate its optoelectronic properties, achieving a range of approximately 30 K within which T_f could be modulated in a timely manner (not requiring extended durations). Although stabilization of T_f remained elusive, it became evident that prolonged cooling times are necessary to gradually decrease it.

Now, I want to rewrite the conclusions in Spanish for my family and the people that does not know English and want to know what is about this work.

Conclusiones

Como principales conclusiones de este trabajo se encuentran la utilización de la TMDSC (Calorimetría Diferencial de Barrido Modulada Térmicamente) que ha permitido reproducir con precisión y analizar la composición de las células solares, la morfología de la capa activa de los transistores y sensores. Al reproducir fielmente la célula solar o la capa activa de un transistor o sensor utilizando un chip de flash DSC, podemos investigar la morfología de la capa activa real mediante calorimetría. Además, gracias al GIWAXS y GISAXS, comprendemos la dirección y el rango de orden en la muestra. Estas técnicas, junto con otros enfoques complementarios, nos permiten comprender y modificar a nuestro antojo la nano y microestructura del material.

Para entender la composición real de una hetero-unión de una placa solar como en el capítulo 3) En este apartado se analiza una mezcla mecánica de 50:50 % en peso de donor y aceptor con un recocido en atmósfera saturada. Se determina que, en realidad, la fase entremezclada tiene sólo un 37,5 % de aceptor.

Para estudiar los polímeros denominados “casi amorfos” como capa activa en transistores. En el capítulo 4) se demuestra como el IDTBT que hasta la fecha es considerado de esta familia, en realidad tiene un alto orden a escala nanométrica aunque no se aprecie ningún orden a escala micrométrica. Éste tiene 4 temperaturas clave. Asociadas a la formación de agregados de la cadena principal y a las cadenas laterales son -10 y 50 ˚C. A los 150 grados la cadena principal comienza a adquirir movilidad y ordenarse y a 250 ˚C el material funde.

Para modificar el estado termodinámico de la fase amorfa a antojo modificando la velocidad de enfriamiento y el estado desde el que se enfría (líquido isotrópico o cristal líquido). En el Capítulo 5, la temperatura ficticia (T_f) de PFO se ajustó para manipular sus propiedades optoelectrónicas, logrando un rango de aproximadamente 30 K dentro del cual T_f podría modularse de manera oportuna (sin requerir tiempos muy largos). Por otro lado, la estabilización de la T_f no se consigue debido a que se necesitaría un enfriamiento excesivamente lento.

7

"En ciencia, algunos experimentos tienen éxito y otros, enseñanza."

John C. Polanyi

7) Bibliography

1. Semiconductores - Qué son, tipos, aplicaciones y ejemplos https://concepto.de/semiconductores/ (accessed Jan 12, 2023).
2. Jenkins, R. et al. A Review of Thermionic Cathodes. *Vacuum* **1969**, *19* (8), 353–359.
3. Segal, M. et al. Material History: Learning from Silicon. *Nature* **2012**, *483* (7389), S43–S44.
4. Moore, G. E. et al. Cramming More Components onto Integrated Circuits With Unit Cost. *Electronics* **1965**, *38* (8), 114.
5. Sarma, K. R. et al. *Flexible Electronics: Materials and Applications*; Wong, W. S., Salleo, A., Eds.; Electronic Materials: Science & Technology; Springer US: Boston, MA, 2009; Vol. 11.
6. Rivnay, J. et al. The Rise of Organic Bioelectronics. *Chem. Mater.* **2014**, *26* (1), 679–685.
7. Someya, T. et al. The Rise of Plastic Bioelectronics. *Nature* **2016**, *540* (7633), 379–385.
8. *Handbook of Conducting Polymers, 2 Volume Set*; Skotheim, T. A., Ed.; CRC Press, 2007.
9. Pron, A. et al. Processible Conjugated Polymers: From Organic Semiconductors to Organic Metals and Superconductors. *Prog. Polym. Sci.* **2002**, *27* (1), 135–190.
10. Lu, H. et al. Conjugated Conductive Polymer Materials and Its Applications: A Mini-Review. *Front. Chem.* **2021**, *9* (September), 6–11.
11. Hurhangee, M. et al. Heteroatom and Bridged-Ring π-Conjugated Polymers and Their Use in Organic Electronics. *Imp. Coll. London* **2016**, No. December.
12. Brédas, J.-L. et al. An Introduction to the Electronic Structure of π -Conjugated Molecules and Polymers, and to the Concept of Electronic Bands; 2016; pp 1–18.
13. Bian, L. et al. Recent Progress in the Design of Narrow Bandgap Conjugated Polymers for High-Efficiency Organic Solar Cells. *Prog. Polym. Sci.* **2012**, *37* (9), 1292–1331.
14. Reynolds, J. R. et al. *Conjugated Polymers*; Reynolds, J. R., Thompson, B. C., Skotheim, T.

A., Eds.; CRC Press, 2019.

15. Kausch, H. H. et al. *The Physics of Polymers: Concepts for Understanding Their Structures and Behavior By Gert R. Strobl (Alber-Ludwigs University). Springer: New York. 1996. Xi + 439 Pp. $39.95. ISBN 3-540-60768-4.*; 1997; Vol. 119.

16. Cabaleiro-Lago, E. M. et al. On the Nature of σ-σ, σ-π, and π-π Stacking in Extended Systems. *ACS Omega* **2018**, *3* (8), 9348–9359.

17. Myny, K. et al. An 8-Bit, 40-Instructions-Per-Second Organic Microprocessor on Plastic Foil. *IEEE J. Solid-State Circuits* **2012**, *47* (1), 284–291.

18. Peng, Z. et al. Understanding, Quantifying, and Controlling the Molecular Ordering of Semiconducting Polymers: From Novices to Experts and Amorphous to Perfect Crystals. *Mater. Horizons* **2022**, *9* (2), 577–606.

19. Marina, S. et al. Semi-Paracrystallinity in Semi-Conducting Polymers. *Mater. Horizons* **2022**, *9* (4), 1196–1206.

20. Seymour, R. B. et al. *Structure—Property Relationships in Polymers*; Springer US: Boston, MA, 1984.

21. Crow. et al. Crystallization Behavior of Polymers https://polymerdatabase.com/polymer physics/Crystalline Polymers.html (accessed Feb 7, 2023).

22. Noël, C. et al. Liquid Crystal Polymers. *Prog. Polym. Sci.* **1991**, *16* (1), 55–110.

23. Arvind, M. et al. Regarding the Role of Aggregation and Structural Order on the Mechanism of Molecular Doping of Semiconducting Polymers : From Solutions to Films Dissertation Malavika Arvind, Universität Postdam, 2021.

24. Wang, Q. et al. Carboxylate-Substituted Polythiophenes for Efficient Fullerene-Free Polymer Solar Cells: The Effect of Chlorination on Their Properties. *Macromolecules* **2019**, *52* (12), 4464–4474.

25. Schick, C. et al. Fast Scanning Calorimetry. *Fast Scanning Calorim.* **2016**, 1–787.

26. Juego de sensores UFS 1/ST (10 unidades) - Descripción general - METTLER TOLEDO https://www.mt.com/es/es/home/products/Laboratory_Analytics_Browse/TA_Family_ Browse/ta_accessories_browse/sensor-set-ufs-1-st.html (accessed Nov 2, 2022).

27. Martín, J. et al. Direct Calorimetric Observation of the Rigid Amorphous Fraction in a

Semiconducting Polymer. *J. Phys. Chem. Lett.* **2018**, *9* (5), 990–995.

28. Yin, H. et al. Calorimetric Glass Transition of Ultrathin Poly(Vinyl Methyl Ether) Films. *Polymer (Guildf).* **2013**, *54* (8), 2067–2070.

29. Erukhimovich, I. et al. Phase Equilibria and Charge Fractionation in Polydisperse Polyelectrolyte Solutions. **2004**, No. June, 2741–2753.

30. Snyder, C. R. et al. Glassy Phases in Organic Semiconductors. *Curr. Opin. Solid State Mater. Sci.* **2018**, *22* (2), 41–48.

31. Schick, C. et al. *Fast Scanning Calorimetry*; Schick, C., Mathot, V., Eds.; Springer International Publishing: Cham, 2016.

32. Di Lorenzo, M. L. et al. The Role of the Rigid Amorphous Fraction on Cold Crystallization of Poly(3-Hydroxybutyrate). *Macromolecules* **2012**, *45* (14), 5684–5691.

33. Shoifet, E. et al. Temperature Modulated Differential Scanning Calorimetry – Extension to High and Low Frequencies. *Thermochim. Acta* **2015**, *603*, 227–236.

34. Richert, R. et al. Non-Linear Dielectric Signatures of Entropy Changes in Liquids Subject to Time Dependent Electric Fields. *J. Chem. Phys.* **2016**, *144* (11), 1–5.

35. Ezquerra, T. A. et al. *Applications of Synchrotron Light to Scattering and Diffraction*; 2009; Vol. 33.

36. Broennimann, C. et al. The PILATUS 1M Detector. *J. Synchrotron Radiat.* **2006**, *13* (2), 120–130.

37. Gutiérrez, a I. et al. La Luz Sincrotrón: Una Herramienta Extraordinaria Para La Ciencia. *Apunt. Cienc. y Tecnol.* **2004**, *12*, 12–37.

38. 7.4: The Wavelength Nature of Matter - Chemistry LibreTexts https://chem.libretexts.org/Bookshelves/General_Chemistry/Map%3A_A_Molecular_Approach_(Tro)/07%3A_The_Quantum-Mechanical_Model_of_the_Atom/7.04%3A_The_Wavelength_Nature_of_Matter (accessed Nov 2, 2022).

39. Accelerators https://www.cells.es/en/accelerators (accessed Oct 26, 2022).

40. Inside the Machine - - Diamond Light Source https://www.diamond.ac.uk/Home/About/FAQs/Inside-the-Machine.html (accessed

Oct 26, 2022).

41. Hirsch, P. B. et al. Elements of X-Ray Diffraction. *Phys. Bull.* **1957**, *8* (7), 237–238.

42. Müller-Buschbaum, P. et al. The Active Layer Morphology of Organic Solar Cells Probed with Grazing Incidence Scattering Techniques. *Adv. Mater.* **2014**, *26* (46), 7692–7709.

43. Gutiérrez-Fernández, E. et al. Nanostructuring Of Soft Matter For Organic Electronics. *Fac. Física* **2019**, *PhD*.

44. Rivnay, J. et al. Quantitative Determination of Organic Semiconductor Microstructure from the Molecular to Device Scale. *Chem. Rev.* **2012**, *112* (10), 5488–5519.

45. Rivnay, J. et al. Quantitative Analysis of Lattice Disorder and Crystallite Size in Organic Semiconductor Thin Films. *Phys. Rev. B - Condens. Matter Mater. Phys.* **2011**, *84* (4), 1–20.

46. Noriega, R. et al. A General Relationship between Disorder, Aggregation and Charge Transport in Conjugated Polymers. *Nat. Mater.* **2013**, *12* (11), 1038–1044.

47. BEAMLINE INFORMATION — en https://www.cells.es/en/beamlines/bl11-ncd (accessed Jan 10, 2023).

48. Elettra Sincrotrone Trieste https://www.elettra.eu/lightsources/elettra/elettra-beamlines/saxs/beamline/page-3.html?showall= (accessed Jan 10, 2023).

49. Magonov, S. N. et al. *Atomic Force Microscopy in Analysis of Polymers*; 2000.

50. Nguyen-Tri, P. et al. Recent Applications of Advanced Atomic Force Microscopy in Polymer Science: A Review. *Polymers (Basel).* **2020**, *12* (5), 1–28.

51. Schönherr, H. et al. *Scanning Force Microscopy of Polymers*; Springer Berlin Heidelberg: Berlin, Heidelberg, 2010.

52. Sukanek, P. C. et al. Spin Coating. *J. imageing Technol.* **1985**, *11* (4), 184–190.

53. Mustafa, H. A. M. et al. Modeling and the Main Stages of Spin Coating Process: A Review. *J. Appl. Sci. Technol. Trends* **2021**, *2* (03), 91–95.

54. Khim, D. et al. Simple Bar-Coating Process for Large-Area, High-Performance Organic Field-Effect Transistors and Ambipolar Complementary Integrated Circuits. *Adv. Mater.* **2013**, *25* (31), 4302–4308.

55. McQuade, J. et al. Solvent Retention and Crack Evolution in Dropcast PEDOT:PSS and

Dependence on Surface Wetting. *ACS Omega* **2018**, *3* (4), 3868–3873.

56. Ellabban, O. et al. Renewable Energy Resources: Current Status, Future Prospects and Their Enabling Technology. *Renew. Sustain. Energy Rev.* **2014**, *39*, 748–764.

57. Vodapally, S. N. et al. A Comprehensive Review of Solar Photovoltaic (PV) Technologies, Architecture, and Its Applications to Improved Efficiency. *Energies* **2022**, *16* (1), 319.

58. Dai, Z. et al. Recent Progress in the Theory of Bulk Photovoltaic Effect. *Chem. Phys. Rev.* **2023**, *4* (1), 011303.

59. Copeland, A. W. et al. The Photovoltaic Effect. *Chem. Rev.* **1942**, *31* (1), 177–226.

60. Aftab, S. et al. Bulk Photovoltaic Effect in 2D Materials for Solar-Power Harvesting. *Adv. Opt. Mater.* **2022**, *10* (23), 2201288.

61. Yao, H. et al. Recent Advances in Single-Junction Organic Solar Cells. *Angew. Chemie* **2022**, *134* (37).

62. Shirakawa, H. et al. Synthesis of Electrically Conducting Organic Polymers: Halogen Derivatives of Polyacetylene, (CH) X. *J. Chem. Soc. Chem. Commun.* **1977**, No. 16, 578.

63. Fukuda, K. et al. The Future of Flexible Organic Solar Cells. *Adv. Energy Mater.* **2020**, *10* (25), 1–10.

64. Tress, W. et al. Organic Solar Cells. In *Springer Series in Materials Science*; 2014; Vol. 208, pp 67–214.

65. Rasmussen, S. C. et al. Conjugated and Conducting Organic Polymers: The First 150 Years. *Chempluschem* **2020**, *85* (7), 1412–1429.

66. Nguyen, V. H. et al. Influence of Block Ratio on Thermal, Optical, and Photovoltaic Properties of Poly(3-Hexylthiophene)-b-Poly(3-Butylthiophene)-b-Poly(3-Octylthiophene). *Molecules* **2022**, *27* (23).

67. Schmatz, B. et al. Perspective on the Advancements in Conjugated Polymer Synthesis, Design, and Functionality over the Past Ten Years. In *Conjugated Polymers*; CRC Press, 2019; pp 107–148.

68. Qian, D. et al. Design, Application, and Morphology Study of a New Photovoltaic Polymer with Strong Aggregation in Solution State. *Macromolecules* **2012**, *45* (24), 9611–9617.

69. G. Yu,* J. Gao, J. C. Hummelen, F. Wudi, A. J. H. et al. Polymer Photovoltaic Cells: Enhanced Efficiencies via a Network of Internal Donor-Acceptor Heterojunctions. *Science (80-.).* **1995**, *270*, 1–3.

70. Vongsaysy, U. et al. Formulation Strategies for Optimizing the Morphology of Polymeric Bulk Heterojunction Organic Solar Cells: A Brief Review. *J. Photonics Energy* **2014**, *4* (1), 040998.

71. Marina, S. et al. INTERPLAY BETWEEN MICROSTRUCTURE/MORPHOLOGY AND THE OPTO-ELECTRONIC PROPERTIES OF MATERIALS FOR ORGANIC PHOTOVOLTAICS.

72. Armin, A. et al. A History and Perspective of Non-Fullerene Electron Acceptors for Organic Solar Cells. *Adv. Energy Mater.* **2021**, *11* (15), 2003570.

73. Lin, Y. et al. An Electron Acceptor Challenging Fullerenes for Efficient Polymer Solar Cells. *Adv. Mater.* **2015**, *27* (7), 1170–1174.

74. Li, S. et al. Energy-Level Modulation of Small-Molecule Electron Acceptors to Achieve over 12% Efficiency in Polymer Solar Cells. *Adv. Mater.* **2016**, *28* (42), 9423–9429.

75. Zhao, W. et al. Molecular Optimization Enables over 13% Efficiency in Organic Solar Cells. *J. Am. Chem. Soc.* **2017**, *139* (21), 7148–7151.

76. Huang, M. et al. Impact of Polarization Effect on Exciton Binding Energies and Charge Transport for the Crystals of Chlorinated ITIC Derivatives. *J. Phys. Chem. C* **2023**, *127* (11), 5597–5603.

77. Lin, Y. et al. High-Performance Electron Acceptor with Thienyl Side Chains for Organic Photovoltaics. *J. Am. Chem. Soc.* **2016**, *138* (14), 4955–4961.

78. Peng, Z. et al. Unraveling the Stretch-Induced Microstructural Evolution and Morphology–Stretchability Relationships of High-Performance Ternary Organic Photovoltaic Blends. *Adv. Mater.* **2023**, *35* (3), 2207884.

79. Tang, L. et al. Morphology and Charge Transport Properties of P(NDI2OD-T2)/Polystyrene Blends. *Macromolecules* **2021**, *54* (23), 11134–11146.

80. Steckmann, T. et al. Ultrathin P(NDI2OD-T2) Films with High Electron Mobility in Both Bottom-Gate and Top-Gate Transistors. *Adv. Electron. Mater.* **2022**, *8* (7), 2101324.

81. Al-Azzawi, A. G. S. et al. A Mini Review on the Development of Conjugated Polymers: Steps towards the Commercialization of Organic Solar Cells. *Polymers (Basel).* **2022**, *15*

(1), 164.

82. Zhu, L. et al. Efficient Organic Solar Cell with 16.88% Efficiency Enabled by Refined Acceptor Crystallization and Morphology with Improved Charge Transfer and Transport Properties. *Adv. Energy Mater.* **2020**, *10* (18), 1904234.

83. Tang, C. W. et al. Two-layer Organic Photovoltaic Cell. *Appl. Phys. Lett.* **1986**, *48* (2), 183–185.

84. Vermeulen, L. A. et al. Stable Photoinduced Charge Separation in Layered Viologen Compounds. *Nature* **1992**, *358* (6388), 656–658.

85. Kim, H. et al. Organic Solar Cells Based on Conjugated Polymers: History and Recent Advances. *Korean J. Chem. Eng.* **2014**, *31* (7), 1095–1104.

86. Heeger, A. J. et al. Plastic Solar Cells: Self-Assembly of Bulk Heterojunction Nano-Materials by Spontaneous Phase Separation. *AIP Conf. Proc.* **2013**, *1519* (11), 47–50.

87. Doumon, N. Y. et al. Ternary Organic Solar Cells: A Review of the Role of the Third Element. *Nano Energy* **2022**, *94* (August 2021), 106915.

88. Chen, X. et al. 18.02% Efficiency Ternary Organic Solar Cells with a Small-Molecular Donor Third Component. *Chem. Eng. J.* **2021**, *424* (May), 130397.

89. Zhong, W. et al. Decoupling Complex Multi-Length-Scale Morphology in Non-Fullerene Photovoltaics with Nitrogen K-Edge Resonant Soft X-ray Scattering. *Adv. Mater.* **2022**, *34* (6), 2107316.

90. Tian, L. et al. Recent Advances of Interface Engineering for Non-Fullerene Organic Solar Cells. *Org. Electron.* **2021**, *93* (March), 106141.

91. Gregg, B. A. et al. The Photoconversion Mechanism of Excitonic Solar Cells. *MRS Bull.* **2005**, *30* (1), 20–22.

92. Mukherjee, S. et al. Significance of Average Domain Purity and Mixed Domains on the Photovoltaic Performance of High-Efficiency Solution-Processed Small-Molecule BHJ Solar Cells. *Adv. Energy Mater.* **2015**, *5* (21), 1500877.

93. Dambhare, M. V. et al. Solar Photovoltaic Technology: A Review of Different Types of Solar Cells and Its Future Trends. *J. Phys. Conf. Ser.* **2021**, *1913* (1), 012053.

94. Ghasemi, M. et al. A Molecular Interaction–Diffusion Framework for Predicting Organic

Solar Cell Stability. *Nat. Mater.* **2021**, *20* (4), 525–532.

95. Riordan, M. et al. The Invention of the Transistor. *Rev. Mod. Phys.* **1999**, *71* (2), S336–S345.

96. Solankia, T. et al. A Review Paper : A Comprehensive Study of Junctionless Transistor. *Natl. Conf. Recent Trends Eng. Technol.* **2011**, No. May, 1–5.

97. Chhowalla, M. et al. Two-Dimensional Semiconductors for Transistors. *Nat. Rev. Mater.* **2016**, *1* (11), 16052.

98. Cao, W. et al. The Future Transistors. *Nature* **2023**, *620* (7974), 501–515.

99. Iwai, H. et al. The Transistor Was Invented 75 Years Ago: A Big Milestone in Human History. *Electrochem. Soc. Interface* **2022**, *31* (4), 65–72.

100. Yin, X. et al. Vertical Phase Separation Structure for High-Performance Organic Thin-Film Transistors: Mechanism, Optimization Strategy, and Large-Area Fabrication toward Flexible and Stretchable Electronics. *Adv. Funct. Mater.* **2022**, *32* (27).

101. Kleemann, H. et al. A Review of Vertical Organic Transistors. *Adv. Funct. Mater.* **2020**, *30* (20).

102. Yan, Y. et al. Recent Progress in Organic Field-Effect Transistor-Based Integrated Circuits. *J. Polym. Sci.* **2022**, *60* (3), 311–327.

103. Wadhera, T. et al. Recent Advances and Progress in Development of the Field Effect Transistor Biosensor: A Review. *J. Electron. Mater.* **2019**, *48* (12), 7635–7646.

104. Liang, Y. et al. Low-Dimensional Hybrid Perovskites for Field-Effect Transistors with Improved Stability: Progress and Challenges. *Adv. Electron. Mater.* **2020**, *6* (9), 2000137.

105. Yuvaraja, S. et al. Organic Field-Effect Transistor-Based Flexible Sensors. *Chem. Soc. Rev.* **2020**, *49* (11), 3423–3460.

106. Surya, S. G. et al. Organic Field Effect Transistors (OFETs) in Environmental Sensing and Health Monitoring: A Review. *TrAC - Trends Anal. Chem.* **2019**, *111*, 27–36.

107. Kumar, B. et al. Organic Thin Film Transistors: Structures, Models, Materials, Fabrication, and Applications: A Review. *Polym. Rev.* **2014**, *54* (1), 33–111.

108. Reséndiz, L. et al. Effect of Active Layer Thickness on the Electrical Characteristics of Polymer Thin Film Transistors. *Org. Electron.* **2010**, *11* (12), 1920–1927.

109. Zhang, W. et al. A Novel Alkylated Indacenodithieno[3,2-b]Thiophene-Based Polymer for High-Performance Field-Effect Transistors. *Adv. Mater.* **2016**, *28* (20), 3922–3927.

110. Wang, W. et al. Probing the Intrinsic Charge Transport in Indacenodithiophene-Co-Benzothiadiazole Thin Films. *AIP Adv.* **2017**, *7* (12).

111. Harkin, D. J. et al. Decoupling Charge Transport and Electroluminescence in a High Mobility Polymer Semiconductor. *Adv. Mater.* **2016**, *28* (30), 6378–6385.

112. Zhang, X. et al. Molecular Origin of High Field-Effect Mobility in an Indacenodithiophene- Benzothiadiazole Copolymer. *Nat. Commun.* **2013**, *4*, 1–9.

113. Bao, B. et al. Electronic Mobility in the High-Carrier-Density Limit of Ion Gel Gated IDTBT Thin Film Transistors. *Chinese Phys. B* **2015**, *24* (9), 1–5.

114. Sommerville, P. J. W. W. et al. Elucidating the Influence of Side-Chain Circular Distribution on the Crack Onset Strain and Hole Mobility of Near-Amorphous Indacenodithiophene Copolymers. *Macromolecules* **2020**, *53* (17), 7511–7518.

115. Li, Y. et al. An Indacenodithiophene-Based Semiconducting Polymer with High Ductility for Stretchable Organic Electronics. *Polym. Chem.* **2017**, *8* (34), 5185–5193.

116. Zhang, W. et al. Indacenodithiophene Semiconducting Polymers for High-Performance, Air-Stable Transistors. *J. Am. Chem. Soc.* **2010**, *132* (33), 11437–11439.

117. Venkateshvaran, D. et al. Approaching Disorder-Free Transport in High-Mobility Conjugated Polymers. *Nature* **2014**, *515* (7527), 384–388.

118. Noriega, R. et al. A General Relationship between Disorder, Aggregation and Charge Transport in Conjugated Polymers. *Nat. Mater.* **2013**, *12* (11), 1038–1044.

119. Marina, S. et al. Common High-Performance Semiconducting Polymers Are Not Amorphous but Semi-Para-Crystalline. **2021**, 1–24.

120. Tool, A. Q. et al. Viscosity and the Extraordinary Heat Effects in Glass. *J. Res. Natl. Bur. Stand. (1934).* **1946**, *37* (2), 73.

121. McKenna, G. B. et al. Some Open Challenges in Polymer Physics*. *Polym. Eng. Sci.* **2022**, *62* (5), 1325–1355.

122. Wilhelm, P. et al. Control of Intrachain Morphology in the Formation of Polyfluorene Aggregates on the Single-Molecule Level. *ChemPhysChem* **2020**, *21* (10), 961–965.

123. Gao, S. et al. Measurement of the Limiting Fictive Temperature over Five Decades of Cooling and Heating Rates. *Thermochim. Acta* **2015**, *603*, 123–127.

124. Yoon, H. et al. An Ultrastable Polymeric Glass: Amorphous Fluoropolymer with Extreme Fictive Temperature Reduction by Vacuum Pyrolysis. *Macromolecules* **2017**, *50* (11), 4562–4574.

125. Badrinarayanan, P. et al. The Glass Transition Temperature versus the Fictive Temperature. *J. Non. Cryst. Solids* **2007**, *353* (26), 2603–2612.

126. Kawamura, T. et al. Crystalline Thin Films of β-Phase Poly(9,9-Dioctylfluorene). *Thin Solid Films* **2011**, *519* (7), 2247–2250.

127. Pirela, V. et al. Unraveling the Influence of the Preexisting Molecular Order on the Crystallization of Semiconducting Semicrystalline Poly(9,9-Di- *n* -Octylfluorenyl-2,7-Diyl (PFO). *Chem. Mater.* **2022**, *34* (23), 10744–10751.

128. Chen, S. H. et al. Cold Crystallization of Poly(9,9-Di- *n* -Octyl-2,7-Fluorene). *Macromolecules* **2007**, *40* (15), 5353–5359.

129. Elshaikh, M. et al. Influence of the Organic Solvents on the α and β Phases of a Conjugated Polymer (PFO). *Dig. J. Nanomater. Biostructures* **2019**, *14* (4), 1069–1077.

130. Liu, B. et al. Discovery and Structure Characteristics of the Intermediate-State Conformation of Poly(9,9-Dioctylfluorene) (PFO) in the Dynamic Process of Conformation Transformation and Its Effects on Carrier Mobility. *RSC Adv.* **2020**, *10* (1), 492–500.

131. Luzio, A. et al. Microstructural Control Suppresses Thermal Activation of Electron Transport at Room Temperature in Polymer Transistors. *Nat. Commun.* **2019**, *10* (1), 3365.

132. Perevedentsev, A. et al. Solution-crystallization and Related Phenomena in 9,9-dialkyl-fluorene Polymers. I. Crystalline Polymer-solvent Compound Formation for Poly(9,9-dioctylfluorene). *J. Polym. Sci. Part B Polym. Phys.* **2015**, *53* (21), 1481–1491.

133. Peng, H. et al. Light Emitting Based on Polymer. In *Polymer Materials for Energy and Electronic Applications*; Elsevier, 2017; pp 243–285.

134. Chen, S. H. et al. Crystalline Forms and Emission Behavior of Poly(9,9-Di- *n* -Octyl-2,7-Fluorene). *Macromolecules* **2005**, *38* (2), 379–385.

135. Eggimann, H. J. et al. How β-Phase Content Moderates Chain Conjugation and Energy Transfer in Polyfluorene Films. *J. Phys. Chem. Lett.* **2019**, *10* (8), 1729–1736.

136. Grell, M. et al. Interplay of Physical Structure and Photophysics for a Liquid Crystalline Polyfluorene. *Macromolecules* **1999**, *32* (18), 5810–5817.

137. Padmaja, S. et al. Crystallization Kinetics in Liquid Crystals with Hexagonal Precursor Phases by Calorimetry. *Zeitschrift für Naturforsch. A* **2010**, *65* (8–9), 733–744.

138. Di Lisio, V. et al. Physical Ageing in Molecular Glasses beyond the α Relaxation. *J. Chem. Phys.* **2023**, *159* (6).

139. Perez-de-Eulate, N. G. et al. Glass Transition and Molecular Dynamics in Polystyrene Nanospheres by Fast Scanning Calorimetry. *ACS Macro Lett.* **2017**, *6* (8), 859–863.

140. Merzlyakov, M. et al. Step Response Analysis in DSC — a Fast Way to Generate Heat Capacity Spectra. *Thermochim. Acta* **2001**, *380* (1), 5–12.

141. Di Lisio, V. et al. Physical Ageing in Molecular Glasses beyond the α Relaxation. *J. Chem. Phys.* **2023**, *159* (6).

142. Shoifet, E. et al. Temperature Modulated Differential Scanning Calorimetry - Extension to High and Low Frequencies. *Thermochim. Acta* **2015**, *603*, 227–236.

143. Levit, R. et al. The Generalized Vogel-Fulcher-Tamman Equation for Describing the Dynamics of Relaxor Ferroelectrics. *Sci. Rep.* **2019**, *9* (1), 1–8.

POLYMAT

eman ta zabal zazu
Universidad del País Vasco
Euskal Herriko Unibertsitatea

ESTO-ES-TODO-AMIGOS